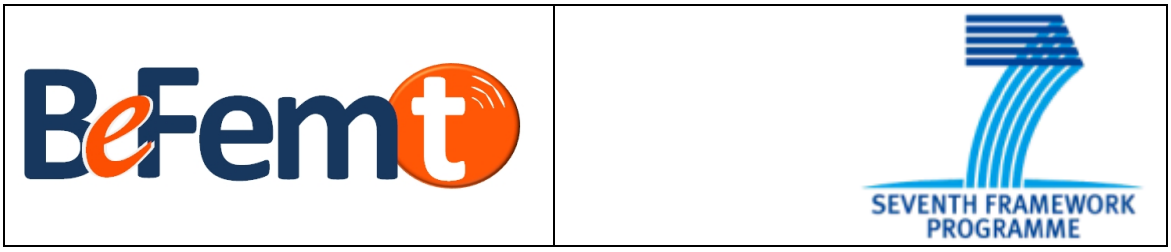

INFSO-ICT-248523 BeFEMTO

D3.2

Promising Interference and Radio Management Techniques for Indoor Standalone Femtocells

Contractual Date of Delivery to the CEC:	**30-06-2012**
Actual Date of Delivery to the CEC:	**30-06-2012**
Author(s):	Mehrdad Shariat, Atta U. Quddus, Mehdi Bennis, Zubin Bharucha, Massinissa Lalam, Masood Maqbool, Sylvie Mayrargue, Chrysovalantis Kosta, Antonio De Domenico, Emilio Calvanese-Strinati, Rajarshi Mahapatra, Carlos H. M. de Lima, Serkan Uygungelen
Participant(s):	**CEA, DOCOMO, SCET, UniS, UOulu**
Workpackage:	WP3 – Radio Access for Stand-alone Femtocells
Estimated person months:	**88**
Security:	**PU**
Nature:	**R**
Version:	1.0
Total number of pages:	**81**

Abstract:
This document summarizes the technical contributions carried out by Work Package 3 (WP3) over the course of the 2.5 years of the BeFEMTO project in respect to Interference management and RRM techniques for Indoor standalone femtocells. Here, a number of technical contributions related to interference management techniques in the downlink and uplink for indoor standalone femtocells including power control, frequency partitioning schemes, as well as interference management on the control channel for macro UEs trapped in the coverage of femtocells are examined. Next, multi-operator indoor band sharing is studied as a means to facilitate coexistence of macro and femtocells. Subsequently, the concept of coordinated Time Division Duplexing underlay at Uplink is investigated in presence of Self-Organizing femtocells. Next, this deliverable investigates the impact of decentralized approaches for radio resource allocation such as multi-user scheduling exploiting location information and opportunistic spectrum reuse combined with Successive Interference Cancellation techniques. Furthermore, different access control policies and their tradeoffs for indoor femtocells in addition to optimizing layer-2 handover parameters are studied. Finally, the benefit of Multiple Input Multiple Output transmission and high order modulation for femtocells is presented with detailed simulation studies.

Keyword list:

Interference Management, Macrocell, OFDMA, Spectrum Sharing, Standalone Femtocell, Power Control, Frequency Partitioning, Radio Resource Management

Executive Summary

This deliverable presents innovative concepts along with the promising results of the research activities carried out during the two years and a half of the BeFEMTO project within Work Package 3 in respect to interference management and RRM techniques. These concepts cover interference management and radio resource management for standalone indoor femtocells as opposed to networked femtocells, which are considered in WP4.

This document consists of four main sections. First, Section 1 summarizes the challenges addressed in this deliverable and also introduces different contributions.

In Section 2, interference management strategies, which are carried out among unplanned indoor standalone femtocells or between them and the overlay macrocells, are explored. First, the critical issue of femto-to-macrocell interference on the control channel is studied, in which interference-reducing techniques such as sparseness yield promising gains for UEs trapped within the coverage of active femtocells are addressed. In addition, interference avoidance techniques including power control and frequency partitioning (via resource restriction) schemes are studied in the downlink. Moreover, multi-operator indoor band sharing is examined as a means to facilitate coexistence of macro and femtocells where full sharing versus partial sharing of macrocell and femtocells spectrum bands is discussed. Finally, the concept of Time Division Duplexing underlay at Uplink is studied where a distributed self-organizing mechanism based on the concept of busy tones is proposed.

Section 3 addresses the impact of decentralized approaches for radio resource allocation. First, a novel scheduler exploiting the wireless spectrum in a two tier-network is proposed. The proposed radio resource management scheme limits the overall interference per Resource Block generated outside the coverage range of a femtocell while reducing the transmission power in each Resource Block. Subsequently, another decentralized approach is proposed for radio resource allocation in femtocell networks based on opportunistic reuse to efficiently control the level of resulting interference on macro performance. Thereafter, an interference-aware Local Cartography RRM technique is presented for standalone femtocell where Power and Resources are allocated to femto UEs efficiently by combining location information. Next, it is focused on a novel RRM and power control scheme combined with Successive Interference Cancellation. Different access control policies for standalone femtocells are also studied highlighting interesting tradeoffs between closed, open and hybrid access. Furthermore, the impact of key handover parameters is evaluated via developing analytical methods. Finally, the benefit of Multiple Input Multiple Output transmission and high order modulation for femtocells is presented with detailed simulation studies.

Section 4 concludes this deliverable and highlights its achievements in the area of small cells.

Authors

Partner	Name	Phone / Fax / e-mail
CEA		
	Antonio De Domenico	Phone: +33 4 38 78 18 17 e-mail: antonio.de-domenico@cea.fr
	Emilio Calvanese Strinati	Phone: +33 4 38 78 17 34 e-mail: emilio.calvanese-strinati@cea.fr
	Rajarshi Mahapatra	Phone +33 4 38 78 62 42 e-mail rajarshi.mahapatra@cea.fr
	Sylvie Mayrargue	Phone: +33 4 38 78 62 42 e-mail: sylvie.mayrargue@cea.fr
DOCOMO		
	Zubin Bharucha	Phone: +49 89 56824 231 e-mail: bharucha@docomolab-euro.com
	Serkan Uygungelen	Phone: +49 89 56824 226 e-mail: uygungelen@docomolab-euro.com
Sagemcom Energy & Telecom		
	Masood Maqbool	Phone: +33 1 57 61 13 63 e-mail: masood.maqbool@sagemcom.com
	Massinissa Lalam	Phone: +33 1 57 61 13 41 e-mail: massinissa.lalam@sagemcom.com
University of Oulu		
	Mehdi Bennis	Phone: +358 40 8241 742 Fax: +358 8 553 2845 e-mail: bennis@ee.oulu.fi
	Carlos H. Lima	Phone: +358 40 8241 775 e-mail: carlosl@ee.oulu.fi
University of Surrey		
	Mehrdad Shariat	Phone: +44 1483 689330 e-mail: m.shariat@surrey.ac.uk
	Chrysovalantis Kosta	Phone: +44 1483 683430 e-mail: c.kosta@surrey.ac.uk
	Atta U. Quddus	Phone: +44 1483 683787 Fax: +44 1483 686011 e-mail: a.quddus@surrey.ac.uk

Table of Contents

Table of Abbreviations

Acronym	Meaning
3G	3rd Generation
3GPP	3rd Generation Partnership Project
4G	4th Generation
ACK/NACK	Acknowledgment / Negative Acknowledgment
AR	Activation Ratio
BeFEMTO	Broadband Evolved Femtocells
BER	Bit Error Rate
BLER	Block Error Rate
BS	Base Station
BW	Bandwidth
CCI	Co-Channel Interference
CDF	Cumulative Distribution Function
CF	Characteristic Function
CLSM	Closed Loop Spatial Multiplexing
CQI	Channel Quality indicator
CRS	Common Reference Symbol
CSG	Closed Subscriber Group
dB	Decibel
DCI	Downlink Control Information
DER	Dynamic Exclusion Region
DFP	Dynamic Frequency Planning
DL	Downlink
eICIC	enhanced Inter-Cell Interference Coordination
eNB	evolved Node B
E-UTRA	Evolved-Universal Terrestrial Radio Access
FDMA	Frequency Division Multiple Access
FFR	Fractional Frequency Reuse
FFT	Fast Fourier Transform
FR	Frequency Reuse
FSM	Femtocell Spectrum Management
FUE	Femtocell User Equipment
HO	Hand Over
HeNB	Home evolved Node B
HetNet	Heterogeneous Network
IC	Interference Cartography
ICI	Inter Carrier Interference
IEEE	Institute of Electrical and Electronics Engineers
IFR	Inverse Frequency Reuse
ISD	Inter Site Distance
KPI	Key Performance Indicator
LC-RRM	Local Cartography RRM
LFGW	Local Femto Gateway
LN	Log Normal
LTE	Long-Term Evolution
LTE-A	Long-Term Evolution Advanced
MBS	Macro Base Station
MCI	Maximum Signal to Interference Ratio
MCM	Measurement Collection Module
MIC	Mean Instantaneous Capacity
MIMO	Multiple Input Multiple Output
MGF	Moment Generating Function
MMSE	Minimum Mean Square Error
MPP	Marked Point Process
MUE	Macrocell User Equipment

ML-MIMO	Multi-User MIMO
OFDM	Orthogonal Frequency Division Multiplexing
OFDMA	Orthogonal Frequency Division Multiple Access
PC	Power Control
PDF	Probability Distribution Function
PDSCH	Physical Downlink Shared Channel
PF	Proportional Fairness
PHY	Physical (Layer)
PMI	Precoding Matrix Indicator
QAM	Quadrature Amplitude Modulation
QoS	Quality of Service
RB	Resource Block
REM	Radio Environment Map
RF	Radio Frequency
RI	Rank Indicator
RRC	Radio Resource Control
RRM	Radio Resource Management
RV	Random Variable
SCME	Spatial Channel Model Extended
SFR	Soft Frequency Reuse
SIC	Successive Interference Cancellation
SINR	Signal to Interference-plus-Noise Ratio
SLN	Shifted Log Normal
SNR	Signal to Noise Ratio
SISO	Single Input Single Output
SON	Self Organized Network
SU-MIMO	Single User MIMO
TTI	Time Transmit Interval
TTT	Time-To-Trigger
UE	User Equipment
UL	Uplink
UMa	Urban Macro
WiMAX	Worldwide interoperability for Microwave Access
WP	Work Package

1. Introduction

The emergence of new data and video services coupled with an increase in the number of user equipments such as smart-phones and tablets, has forced mobile operators to examine new ways for increasing coverage, boosting data rates and lowering capital and operating expenditures (CAPEX and OPEX) of their mobile networks. One approach for improving the poor macrocell indoor coverage and enhancing the spectral efficiency has been the utilization of femtocells. The potential cost reduction combined with the prediction market growth make the femtocell concept a lucrative option for mobile operators. Recently, femtocells have been receiving a growing interest from both academia and industry. Femtocells are small cellular base stations which can be deployed in residential, enterprise, or outdoor areas. Femtocells connect several mobile phones to the operator's network via an existing broadband connection (such as DSL or cable). Among the benefits provided by femtocells include boosting the spectral efficiency of the network, improving the poor macrocell indoor coverage, and offloading the macrocell network. Although femtocells provide several benefits for operators and users alike, their massive deployment comes with a number of technical challenges. Notably, the most important and detrimental problem facing femtocell networks is the presence of interference among neighbouring femtocell networks, and between the femtocell network and the macrocell network.

This report presents the innovative concepts along with results of the research activities carried out during the two years and a half of the BeFEMTO project within Work Package 3. This document consists of four sections.

An introduction is given in Section 1 summarizing the challenges addressed in this deliverable.

In Section 2, interference management approaches between unplanned indoor standalone femtocells and overlay macrocells are investigated. First, the problem of femto-to-macrocell interference on the control channel is studied and efficient interference reduction techniques are proposed. Next, on data channel part, a novel low-complexity distributed Inter-Cell Interference Coordination (ICIC) scheme is proposed for the emerging multi-cell Heterogeneous Networks (HetNets). Furthermore, a complementary dynamic algorithm is introduced to mitigate interference for victim macro user equipments which are impacted by an aggressor femto cell in the vicinity. The algorithm exploits the channel condition of the victim Macrocell UE (MUE) so that the Soft Frequency Reuse (SFR) in femtocell only implicates the least number of required subbands. Moreover, multi-operator indoor band sharing is examined as a means to facilitate femto deployments under current macro network. Finally, Time Division Duplexing (TDD) underlay at Uplink (UL) Frequency Division Duplexing (FDD) bands is investigated where a distributed self-organizing mechanism based on the concept of busy tones is proposed.

Section 3 deals with decentralized approaches for RRM. First, a novel scheduler exploiting the wireless spectrum in a two tier-network is proposed to limit interference per Resource Block (RB) while reducing the transmission power per RB. Furthermore, another decentralized approach is proposed for radio resource allocation in femtocell networks based on opportunistic reuse of spectrum. Thereafter, an interference-aware Local Cartography-based Radio Resource Management (LC-RRM) technique is presented for standalone femtocell where RRM is combined with location information to enhance the efficiency of the scheme. Next contribution focuses on a novel RRM and power control scheme combined with Successive Interference Cancellation (SIC). Here, SIC is used to allow a macrocell user and a femtocell user to share a common channel on UL to a femtocell access point. Different access control policies for standalone femtocells are also studied highlighting interesting tradeoffs between different schemes. Furthermore, an analytical model is developed to more efficiently study the impact of critical HO parameters on the performance of the system. Finally, the advantages of Multiple Input Multiple Output (MIMO) transmission and high order modulation for femtocells is evaluated based on detailed simulation studies

Section 4 highlights the achievements of this deliverable in the area of heterogeneous networks and small cells.

2. Interference Management for Indoor Standalone Femtocells

This section describes interference management approaches between unplanned indoor standalone femtocells and planned overlay macrocells, as well as between indoor standalone femtocells themselves. The first subsection tackles various interference avoidance techniques, while the second subsection deals with the concept of multi-operator indoor band sharing. The third subsection presents the concept of TDD underlay at Uplink FDD bands, in which case standalone femtocells opportunistically reuse the UL macrocell spectrum in a TDD manner.

2.1 Interference Avoidance Schemes

2.1.1 Problem Statement

The rapidly increasing demand for capacity is served by higher bandwidth allocation, but since bandwidth is scarce and expensive, a key to substantial throughput enhancement is to improve the reuse of radio frequency resources. Smaller cell sizes enable the efficient spatial reuse of spectrum [1]. While decreasing the cell size boosts system capacity, the cost involved is becoming increasingly prohibitive, due to the required installation of new network infrastructure. Studies indicate that a significant proportion of data traffic originates indoors [2]. Poor signal reception caused by penetration losses through walls severely hampers the operation of indoor data services in state-of-the-art systems. The concept of femtocells, in which Home evolved NodeBs (HeNBs) are placed indoors, has therefore attracted considerable interest in recent times. HeNBs are low-cost, low-power, short-range, plug-and-play base stations, which aim to extend and improve macro-cell coverage in indoor areas. HeNBs are directly wired to the backbone network and UEs located indoors (if allowed) communicate directly with them. HeNBs therefore offload indoor users from the macro-cell, thus potentially enhancing the capacity both, indoors (by bypassing the wall penetration loss problem) as well as outdoors (by freeing up resources). There are several obvious advantages from femtocell deployment, the most important of which is that radio resources can be shifted to outdoor users, yielding better user performance (satisfied user criterion) and coverage. Another selling point for operators is that high throughput coverage is extended to the indoor environment where it is most needed [2].

Much research has recently been devoted to the issue of interference in co-channel femto-to-macro Downlink (DL) interference [3][4][5][6][7]. These studies have consistently shown that a coverage-hole exists when co-channel femtocells are deployed in a macro-cell overlay network. Many of these studies propose that open-access femtocells help alleviate this problem. However, in recent 3GPP discussions, it has been decided that femtocells are solely operate in the closed-access mode, i.e., each HeNB maintains a list of UEs that are allowed access to it. Any UE which is not a member of this so-called Closed Subscriber Group (CSG) must attempt to maintain communication with its serving macro evolved NodeB (eNB) despite being in close proximity to the HeNB. While femtocells promise substantial coverage and capacity gains [2][8][9][10], their random deployment introduces additional interference to the system, particularly for macro UEs who are not part of a CSG. A rigorous study must therefore be conducted to assess the impact of femtocell deployment on co-channel macrocell UEs. Furthermore, the most recent study item [11] urges the investigation of interference management techniques that are backwards compatible with Long Term Evolution (LTE) Rel-8/9 UEs for co-channel deployments of femtocells.

In this direction, an extensive research is going on at the moment to resolve the cross-tier interference problems in macro/femto HetNets. Solutions based on power control, Fractional Frequency Reuse (FFR) and SFR have already been discussed in the literature. These solutions could be dynamic or static. ICIC is an approach through which base stations could coordinate among each other to mitigate an arising interference condition.

Currently, ICIC in macro/femto HetNets is an active area of research both in academic institutions and industry. The authors of [12] have provided an overview of different categories of ICIC techniques: time-domain, frequency-domain and power control based. A comparison of these techniques is carried out using system level simulations. However, only one macro base station is considered hence macro-to-macro aspect is not taken into account. In [13], performance evaluation of a dynamic and a static ICIC technique is carried out. Time/frequency silencing is used to mitigate interference for a victim MUE at the expanse of reduction in femto performance owing to partial resource utilization. A dynamic ICIC algorithm is presented in [14] that addresses the problem of interference within the femtocell network. It

has been shown that the proposed algorithm outperforms the reuse 1 in terms of user data rate and delay. Interface X2 is used between femto and macro cells in [15] to mitigate the interference caused by femto to a victim MUE. Resource partitioning is employed to deter the usage of same resources by the victim MUE and the aggressor femto. The authors of [16] have also proposed a frequency partitioning scheme for macro/femto networks. With the knowledge of resources shared among macro and femto cells, the macro base stations allocate resources to the victim MUE in the non-shared part.

In this section we explore novel interference coordination /avoidance techniques to address the omissions in the literature. In particular, we focus on areas that have not been sufficiently covered like the issue of control channel interference in presence of femtocells. Furthermore, some new dynamic ICIC schemes are proposed to control the interference on data channel via restricting frequency resources or the power allocated to the strong interferers (eNBs/HeNBs).

2.1.2 Control Channels Interference Management

Femtocells promise substantial gains in system spectral efficiency due to an enhanced reuse of radio resources. Femtocells may be employed in a co-channel fashion such that the bandwidth used by the macro-cell is reused by the femtocell. Femtocells maintain an exclusive list of UEs that they serve. In this case, a foreign macro UE trapped inside a femtocell experiences heavy interference from this femtocell. As per the current 3rd Generation Partnership Project (3GPP) discussions for Rel-10, this part investigates the issue of femto-to-macro interference on the control channel. The control channel is very crucial because if it is incorrectly decoded, the following data region is completely lost. In line with the 3GPP discussions on the ICIC topic, interference-reducing techniques that are backward compatible with Rel-8/9 UEs are introduced in here. The use of these techniques results in a significant improvement of control channel performance for trapped macro UEs.

This sub-task addresses an issue that has so far not been sufficiently discussed, i.e., the performance of the DL control channel in the presence of femtocell deployment. Femtocell research at this point is mature enough to allow for a detailed and rigorous performance assessment of the various elements that comprise the air interface. Emphasis is given to the control channel performance for macro UEs that are trapped in the coverage of one or more femtocells. The control channel is especially important because if it cannot be correctly decoded, the ensuing data is unintelligible. Based on this, certain LTE Rel-8/9-compliant interference management techniques are introduced and it is shown that they help improve the performance of the control channel for the vulnerable macro UEs.

The DL of an LTE Orthogonal Frequency Division Multiple Access (OFDMA)-FDD system is considered where the system bandwidth, W , is divided into N_{RB} Resource Blocks (RBs), each of bandwidth W_{RB} so that $W = N_{RB}W_{RB}$. The RB represents the basic OFDMA time-frequency unit [17]. Each RB contains N_{RE} Resource Elements (REs). One slot in the time-domain consists of N_{OFDM} Orthogonal Frequency Division Multiplexing (OFDM) symbols. Two slots in the time-domain, i.e., $2N_{OFDM}$ symbols and N_{RB} RBs in the frequency-domain make one OFDM subframe as shown in Figure 2-1. The subframe consists of a control and a data region. Interspersed within these are Common Reference Symbols (CRSs) which are used to estimate the channel. Figure 2-1shows the CRS distribution for the one transmit antenna case. Their density increases for the two and four transmit antenna cases.

The control region can span between one and three OFDM symbols and always occurs at the start of every subframe. Since the control region is pertinent to this work, it will be described in further detail here. The DL control region consists of three physical channels.

The Physical Control Format Indicator CHannel (PCFICH) carries the control format indicator, indicating the number of OFDM symbols (1, 2 or 3) used for the transmission of DL control channel information in each subframe.

The Physical Hybrid-ARQ Indicator CHannel (PHICH) carries UL hybrid-ARQ ACK/NACK information indicating whether the eNB has correctly received an UL transmission. Four REs constitute a Resource Element Group (REG). Nine REGs make a Control Channel Element (CCE). The PCFICH always occupies four REGs and the number of REGs that the PHICH may occupy depends on the system bandwidth and a system-wide parameter, Ng . Further details can be found in [18].

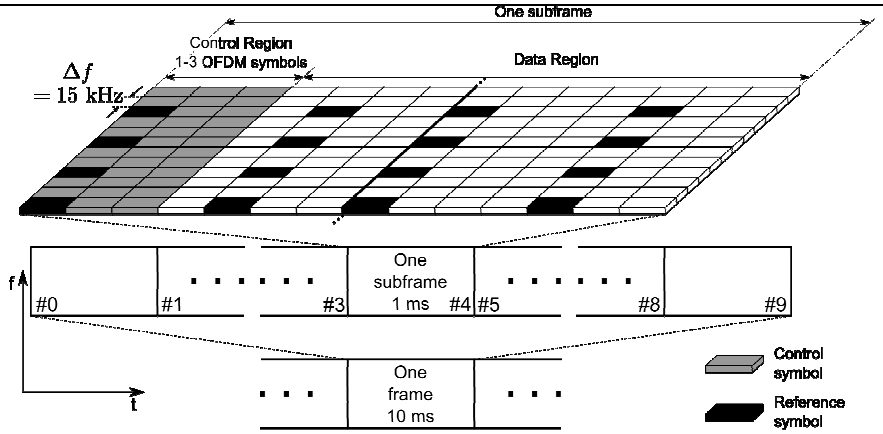

Figure 2-1: Frame structure for LTE systems operating in the FDD mode. Each 1 ms subframe consists of two slots with each slot containing several REs of 15 kHz bandwidth each. Ten subframes together make one frame.

The third physical channel is known as the Physical Downlink Control CHannel (PDCCH) and it carries the DL control information which includes transmission resource assignments and other control information for a UE or groups of UEs. The PDCCH belonging to any UE occupies any of {1, 2, 4, 8} CCEs depending on the prevailing channel conditions between the UE and the eNB.

The PCFICH always occurs exclusively on the first OFDM symbol of the control channel. The PHICH may occupy all available OFDM symbols, but this is not a mandatory requirement. The PDCCH is distributed over all the available OFDM symbols of the control channel. It is important to note that in the context of the subframe, the control channel is very crucial. If the PCFICH or PDCCH are incorrectly decoded, the data region is lost. This is the premise of the research done in this work and is particularly important in a scenario with co-channel heterogeneous network deployment due to detrimental femto-to-macro interference.

The redundant repetitions of the PCFICH (four) and PHICH (three) are equally distributed in the frequency domain in order to exploit frequency selective fading [17]. The locations of these two physical channels are subject to a cyclic shift dependent on the Physical Cell Identity (PCI) in order to reduce collisions of these channels between two neighbouring cells. For further details on the mapping of PCFICH and PHICH to REs, the reader may refer to [18]. In order to prevent the UE from attempting to blindly search the entire control channel in the frequency domain for its associated PDCCH, in LTE, each UE has a limited set of CCE locations where its PDCCH can be located. Each UE is assigned a cell radio network temporary identifier (C-RNTI), which is an identifier, unique within the cell and allocated by the eNB. This C-RNTI is used to determine the possible location, known as the search space, of the UE's PDCCH. The CCEs available for use by PDCCHs are sequentially numbered and interleaved [19]. This is again done in order to exploit the channel's frequency selectivity. The PDCCH assigned to a UE occupies consecutively numbered CCEs, which, due to the interleaving are spread in the frequency domain. Finally, the interleaving also depends on the subframe index within the frame being considered so as to further randomize PDCCH collisions from neighbouring cells. Further details on PDCCH assignment may be found in [20]. For the remainder of this work, only PCFICH and PDCCH are considered due to their significantly different RE occupancy. Figure 2-2 shows an example of the loading in part of the control region of an LTE subframe. In this example, the control region is three OFDM symbols long and the CRS distribution for the two antenna case is shown. As is seen, the PDCCH is distributed across all available OFDM symbols. One repetition each of the PHICH (occupying 24 REs) and the PCFICH (occupying 4 REs) is shown.

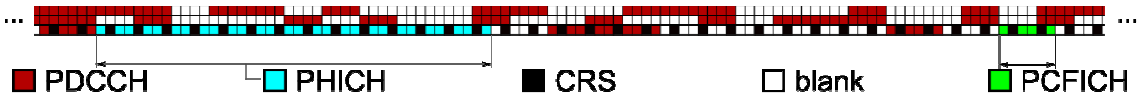

Figure 2-2: An example of the loading in part of the control region of a subframe.

2.1.2.1 System model

The simulation area comprises a one tier tessellated hexagonal cell layout. Each hexagon represents a

sector, thus implying that the eNBs is situated at the junction of three hexagonal sectors. Statistics are taken only from the central sector. However, users are distributed in all sectors in order to simulate the wrap-around effect. For each sector, the azimuth antenna pattern, $A(\phi)$, is described as in [22]. According to the simulation requirements described in [22], the 5x5 grid model is used in this work to simulate the femtocells. This setup models a single-floor building with 25 apartments, occurring in a 5x5 grid. An active HeNB may exist in an apartment with probability p_{active}. Every apartment that contains an active HeNB also contains exactly one associated femto UE. These are dropped randomly and uniformly within the apartment with a specified minimum separation from the HeNB. In addition to this, macro UEs are also randomly and uniformly dropped within the tiered hexagonal system. As a result, it is possible that a macro UE lies within the confines of an apartment. Since the method of access is strictly closed, such macro UEs, despite their indoor locations, are served by the eNB situated outdoors. In such a situation, these vulnerable macro UEs suffer severely from interference originating from the nearby HeNBs. To assess the impact of the interference management techniques, macro UEs lying within a certain path loss threshold, L_t, are identified and analyzed for achieved Signal-to-Interference-plus-Noise Ratio (SINR).

Three path loss models are used depending on the type of link [22], i.e., whether the link is purely outdoor, outdoor-to-indoor or purely indoor. Log-normal shadowing is added to all links. Correlated shadowing maps are applied such that the correlation in the shadowing values of two points is dependent on the distance between them. Shadowing standard deviation and auto-correlation shadowing distances for the macro and femtocells are taken from [22]. Fast fading channels are simulated using the delay profiles for the UMi and InH models provided in [23]. Due to the presence of multiple receive antennas, maximum ratio combining (MRC) is made use of. The gain from MRC is approximated by simulating two individual, uncorrelated receive streams and adding the achieved SINR on each of them [24].

2.1.2.2 Proposed algorithm

Typically, the HeNB is expected to serve a very small number of UEs (system-level evaluation of LTE assumes one UE per femtocell). Furthermore, since the transmission distances between the serving eNB and the UE within the femtocell are much shorter than those of overlay macro-cell, channel conditions between transmitter and receiver are very good. Due to this, the aggregation levels assigned to femto UEs are usually low. The aggregation level is the number of CCEs that are used for transmission of the PDCCH and can take values in {1, 2, 4, 8}. Clearly, worse channel conditions lead to higher aggregation levels being used. As a result of the low number of physical control channels to be transmitted, normal LTE operation would then prescribe a control region of size one, i.e., one OFDM symbol in the femto layer, with the rest of the subframe used for data transmission. The interference management techniques described in the following subsections exploit this knowledge in different ways.

2.1.2.2.1 Blank Data Region

The control region on the femto layer being one symbol long, followed by data, would cause high DL interference to the entire control region of a macro UE trapped within the coverage of the femtocell. One method of reducing the interference caused to such macro UEs is to simply not transmit any data in the data region. Clearly, doing so on all subframes would result in a complete loss of data capacity on the femto layer. However, doing this on only some subframes would enable the macro UE to reliably decode all three channels (especially the PDCCH due to its time-spread nature) on such subframes. Such a technique is completely transparent to the UE and therefore backward compatible. One possible disadvantage of this technique is that the reduced density of the data region results in a loss of capacity on the femto layer.

2.1.2.2.2 Sparseness in the Control Channel

Since the PCFICH resides only in the first OFDM symbol, their performance in the macro layer would be severely degraded if the femto control region is limited to one OFDM symbol only. A very simple method of reducing this interference is to make the control region of the femtocell as sparse as possible so as to reduce the interference caused to PCFICH. This can easily be done by forcing HeNBs to always use a control region of size three OFDM symbols regardless of the size of the physical control channel payload. Doing this will spread the PDCCH in the femto layer over the three OFDM symbols, thus reducing the interference imposed on PCFICH. Such a technique is completely transparent to the UE and therefore backward compatible. One possible disadvantage of this technique is that the reduced size of the data region results in a loss of capacity on the femto layer. However, previous studies [8] have shown that very high capacities are achieved in the femtocell. Therefore, this technique is expected to result only in a

modest capacity reduction; certainly less than the loss of capacity caused by the technique shown in 2.1.2.2.1.

2.1.2.2.3 Power Control

Since favourable channel conditions exist within femtocells, power control can be utilized to reduce the control channel interference caused to trapped macro UEs. A simple power control scheme which adjusts the HeNB transmit power based on the reference signal received power can be implemented [21] such that the HeNB transmit power, P_{HeNB}, is adjusted as

$$P_{HeNB} = \max(\min(x, P_{\max}), P_{\min}) \quad [dBm] \tag{2.1}$$

where $x = \alpha(\overline{R_{CRS}} + 10\log_{10}(N_{RB}^{DL} N_{SC}^{RB})) + \beta$. Here, $P_{\max}$ and $P_{\min}$ are the maximum and minimum allowable HeNB transmit powers, respectively, $\overline{R_{CRS}}$ is the mean measured reference signal received power (RSRP) from the strongest co-channel macro-cell (in dBm), N_{RB}^{DL} is the number of DL RBs, N_{SC}^{RB} is the number of subcarriers per RB, α is a linear scalar that allows altering the slope of the power control mapping curve and β is a parameter (in dB) that is used to alter the exact range of $\overline{R_{CRS}}$ covered by the dynamic range of power control. Again, this technique is backward compatible since the power control method does not rely on any UE measurements. It is assumed that the HeNB is equipped with a DL receiver in order to determine $\overline{R_{CRS}}$. The trade-off of using this technique is a reduced data capacity due to power control. However, past studies have shown that very high data capacities are possible within the femtocell. Therefore, despite power control, the femto UEs are expected to experience high data capacities.

2.1.2.3 Simulation results

It is assumed that the control region on the macro layer is always three OFDM symbols long. This, however, is not the case for the femto layer, where the size of the control region depends on the interference management scheme being used. Both macro and femtocells utilize the entire system bandwidth W. The useful received signal power observed by UE u (where u is the user index) on OFDM symbol $t \in \{1, 2, 3\}$ on RE n is given by

$$Y_{n,t}^{u} = G_{n,t}^{v,u} P_x \tag{2.2}$$

Where $G_{n,t}^{v,u}$ is the channel gain between UE u and its serving HeNB or eNB, v, on symbol t, and the transmit power, P_x, represents either the eNB or HeNB transmit power depending on which entity the UE is served by. The aggregate interference $I_{n,t}^{u}$ seen by UE u is composed of eNB and HeNB interference

$$I_{n,t}^{u} = \sum_{i \in M_{\text{int}}} G_{n,t}^{i,u} P_m + \sum_{j \in F_{\text{int}}} G_{n,t}^{j,u} P_f \tag{2.3}$$

where $G_{n,t}^{i,u}$ accounts for the channel gain between interferer y and UE u on symbol t. The set of instantaneous eNB and HeNB interferers on symbol t and RE n is denoted by M_{int} and F_{int} respectively. Note that the sets M_{int} and F_{int} change across OFDM symbols and subframes due to the PDCCH interleaving and cyclically shifted PCFICH and PHICH locations. The SINR observed on RE n and symbol t at UE u therefore amounts to

$$\gamma_{n,t}^{u} = \frac{G_{n,t}^{v,u} P_x}{I_{n,t}^{u} + \eta} \tag{2.4}$$

where η accounts for thermal noise per RE. In order to calculate the effective SINR across all the allocated REs on any of the control channels belonging to UE u, a mapping to the capacity-domain is first made and this is then re-translated into the SINR domain as explained in [25]. Therefore, the effective SINR for UE u on the control channel y (y representing either the PDCCH or PCFICH) is calculated as

$$\gamma_y^u = F^{-1}\left(\sum_{p \in N_{RE,y}^u} F\left(\gamma_p^u\right) \right) \quad (2.5)$$

where $N_{RE,y}^u$ is the set of REs allocated to the control channel y of UE u . Each element $p \in N_{RE,y}^u$, y is an ordered set $p_1 = (n_1, t_1)$ containing an RE index and a time instant, indicating the position of the RE in question. The capacity $F\left(\gamma_p^u\right)$ is calculated using the attenuated and truncated Shannon bound, as described in [7]. According to this bound, capacity saturates beyond a certain SINR or becomes zero below a certain SINR in order to avoid unrealistically high or low values.

For the results shown in the following subsections, the simulation parameters shown in Table 2-1 are used. Three classes of UEs are considered:

- Trapped macro UEs: These are UEs that are vulnerable macro UEs which have a path loss of $\leq L_t$ dB to any HeNB. Such macro UEs experience very high levels of DL interference from the aggressor HeNBs. The interference management techniques explained in 2.1.2im to reduce the interference experienced by this set of macro UEs.
- Untrapped macro UEs: This forms the set of macro UEs which are not trapped in the coverage of any femtocell, i.e., they have a path loss of $> L_t$ dB to any HeNB.
- Femto UEs: These are the UEs served by HeNBs.

Parameter	**Value**
Avg. 5x5 apartment blocks per macro-cell sector	4
Avg. Macro UEs per macro-cell sector	10
Inter-site distance	500 m
Individual apartment dimensions	10 m x 10 m
HeNB activation probability	0.1
Number of REs per RB	12
Tot. Number of available RBs	50
Tot. Number of subcarriers per RB	12
Thermal noise per RB	-144 dBm
Max. eNB transmit power per sector	46 dBm
Max. HeNB transmit power	20 dBm
Min. HeNB transmit power	-10 dBm
eNB antenna gain	14 dBi
Sectors per eNB	3
Min. Distance between macro UE and eNB	35 m
Min. Distance between femto UE and HeNB	20 cm
Number of HeNB/eNB Rx antennas	2
Number of macro/femto UE Rx antennas	2
Wall penetration loss	20 dB
Power control slope factor	1
Power control dynamic range factor	40 dB
Path loss threshold	85 dB

Table 2-1: Simulation parameters

2.1.2.3.1 Sparseness and Blank Data Regions

The results shown in this subsection only compare sparse and non-sparse schemes. Power control is not employed and all HeNBs transmit with maximum power. Figure 2-3 shows Cumulative Distribution Functions (CDFs) of the effective SINR for the PDCCH

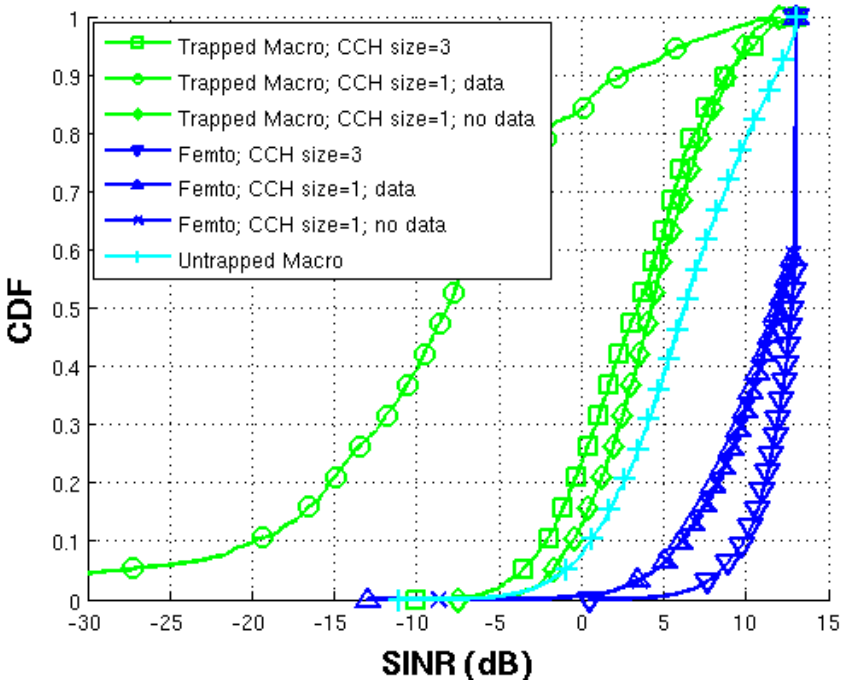

Figure 2-3: Comparison of the sparse control channel scheme and two non-sparse schemes for PDCCH. For the macro layer, the best performance is observed with the non-sparse scheme with a blank data region. For the femto layer, the sparse scheme performs best.

As a basis for comparison, the effective SINRs achieved by trapped macro UEs are plotted against those achieved by the untrapped macro UEs. The aim of the interference management techniques detailed in 2.1.2.2 is to bring the performance of the trapped macro UEs as close as possible to that of the untrapped macro UEs. This figure compares the performance of a sparse femto control channel, i.e., when it is three OFDM symbols long to the case when it is not sparse, i.e., only one OFDM symbol long. The latter case is further divided into two possibilities: one where the second and third OFDM symbols are filled with data and the other where they are left empty as explained in 2.1.2.2.1. It is clearly seen that the sparse scheme and the scheme with a blank data region significantly outperform the scheme where the data region is occupied by approximately 12 dB. The reason for this is obvious: since the PDCCH is distributed over all three OFDM symbols, spreading the PDCCHs of the femto layer over the three available OFDM symbols or forcing them to occupy only the first one and leaving the other two symbols blank results in a reduction of PDCCH interference.

Focusing on the two well-performing schemes, it is seen that at the mid-to-low SINR regime, the non-sparse scheme outperforms the sparse one by approximately 2 dB, since in this case, two out of three OFDM symbols contain no PDCCH collisions. For femto UEs, it is seen that the sparse control region is more beneficial for PDCCH because this reduces the probability of collision from active HeNBs in neighbouring apartments. Figure 2-4 shows CDFs of the effective SINR on the PCFICH. Due to the PCFICH being located strictly in the first OFDM symbol, these results do not differentiate between an occupied and unoccupied data region. Here, the comparison is only between a sparse and a non-sparse control region. In contrast to the previous results, here, it is seen that the sparse control region shows an improved performance for the untrapped macro UEs as well as the femto UEs. This is because the PCFICH strictly occurs in the first OFDM symbol, regardless of the control channel size. A sparse control channel, therefore, obviously results in reduced PCFICH collisions and leads to a performance improvement.

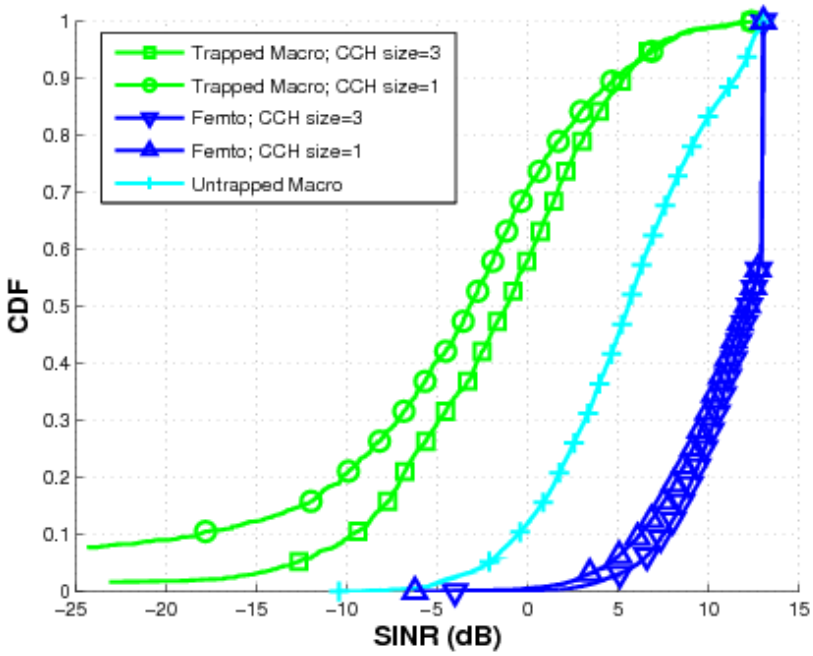

Figure 2-4: Comparison of the sparse and non-sparse control channel schemes for PCFICH. Here, the sparse scheme is consistently better than the non-sparse one.

2.1.2.3.2 Power Control

It is seen from Figure 2-3 and Figure 2-4 that a sparse control region produces satisfactory PDCCH performance. However, even though the sparseness improves PCFICH performance over the benchmark, it is seen in Figure 2-4 that the SINRs are still very low – potentially leading to a loss of the subframe. As a result, this subsection investigates the effects of enhancing control channel sparseness with power control.

Figure 2-5 shows the performance of sparseness supplemented with power control. It is clearly seen that when the control region on the femto layer is one symbol long and the other two symbols are filled with data, power control helps improve the performance by approximately 10 dB. However for the cases when the control region is sparse or when the two symbols are not filled with data, power control only results in a minor performance improvement. In employing power control, the femto layer undergoes approximately 5 dB degradation in performance. Despite this, the SINR performance still remains satisfactory on the femto layer.

Figure 2-6 examines the PCFICH performance. Here, it is clearly seen that power control helps improves the PCFICH performance by approximately 5 dB. The femto layer suffers a corresponding 5 dB degradation in performance. However, the SINRs still remain satisfactory.

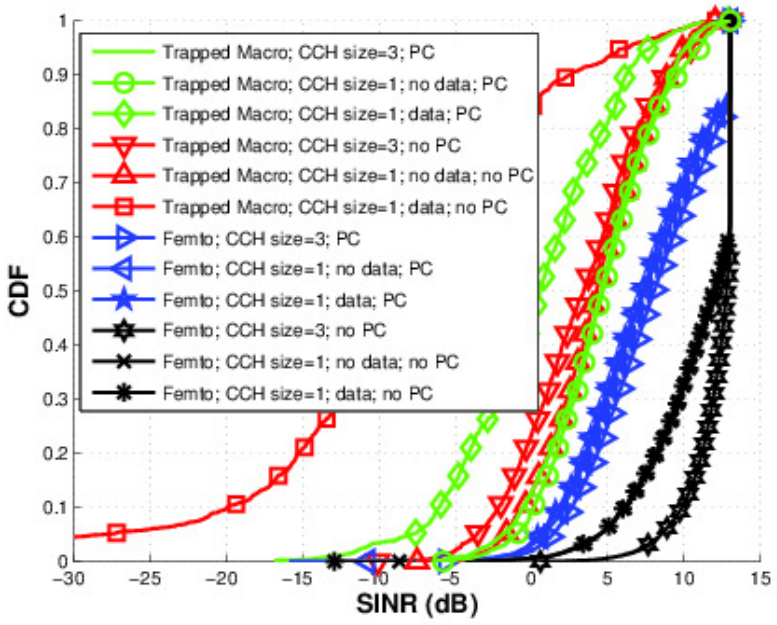

Figure 2-5: Effects of HeNB power control on the PDCCH.

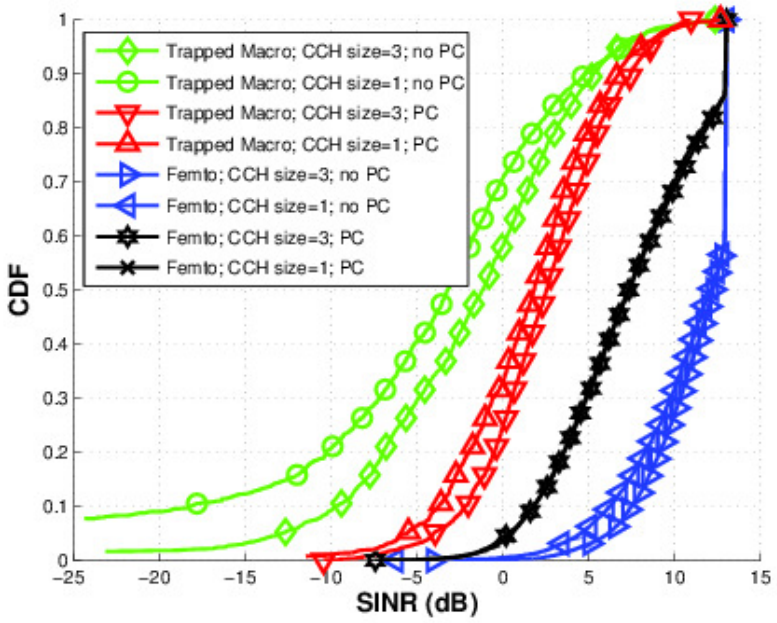

Figure 2-6: Effects of HeNB power control on the PCFICH.

2.1.3 Data Channels Interference Management through Flexible Frequency Reuse

Having covered the problem of Interference on control channel in presence of femtocells, in this sub-section we narrow down our focus on Data Channel Interference Management. As mentioned, in the future, a mass deployment of overlaid networks i.e. remote radio heads (relays) and low-power nodes (e.g. femtocells, picocells) is expected to extend the radio coverage in licensed bands and to provide a large number of bandwidth-hungry multimedia services. However, their heterogeneity will cause higher inter-cell interference if their operation is not coordinated. Thus, investigation of inter-cell interference mitigation techniques is urgently required.

Interference avoidance through ICIC is a promising inter-cell RRM technique which, by applying radio

resource restrictions, provides favourable radio conditions across subsets of users that are severely impacted by the inter-cell interference; and thus attains high spectral efficiency.

2.1.3.1 System model

By the geometric nature of a typical homogeneous cellular system, cell-edge UEs are the most disadvantaged members of the network as in addition to the higher path loss experienced by the attached sector, significant interference is received from close-by cells. Any optimal or suboptimal inter-cell RRM with a throughput maximization objective will avoid scheduling these disadvantaged UEs, since their contribution to the overall throughput is negligible. Therefore, by employing interference avoidance on such UEs, the network can effectively extend their minimum required data rates.

We consider a LTE system based on OFDMA technology with a set of inter-connected eNBs $S = \{1, 2, \ldots, S\}$ with total S eNBs, K UEs and N RBs. It is been assumed that the transmit power on each RB is the same and fixed. For simplicity, if specific RBs termed as 'restricted' are not scheduled at all (P_w=0).

To define a possible set of in-group interfering eNBs we use the power-set expression $P(\ )$. For example, the power-set of $\{x, y\}$ is $\{\}$, $\{x\}$, $\{y\}$, $\{x, y\}$. Following this, we can construct all possible subsets of eNBs that can interfere with eNB i using the following notation $P(S \setminus \{i\})$. Note that the power-set $|P(S \setminus \{i\})|$ contains 2^{S-1} combinations.

It is been also assumed that the served users can measure the separate levels for different sources of interference by employing cell-specific orthogonal reference sequences. With the help of g^i, i.e. an index to represent the subset of the $P(S \setminus \{i\})$, the SINR is conveniently constructed with a list of non-restricted interferences as:

$$\gamma_{k,n}^{i,g^i} = \frac{P_w \cdot H_{k,n}^{i}}{P_w \cdot \sum\limits_{\substack{j \neq i \\ j \notin g^i}} H_{k,n}^{j} + N_w} \tag{2.6}$$

Here, $\gamma_{k,n}^{i,g^i}$ denotes the instantaneous SINR at UE k that is connected to eNB i excluding the g^i interfering eNB group. The $H_{k,n}$ denotes the channel gain which includes all key fading components (path loss, shadowing, multi-path) that UE k experiences on RB n. On the same notation, the super-indexes i and j represent the desired and interfering link, respectively. We define $f(\ )$ as a mapping function where the instantaneous SINR is converted through achievable data rate as:

$$r_{k,n}^{i,g_i} = f\left(\gamma_{k,n}^{i,g_i}\right) \tag{2.7}$$

The general problem of using interference avoidance through ICIC in an interference-limited multi-cell system is formulated below:

$$\text{maximize} \quad \sum_{i}\sum_{g^i}\left(\sum_{k=1}^{K}\sum_{n=1}^{N} U_{k,n}^{i,g^i} \cdot \rho_{k,n}^{i,g^i}\right); \qquad U_{k,n}^{i,g^i} = (r_{k,n}^{i,g^i})^x \cdot (d_k^i)^y; \quad x, y \in \mathrm{N}^+, \tag{2.8}$$

$$\text{subject to} \quad \underbrace{\sum_{g^i}\sum_{k=1}^{K}\overbrace{\rho_{k,n}^{i,g^i}}^{\text{V1}}}_{\text{X1}} + \underbrace{\sum_{j \in g^i}\sum_{g^j}\sum_{k=1}^{K}\overbrace{\rho_{k,n}^{j,g^j}}^{\text{V2}}}_{\text{X2}} \in \{0, 1\}; \ \forall\, n \tag{2.9}$$

The optimization problem here is used with the multi-option utility measure in order to favour a varying degree of emphasis on user throughput and fairness; x and y exponents are defined, respectively. For instance, the x=1 and y=0 option or other non-zero x options, aim to maximize the aggregate sector throughput as the utility shows minimal benefit to the deprived users. Therefore, other non-zero y options of the utility can give more gain to these users.

The variables V1 and V2 in constraint (2.9) are binary variables. Therefore, it is implied by 1 or 0 whether the RB n is assigned for UE k on eNB i excluding the interfering eNB group g^i or not. The term X1 makes certain that each RB cannot be assigned to more than one user and more than one interfering eNB group, which is restricted. In a similar way, the term X2 propagates this inter-relationship among all eNBs within interfering eNB group g_i. The equation X1 + X2 ensures that the allocation to simply one

UE can happen if the RB n is not restricted by g_i.

The complexity cost quoted by the above binary linear solution increases significantly with the number of i, k, n variables and number of subsets in g^i. Solving this global optimization problem on a network-wide scale and accounting for all variables can be a large computational burden.

2.1.3.2 Proposed algorithm

With some loss of optimality, this complex solution can be also decomposed into several sub-solutions at a time with a small set of interfering eNBs and RBs; thus reducing the computational run time significantly. The use of a predetermined dominant interference set with a small set of available RBs was investigated in [26]. However, the limitation of the small set of available RBs can degrade significantly the diversity gain stemming from channel variability. This limitation led us to look into other ways of decomposing down the above problem without losing the optimality nor the performance yielded from the multi-user diversity.

With minimal loss of optimality, this complex solution can be simplified into two sub-problems i.e. the user allocation sub-problem and the inter-cell restriction sub-problem. The former can reside in the local processing unit in each eNB whereas the later should remain in the processing controller of the network. To describe with few words, the sub-problem which can reside in eNB issues a candidate list of best users for possible inter-cell restrictions for each RB (or groups of RBs). Afterwards, the sub-problem which stays in the network controller decides for each eNB which restrictions to be set. This simplification allows fast execution over the RBs, while keeping the optimality of the initial solution. By using effective linear optimization tools [27], the solution can be approximated quickly even for HetNet scenarios where numerous low-power eNBs potentially can exist.

2.1.3.2.1 eNodeBs procedure

The eNB-level procedure is to issue a candidate UE list for each possible inter-cell restriction. Let us then denote with indices '*j1*' and '*j2*' the IDs for first and second interfering eNBs, respectively. This means that the possible interfering in-eNB scenarios are as follows: {} {$j1$} {$j1$, $j2$} {$j2$}. We refer to each possible interfering in-eNB scenario as a mode. Therefore, four possible modes are indicated, i.e. mode 1, mode 2, mode 3 and mode 4. In this work, the latter mode is omitted since it provides insignificant performance improvement for the extra inter-cell signalling and computational complexity involved. For notational convenience, we use a generalized interference group i.e. $G_{k,n}^m$ to indicate these possible three modes in each RB: 1) $G_{k,n}^1 = \{\}$, 2) $G_{k,n}^2 = \{j1\}$, 3) $G_{k,n}^3 = \{j1, j2\}$. In each mode, a utility matrix is prepared at each eNB using the target fairness criteria as follows:

$$U_{k,n}^m = (r_{k,n}^m)^x / (d_k)^y; \qquad x, y \in \mathrm{N}^+ \tag{2.10}$$

Here, we define the user demand d_k as the average throughput of UE k divided with the average throughput across all UEs. The max argument function can solve and determine the best user for each mode:

$$I_n^m = \arg\max_k \{ U_{k,n}^m \} \tag{2.11}$$

It is evident that in scenarios where channel variability may exist across the interference channel, the best user for each mode may not be the same in other modes. Based on the candidate UE list I_n^m, the refined utility A_n^m and interfering group G_n^m can be expressed as:

$$A_n^m = U_{k,n}^m (I_n^m) \tag{2.12}$$

$$G_n^m = G_{k,n}^m (I_n^m) \tag{2.13}$$

2.1.3.2.2 Network level procedure

The central entity collects the refined lists A_n^m, G_n^m from each eNB and constructs the united list $A_n^{i,m}$, $G_n^{i,m}$, respectively. Each decision can be taken independently across all RBs. For each RB, an optimal solution on which mode an eNB should transmit can be given by a network controller. As each decision is independent, this centralized problem can be distributed between up to N different network processing entities. The distributed optimization problem for each processing entity can be modelled as:

$$\text{maximize} \quad \sum_{i}\sum_{m=1}^{3} A^{i,m} \cdot \rho^{i,m}; \tag{2.14}$$

$$\text{subject to} \quad \underbrace{\sum_{m=1}^{3} \overbrace{\rho^{i,m}}^{\text{V1}}}_{\text{X1}} + \underbrace{\sum_{j \in G^{i,m}} \sum_{m=1}^{3} \rho^{j,m}}_{\text{X2}} \quad \begin{matrix} \in \{0, 1\} \\ or \\ \in [0, 1] \end{matrix} \tag{2.15}$$

Based on eNB's candidate list and user's achieved utility, the network controller will decide in which mode an eNB will benefit more to the overall network. The constraint in (2.15) can be solved via either binary linear programming or linear programming relaxation by rounding the solution to the nearest binary value.

Here, the rounded variable V1 in term X1 indicates by one or zero whether it is beneficial for the current RB to be used by eNB *i* on mode *m* or not. As mentioned earlier, only three modes are specified on each RB. The term X1 ensures that each eNB has been assigned to only one mode. However, in the case where no modes are indicated, the eNB *i* will be restricted to benefit the other interfering eNBs. In a similar way, the term X2 propagates this inter-relationship to the first and the second dominant interfering eNBs. To resolve any in-eNB conflicts among the eNB *i* and the two dominant interfering eNBs *j*1 and *j*2 in $G^{i,m}$, the rounded sum of X1+X2 should be either 0 or 1.

The solution given by (2.14) is returned to all eNBs involved. According the solution, each eNB should now assign the best user from the candidate list (or not assign at all). By removing the user allocation process from the ICIC problem, the computational complexity is significantly reduced. The revised problem has a lower complexity bargain increases only with the number of interfering eNBs and the number of indicated modes.

2.1.3.3 Simulation results

The simulation study is performed on the downlink using the available system-level simulator in order to evaluate the performance of the proposed distributed ICIC vs. the state-of-the-art interference avoidance schemes. Since the existing platform is based on classical frequency reuse (reuse-1) and no benchmark schemes are employed, these were implemented under the proportional fairness (PF) scheduler. To distribute the proposed algorithm, several network-processing entities are placed at various locations of the network. Apart from the outdoor eNB network, a closed-access low-power HeNB (Home eNB) network is implemented to simulate a multi-cell indoor scenario. In the case of the indoor scenario, the multi-user diversity is limited as the number of served users is fixed to one. Each HeNB block is accompanied by a network gateway, i.e. Local Femto Gateway (LFGW) that can deal with some processing tasks.

We use the average cell throughput as the system performance and the 5th percentile point of CDF of UE throughput to represent the critical performance. For fair comparison, the total transmitted power in each eNB (or HeNB) is fixed and the same for all the investigated techniques. To avoid excessive interference from HeNB network, a High-Interference Indicator (HII) signalling [7] is used on behalf of outdoor UEs to indoor HeNB to suppress the excessive interference on allocated RBs. Similarly, to observe the trends from employing avoidance schemes in the low-power deployment, we assume that the all indoors UEs served by HeNB experience the same interference from the eNB network in all schemes.

Figure 2-7 shows the CDF of UE throughput for five major different schemes employed by outdoor deployment i.e. reuse-1 (FR1), reuse-3 (FR3), FFR [28], and the proposed ICIC scheme in which one (ICIC-1) or two (ICIC-2) dominant interference(s) can be mitigated. To avoid ambiguity, each of the evaluated schemes is associated with a specific marker and colour.

For simplicity of illustration and for convenience in overall performance, we display the system and critical performance for all the schemes in Figure 2-8. In the same way, Figure 2-9 shows the overall performance in the indoor deployment for all different schemes employed.

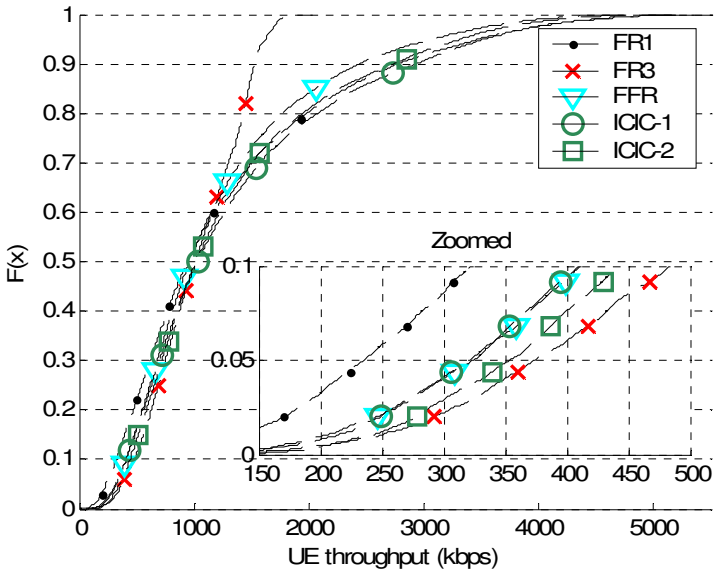

Figure 2-7: CDF of the UE throughput for major schemes in the outdoor deployment

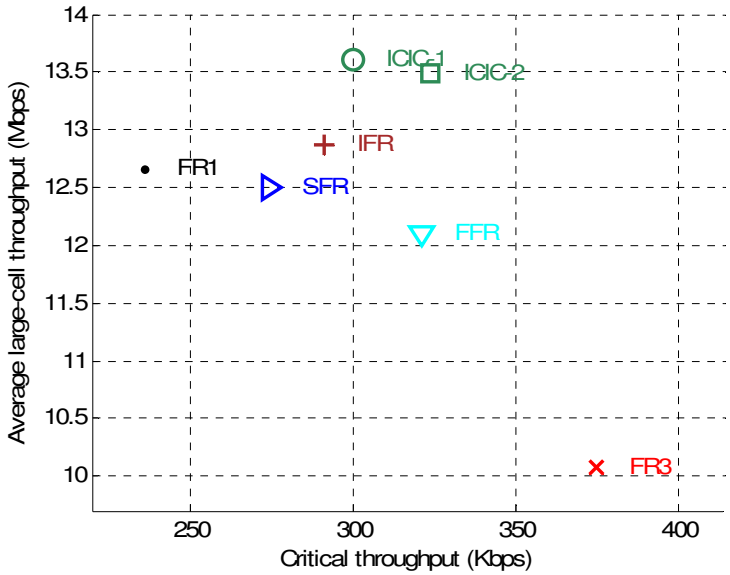

Figure 2-8: Average cell throughput vs. critical throughput for all the different schemes in outdoor

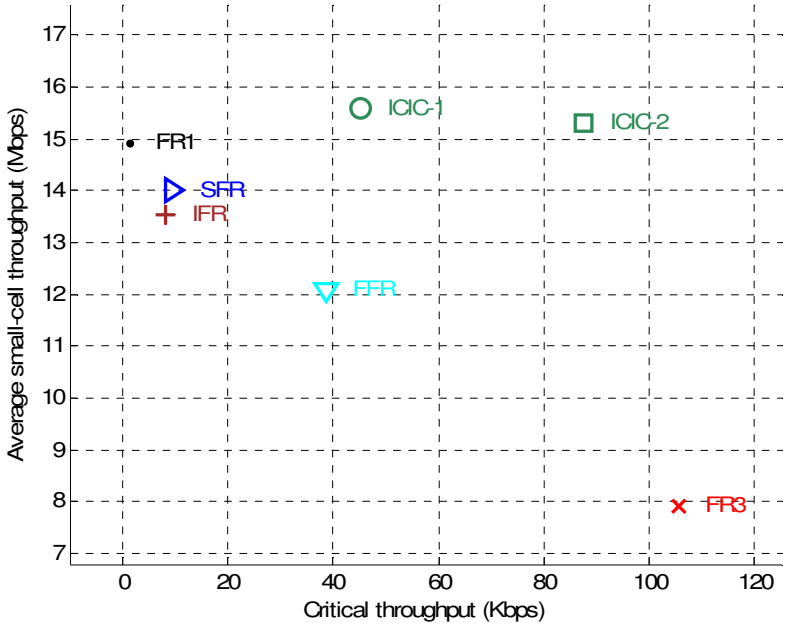

Figure 2-9: Average cell throughput vs. critical throughput for different schemes in indoor

As expected for all multi-cell deployments, the FR1 scheme shows minimum cell-edge performance since no interference is mitigated. On the other hand, the FR3 exhibits superior critical performance by sacrificing a big chunk of its system throughput. A good compromise is the FFR which employs a mixture of reuse-1 and reuse-3. Similar to the FFR, the SFR with power amplification and power restriction technique in different regions shows an analogous performance trade-off [29]. Interestingly, the invert frequency reuse (IFR) [30] achieves a cell-throughput gain compared with FR1, however this trend can be observed only in the eNB deployment. This scheme is more susceptible (compared to SFR and FFR schemes) in unplanned deployments, such as HeNB network, where the operation or the location can vary from house to house. The proposed scheme outperforms all schemes in average cell performance and by mitigating up to two dominant interferences, the ICIC-2 slightly surpasses the eNB FFR in critical performance; however, at the expense of system performance. The same performance trend for the proposed scheme can be observed in Figure 2-9 for indoor scenarios. Here, the ICIC-2 can narrow down the gap to FR3 in critical performance.

2.1.4 Victim User Aware Soft Frequency Reuse in Macro/Femto HetNet

Co-channel deployment of macro/femto HetNets is very attractive from spatial frequency reuse point of view. However, as discussed, assuming CSG femto base station (called HeNB), the co-channel deployment may lead to some highly undesirable interference limited scenarios.

In this section, another dynamic ICIC mechanism is presented to mitigate the interference caused by an aggressor HeNB to its nearby MUE which does not belong to its CSG. This is one of the critical scenarios in the downlink of a co-channel macro/femto deployment [26].

We present here a dynamic algorithm to protect the MUEs which find themselves close to a femtocell. Instead of completely muting the subbands (to be used by a victim MUE) in a femtocell, we suggest to only reduce the transmission power on these subbands. It is shown that the latter yields higher femtocell average throughput while providing a significant protection to a victim MUE nearby. In addition, the choice of these subbands is carried out in a dynamic manner so as to exploit the victim MUE's channel conditions. By doing so we could reduce the number of subbands over which femtocell has to reduce its transmission power. The victim MUE will experience an improvement in Channel Quality Indicator (CQI) of the subbands over which aggressor femtocell has reduced its power. At the macro end, Proportional Fair Scheduling (PFS) per subband will automatically schedule the victim MUE over the subbands over which it has better CQI.

2.1.4.1 Proposed algorithm

In order to describe our dynamic interference mitigation algorithm, we first introduce the relative scenario. We consider a HeNB in the coverage area of a macro base station (MeNB). Both macro and femto transmit on same set of subbands **S**. An MUE u_k^m finds itself close to the HeNB nominated as an aggressor HeNB. This MUE is declared as a victim. Let u_n^f be an HUE served by an HeNB, $\boldsymbol{\delta}_k^{\mathbf{m}}$ be the set of SINR values of all the subbands of **S** reported by an MUE to its serving MeNB, $\mathbf{p}_k^{\mathbf{m}}$ be the set of power received (accounting both the pathloss and shadowing) from neighbouring cell by an MUE, $\mathbf{u}_{victim}$ be the set of MUEs which are victim of HeNBs and $\mathbf{B}_k^{(l)}$ be the matrix in which every row includes subband index of $|\mathbf{l}_k|$ best subbands in terms of SINR for a victim macro user k.

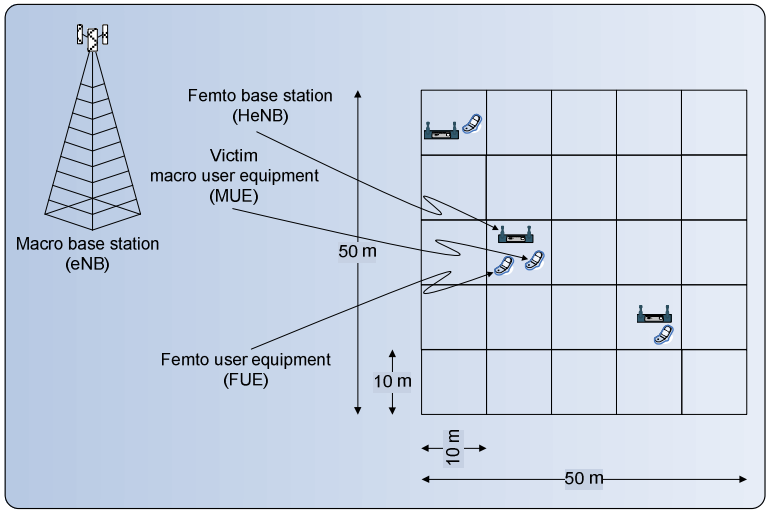

Figure 2-10: Femto to macro interference scenario in the downlink.

The pseudo code for proposed algorithm is given hereafter:

Algorithm

MeNB:

Initialization:

$\mathbf{u}_{victim} = \phi$,

$\mathbf{B}_k^{(l)} = \phi$

Action Phase:

Every macro user u_k^m sends periodically the vector $\mathbf{p}_k^{\mathbf{m}}$ to its serving MeNB. Whenever, MeNB receives the periodic report from a user u_k^m, it performs the following steps:

if the strongest interferer in the vector $\mathbf{p}_k^{\mathbf{m}}$ is a femto base station

$\mathbf{u}_{victim} \leftarrow u_k^m$

find $\mathbf{l}_k$ best subbands in terms of SINR from $\boldsymbol{\delta}_k^{\mathbf{m}}$

if $\mathbf{l}_k \notin \mathbf{B}_k^{(l)}$

$\mathbf{B}_k^{(l)} \leftarrow \mathbf{l}_k$

ask the aggressor HeNB to reduce the power on $\mathbf{l}_k$ these subbands through X2 interface.

else

If $u_k^m \in \mathbf{u}_{victim}$

	ask the aggressor HeNB that it could restore the power on $\mathbf{B}_k^{(l)}$ these subbands through X2 interface. $\mathbf{u}_{victim} = \mathbf{u}_{victim} - u_k^m$ **end if** **end if** **end if**
HeNB:	***Initialization:*** Distribute total cell power equally among all subbands of set **S.** Transmit all the subbands with equal power. ***Action Phase:*** HeNB receives message from MeNB to reduce or restore the power on $\mathbf{l}_k$ subbands. HeNB reduces or increases the power on $\mathbf{l}_k$ subbands and redistributes it across other subbands while keeping the power budget same.

2.1.4.2 System model

2.1.4.2.1 Channel model

The radio channel between an UE u and an (H)eNB b suffers from long-term as well as short-term variations. The long-term propagation loss $l_p^{(b,u)}$ encompasses the path loss and the lognormal shadowing $l_{Sh}^{(b,u)} \sim \tilde{\mathcal{N}}\left(0, \sigma^{(b)}\right)$. These components are computed according to the model 1 of [31]. Since the antenna gain of the UE $g^{(u)}$ and that of (H)eNB $g^{(b)}$ are also fixed entities, we subtract the two from the propagation loss and the resultant long-term variations loss $L^{(b,u)}$ can be written as:

$$10\log_{10}(L^{(b,u)}) = g^{(u)} + g^{(b)} - l_p^{(b,u)} - l_{sh}^{(b,u)} \tag{2.16}$$

where all the terms on the right hand side of the equation above are in decibels. The short-term part represents the fast fading. It is generated by using the MIMO spatial channel model extended (SCME) introduced in [32] which supports bandwidths higher than 5 MHz (since the bandwidth used in our system simulations is 10 MHz). For Doppler effect, a velocity of 3 km/h has been considered. As for power and delay profile, the urban macro (UMa) model has been taken into account. From the temporal representation, the frequency domain response is derived using FFT of size N_{FFT}. The number of useful subcarriers N is bandwidth specific and can be referred from [33].

2.1.4.2.2 Subcarrier SINR

Minimum Mean Square Error (MMSE) receiver is applied on each subcarrier to detect each layer. Since in this studied subject we have only considered Single Input Single Output (SISO) systems, only one layer is considered in the detection process. Ignoring the fast fading gain associated with interfering (H)eNB, post-receiver SINR of subcarrier n for a UE u is calculated.

2.1.4.2.3 Effective SINR

Channel gains experienced by subcarriers are likely to be different over the whole band due to the small coherence bandwidth (inversely proportional to the delay spread) of the multipath channel. Hence, different subcarriers (and subbands) may suffer from different SINR and the error rates on these subcarriers may not be the same. Therefore, block error rate (BLER) of the coded block (transmitted over multiple subcarriers) cannot be obtained through direct averaging of these error rates. In order to obtain a single SINR value of multiple subcarriers that could correspond to this BLER, certain physical abstraction models are used. The resultant single value is called the effective SINR. In our System Level Simulations (SLS), we have used the physical abstraction model Mean Instantaneous Capacity (MIC) [34]. As for CQI, we have chosen "higher layer configured subband" reporting [20], so that the CQI for subband s is computed based on effective SINR. Each subband is comprised of N_{Sc} subcarriers. The set of subbands

for which a UE has to send CQI reports back to (H)eNB is configured by Radio Resource Control (RRC). While considering FFR, RRC only asks for reports on the subbands that are used by a particular (H)eNB. The instant of these reports is also set by RRC. In our simulations, we have considered aperiodic reporting every Transmission Time Interval (TTI).

2.1.4.2.4 System-level simulation assumptions

LTE Parameter	**Value**
Carrier frequency	2 GHz
Bandwidth W	10 MHz
Subcarrier spacing	15 kHz
Number of subcarriers N	600
Number of subbands $\|\mathbf{S}\|$ associated with W	9
Thermal noise density N_0	-174 dBm/Hz
eNB Parameter	**Value**
Inter-site distance	500 m
Number of UEs dropped per eNB	10
Probability of UE to be indoor	0.35
Transmission power	46 dBm
Antenna gain $g^{(b)}$	14 dBi
Antenna pattern	$-\min\left\{12\left(\frac{\theta}{70}\right)^2, 20\right\}$ dB where θ is in degrees.
Shadowing standard deviation	8 dB
Shadowing correlation	0.5 inter-site
	1 intra-site
HeNB Parameter	**Value**
Model	5x5 grid
Number of clusters dropped per macro cell	1
Deployment probability inside a block	0.1
Transmission power	10 dBm
Antenna gain $g^{(b)}$	0 dBi
Shadowing correlation	0
Number of UEs dropped per HeNB	2

Table 2-2: Simulation Parameters

Simulation parameters are summarized in Table 2-2. Monte Carlo approach is used with a significant number of runs where each run lasts several TTIs. The macro cellular network is composed of 7 sites with 3 sectors per site. Each sector is assumed to be covered by one eNB. The geographical positions of eNBs are fixed throughout the simulations and follow classical hexagonal cell deployment. Deployment of femtocells is carried out with the help of 5x5 grid model [31]. On average, one 5x5 grid is randomly dropped per macro cell. A bird view of a 5x5 grid is shown in Figure 2-10. Each 5x5 grid is composed of 25 blocks. Every block inside a cluster is a square shape of 10 m× 10 m. A femtocell is hosted by block inside the grid.

The presence of HeNB inside a block is governed by the probability of femtocell deployment. The position of HeNBs inside a block follows uniform random distribution. HUEs are uniformly dropped inside the block near their serving HeNB and attachment is forced toward it. The drop is performed until all HeNB have a given number (two in our case) of HUEs. MUEs are dropped into a macro cell using uniform random distribution such that a certain number of MUEs are attached to an eNB according to the best link criteria and a given percentage of MUEs finds itself inside the 5x5 grids.

The positions of 5x5 grids, HeNBs, MUEs and HUEs are drawn through uniform distribution at the start of each run and stay the same throughout the TTIs of the run. We assume PFS per subband in both the eNB and the HeNB with 10 MHz of system bandwidth. We compare three scenarios in terms of victim

MUE and HUE throughputs: no mitigating action in aggressor HeNB, full muting of four subbands in aggressor HeNB and reducing power by 75% on four subbands in the aggressor HeNB. We assume X2 interface between macro and the femto for transferring the information related to interference mitigation. The throughput calculation is carried out from the effective SINR for each scheduled UE by using truncated Shannon bound, in adequation with the approach adopted in [83].

2.1.4.3 Simulation Results

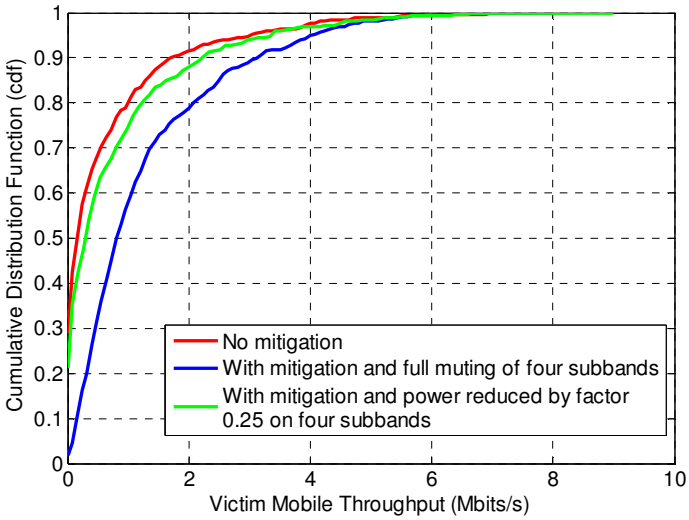

Figure 2-11: CDF of average victim mobile throughput

The Monte-Carlo simulation results for the proposed algorithm are discussed in this section. The CDF of user throughput for the victim MUE is given in Figure 2-11. Significant improvement could be seen in the values of victim MUE throughput for complete muting of four subbands (over which victim MUE has the best radio quality) in the aggressor femtocell. For the case of soft frequency reuse (SFR), instead of muting the four subbands only the power on four target subbands is reduced by a factor of 0.75 by the aggressor cell. We can notice that improvement in victim MUE throughput with SFR as compared to the full muting is lower. However, it is important to look at the impact of the two actions at the femtocell end. That is why in Figure 2-12, CDF of femtocell throughput is given. It can be seen that the performance of SFR in this case is better than complete muting and is quite close to reuse 1. In order to appreciate the comparison, the average values of victim MUE throughput and femtocell throughput are given in Table 2-3. A significant improvement could be seen in the by using SFR in combination with our proposed algorithm.

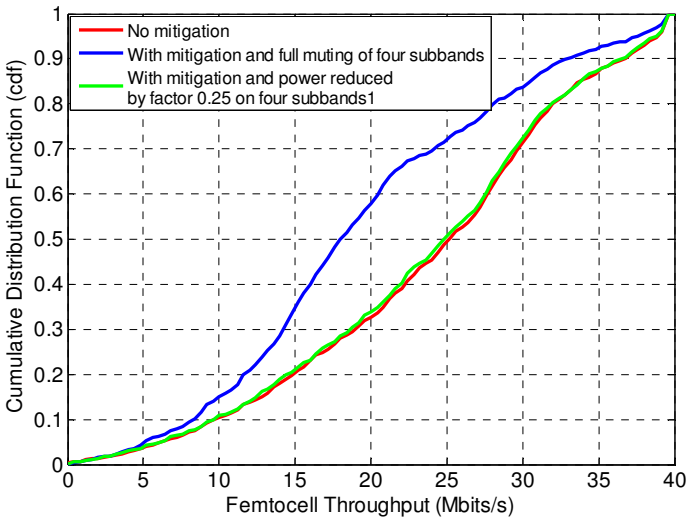

Figure 2-12: CDF of average femtocell throughput

Parameter	No mitigation in aggressor HeNB	Power reduction factor in aggressor HeNB over 4 subbands	
		0	0.5
Femtocell Throughput (Mbps)	23.83	19.48	23.60
Victim MUE Throughput (Mbps)	0.61	1.26	0.76

Table 2-3: Simulation Results

2.1.5 Conclusions

In this section, initially we investigated the impact of femto interference on control channel and efficient algorithms were proposed to address this issue. Thereafter, we narrowed down our focus on data channel. We proposed a low-complexity distributed ICIC scheme for the emerging multi-cell HetNets, which has very low optimality gap. The proposed ICIC scheme was simplified from the global optimum into two smaller problems, the network level problem and eNB-level problem. It has been observed through a simulation study that the proposed scheme can increase both the critical performance and the system performance of the network. Furthermore, we have proposed a complementary dynamic algorithm to mitigate interference for victim macro user equipments which are impacted by an aggressor femto cell in the vicinity. Our algorithm exploits the channel condition of the victim MUE so that the soft frequency reuse in femtocell should only implicate the least number of required subbands. We have shown that the proposed algorithm not only improves the throughput of the victim MUE but also maintains femtocells throughput. Though full muting of subbands in the femtocell performs better in case of victim MUE throughput but degrades the performance of the femtocell in terms of throughput because of lesser resources used in the aggressor cell.

2.2 Multi-Operator Indoor Band Sharing

2.2.1 Problem Statement

Indoor band sharing is one possibility to allow femtocell-macrocell co-existence. As the transmission powers indoors are significantly lower than outdoors, indoor band-sharing is likely to cause less impact to outdoor macrocell operation. However, the unplanned deployment of femtocells can still cause femto to macro interference in dense femto deployments. Given the fact that LTE operators have disjoint frequency allocations, if a femtocell (in an indoor environment) uses the frequencies of another operator (that happens to be relatively further away) instead of using the frequencies of its own operator (due to close proximity), it is going to contribute to solve the femto to macro interference (and vice versa). This is valid in case the macro BSs of different operators are not co-located. This scenario is similar to static flexible frequency reuse scenarios where femto users play as the critical cell-edge users of conventional macro deployment. On the other hand, considering scenarios where the operators' networks are co-located, the proposed solution as above is not efficient as the eNBs of both operators are co-located and HeNB is practically located close to the eNBs of both operators as depicted in Figure 2-13.

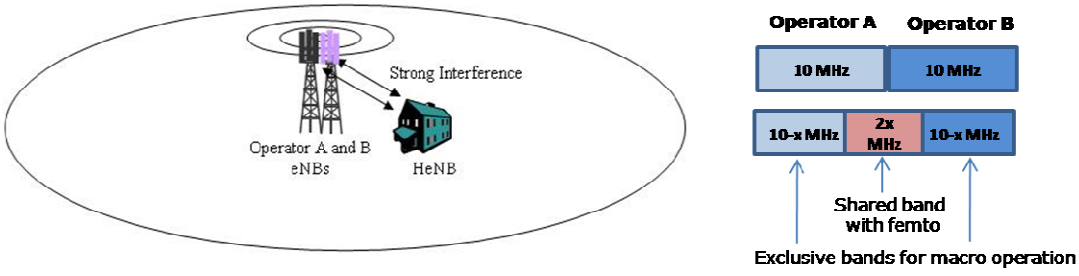

Figure 2-13: HeNB located close to eNB of one operator as compared to other

2.2.2 System model and proposed solution

A possible solution in such scenarios is each operator shares a small portion of its allowed bandwidth for indoor operation where that chunk of spectrum is managed by both operators in a shared manner. Generally, partial sharing may not be favourable solution due to loss of spectral efficiency (on femto side) but in this particular scenario we justify that the loss in spectral efficiency can be greatly recovered by targeting higher modulation and coding schemes for indoor operation considering very robust performance on femtocells. For this scenario, it is worth investigating what should be the principal of band sharing based on the density of the network.

2.2.3 Simulation results

To evaluate the efficiency of proposed scheme a set of simulation studies is carried out on the downlink of an OFDMA-based cellular environment comprising 19 cells. Each cell is assumed to comprise some HeNBs distributed around based on 5x5 grid model. The interference is calculated from the neighbouring cells as well as serving eNB / HeNBs for femto / macro users, respectively. The rest of the simulation parameters are as in Table 2-4.

Topology	19 cells + 5x5 Grid (data from central cell only)	
Inter-Site distance	500 m	
Speed	5 km/h	
Femto deployment and activation ratio	0.1	
Shadowing standard deviation	Macro: 8 dB	Femto: 10 dB
Shadowing correlation distance	Macro: 50 m	Femto: 3m
Traffic	Full Buffer	
Scheduler	RR	
Case	Co-located Operators	

Table 2-4: Simulation parameters

2.2.3.1 Full sharing with indoor femtocells

In this scenario, while the operators utilize separate bands of spectrum for macro transmission, they will share the entire spectrum with their corresponding femtocells. This mode of operation enables high level of local reuse at femto sides over all the bandwidth but at the same time can introduce more interference on the macro level.

Figure 2-14 shows the CDF of user SINR for this scenario assuming deployment of 20 grids per sector, each with activation ratio of 0.1. Here, the CDF of MUE SINR is also depicted for the conventional system (Full Macro partitioning) as well as full macro sharing for benchmarking purposes. As it can be seen, FUEs can enjoy very high SINR values in this scenario (in purple line) reflecting high level of spectral efficiency (considering full sharing of the spectrum). However, this would be at the cost of performance on the macro side in such relatively dense scenarios. Performance-wise, it is clear that such sharing at femto level can impact the performance of MUEs in similar degree as full macro sharing without any femtocells (in green line).

Next, we try to study the effect of femto density (in number of grids per sector) on the overall performance of the system.

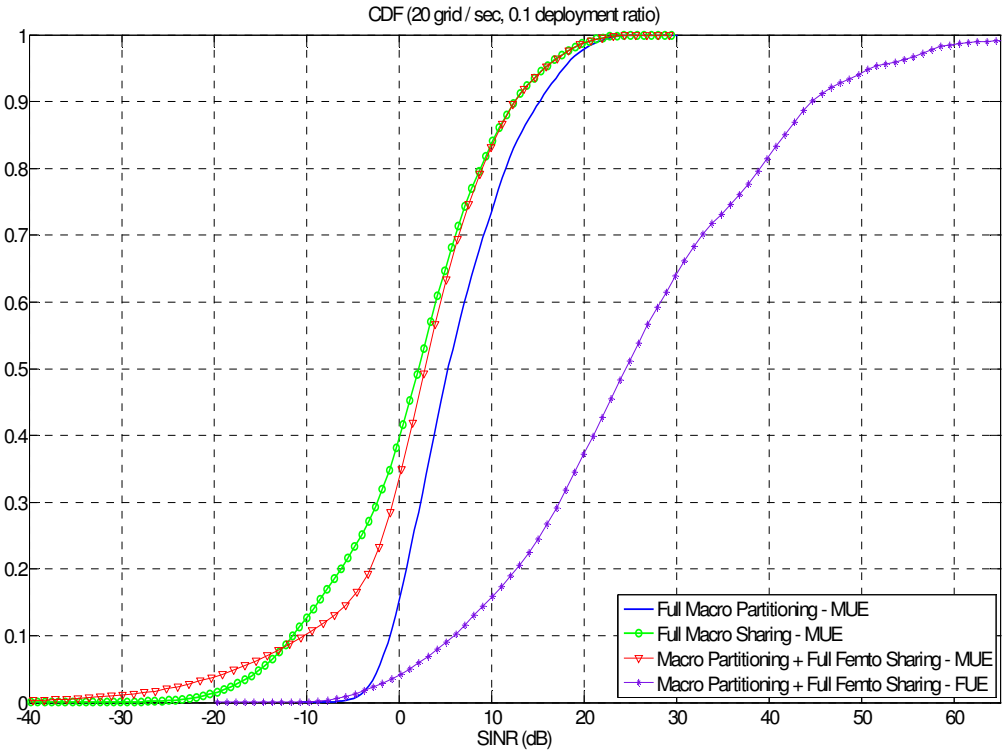

Figure 2-14: Full sharing with indoor femtocells for dense deployment

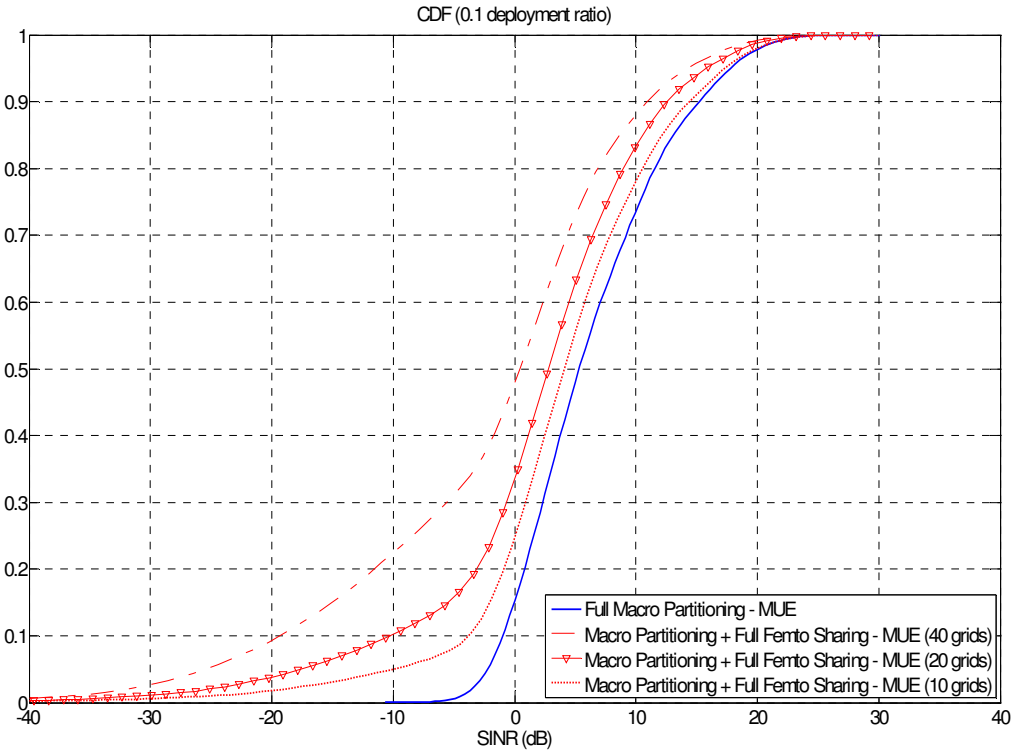

Figure 2-15: The effect of femto density on the performance of system in full sharing scenario

Figure 2-15 shows the performance of MUEs in case of full sharing for different levels of femto density. As it can be seen, increasing the number of grids per sector would more severely impact the performance of MUEs compared to the first simulation case. On the other hand, medium to low deployment of femto grids (10 grids / sect) can significantly improve the performance of MUEs where close performance to benchmark (in blue) can be achieved.

2.2.3.2 Partial sharing with indoor femtocells

In this scenario, the operators will share partially the spectrum with their femtocells. In other words, each operator would enjoy its own exclusive band of operation isolated from inter-operator or femto interference whereas they share a specific chunk of spectrum with their femtocells. This mode of operation reduces the level of local reuse per femtocell however it can better protect the macro operation in particular for dense deployment. To recover the loss resulting from bandwidth limitation for femtocells, it is possible to exploit higher modulation and coding schemes for femto operation compared to conventional macro systems. This is a feasible solution considering the very high performance of femto users (in terms of FUE SINR) as mentioned above resulting from the low level of pathloss on serving links between FUEs and HeNBs in addition to better natural isolation from the walls. It is a also worth noting that individual HeNB typically supports limited number of users compared to Macro stations and as a result requires less bandwidth to provide sufficient service per serving user.

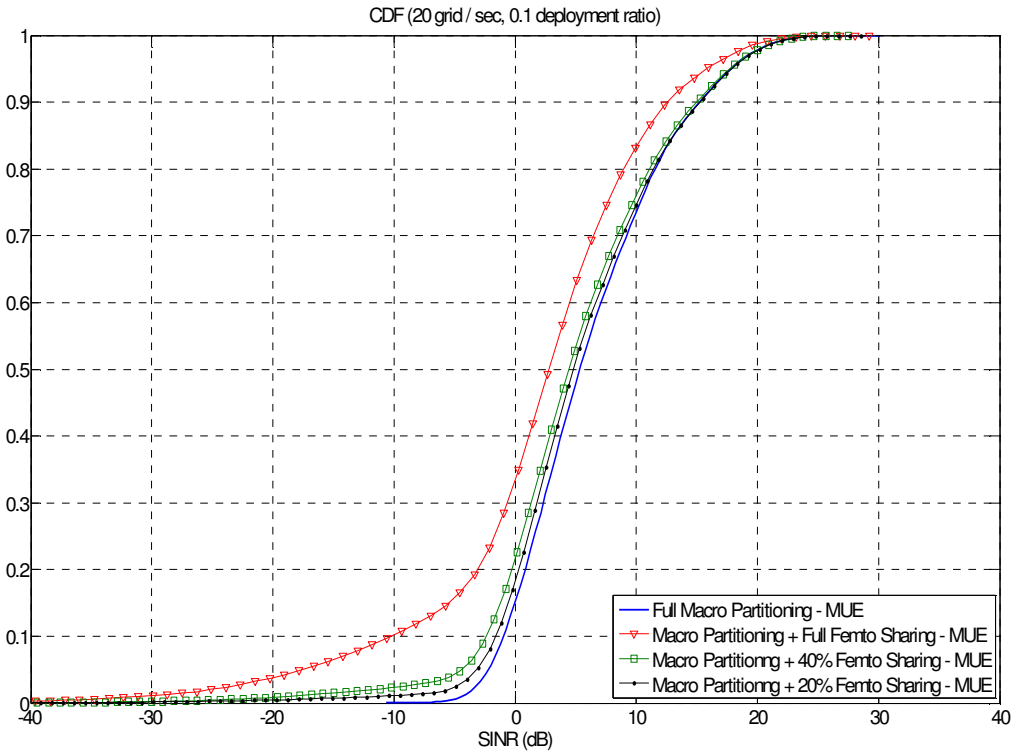

Figure 2-16: The effect of partial sharing on the performance of system

Figure 2-16 shows the performance of system in dense deployment of femto cells (20 grids /sec) for different levels of sharing. As it can be seen, by reducing the available bandwidth for indoor sharing, the performance of MUEs can be greatly recovered in even dense deployment scenarios. This provides a tunable measure to adapt the performance and operational point of the system based on the density and topology of network as well as the target level of service for MUEs (according to the preferences of operators).

2.2.4 Conclusions

In this section, we have investigated the impact of multioperator band sharing within indoor femtocells considering different contributing parameters as well as the impact of level of sharing. As shown, this study clearly shows the necessity of an adaptive algorithm where the level of sharing with femtocells

should be controlled based on the density of femto deployment (and the activation ratio) per sector. Such information can be accessed via the backhaul interfaces between femto cells and corresponding "umbrella" macro sites at the configuration phase of individual femto cells, i.e. where the femto cells are turned on and get activated for the operation. Regarding the time scale of operation, this algorithm can run as a complementary scheme on much longer time span compared to dynamic RRM algorithms to ensure stability and to average out the transitional changes in the topology and density of network.

2.3 Coordinated TDD Underlay in Self-Organizing Femtocells

2.3.1 Problem Statement

The focus is on uplink TDD-underlaid femtocell deployment coexisting with the legacy macrocell. A distributed self-organizing mechanism based on the concept of busy tones is proposed, which relies on *minimal* signalling among tiers, so as to coordinate the underlaid femtocell tier and reduce co-channel interference. A statistical modelling framework based on stochastic geometry is used to capture network dynamics and channel variations. In particular, the impact of fading correlation is used to obtain closed-form expression of network-wide utility metrics. We also use higher-order statistics through the concept of cumulants to recover the distribution of co-channel interference and evaluate the overall system performance in terms of femtocell outage probability and average channel capacity.

2.3.2 System model

Radio links are degraded by path-loss and shadowed fading, which is assumed to be independent over distinct network entities and positions. A signal strength decay function $l(r) = r^{-\alpha}$, where α is the path loss exponent, describes the path loss attenuation, while the received squared envelop due to multi-path channel fading and shadowing is represented by X with CDF and Probability Distribution Function (PDF) denoted $F_X(x)$ and $f_X(x)$. A given interferer disrupts the communication of the tagged receiver with an interfering component given by:

$$p_r = pl(r)x \tag{2.17}$$

where p represents the interferer's transmit power, r is the separation distance from that interferer to the tagged receiver, and x corresponds to the channel shadowed fading. In this study we make use of the composite distribution of the received signal due to the LN-shadowing and Nakagami-m fading [35]. In addition, the underlaid tier is composed of femtocells uniformly scattered over the deployment area, while a single reference Macro Base Station (MBS) represents the overlaid tier. Active femtocells constitute a homogeneous Poisson Point Process (PPP) with density λ. Thus, the number of active femtocells in an arbitrary region R of area A is a Poisson random variable with parameter λA. The fading effect is incorporated into the model as a random mark associated with each point of Φ. By virtue of the Marking theorem, the resulting process corresponds to a Marked Point Process (MPP) with intensity $\lambda.f_X(x)$. In addition, an MPP Φ, whose points belong to the stationary point process Φ, is defined as $\Phi = \{[\varphi, x]; \varphi \in \Phi\}$. In the TDD underlay at UL FDD, femtocell transmissions are time multiplexed in the UL of the macrocell tier which operates in FDD mode. In addition, we make the assumption that the Macrocell User (MU) does not interfere with the tagged receiver but opportunistic strategies which allow femtocells to dynamically coordinate their transmissions so as to reduce the CCI are still needed. In the following, we introduce such a strategy which is based on regular busy tones enabling nearby femtocells to coordinate their simultaneous transmissions in a totally decentralized manner, thereby leveraging on the DL/UL channel reciprocity.

2.3.3 Coordination Mechanisms

The self-organizing coordination mechanism carried out by femtocells is triggered when the tagged femtocell receiver (FUE) experiences an aggregate CCI above a predefined triggering threshold. There are two distinct decision criteria which self-organizing femtocells employ in a totally distributed manner. On one hand, potential interferers coordinate based solely on the received signal strength from the tagged receiver (and we refer to it as **CM1**). On the other hand, **CM2** refers to the case where potential interferers use the received beacon to estimate their channel gain to the tagged receiver, and then use their

intending transmit power to compute the interference they cause on that receiver (similar to the busy burst concept). In the latter, interferers do not coordinate only by detecting the victim receiver, but use the received beacon to estimate if their interference component is above a coordination threshold. In addition, we consider a probability of being active in a given spectrum chunk by ν.

Formally speaking, in CM1, the event that surrounding interferers detect the victim receiver's beacon signal p_b above the predefined coordination threshold ρ_{th} is denoted by [36]

$$\Xi_1 = \left\{ p_b R^{-\alpha} X \geq \rho_{th} \right\} \tag{2.18}$$

Without loss of generality, we introduce the following indicator function:

$$1_{\Xi_1}(p_b R^{-\alpha} x) = \begin{cases} 1 & p_b R^{-\alpha} x \in \Xi_1 \\ 0 & otherwise \end{cases} \tag{2.19}$$

which defines the first coordination region denoted by R_1 and is composed of FBSs that detect under the assumptions of Ξ_1 the victim receiver in their vicinity. In accordance with the formulation $\Phi_1 = \left\{ [\varphi, x]; p_b R^{-\alpha} x \geq \rho_{th} \right\}$. Similarly, femtocells in R_2, which do not detect the victim MU, form a complimentary process denoted by $\Phi_2 = \left\{ [\varphi, x]; p_b R^{-\alpha} x < \rho_{th} \right\}$. Notice that the coordination regions R_1 and R_2 are disjoint and statistically independent. Our focus is to characterize the aggregate interference perceived by the tagged receiver within an observation region using tools from Stochastic Geometry.

In the uncoordinated deployment, FUEs are time-multiplexed in the UL of the macrocell tier. Without loss of generality, we assume that the tagged receiver operates in the first of the two spectrum chunks which composes the UL frame structure. Hence, the aggregate interference is caused by transmitters (FUEs) which operate in the first time slot and belong to the point process with intensity $\nu\lambda f_X(x)$. By observing that transmitters independently access either slot with *equal* probability, and that all interfering nodes communicate with the fixed transmit power p, we derive the cumulants for the uncoordinated TDD-underlay case as follows:

$$\kappa_n(\tilde{\Phi}) = \frac{2\nu\pi\lambda p^n}{n\alpha - 2}\left(R_m^{2-\alpha n} - R_M^{2-\alpha n}\right) E_X[0, \infty, n] \tag{2.20}$$

On the other hand, in the coordinated case, two cases are of interest. In the first case, femtocells self-organize upon detecting the beacon, however no reciprocity is accounted for. In this case, the nth cumulant is given as:

$$\kappa_n(\tilde{\Phi}_2) = \frac{2\nu\pi\lambda p^n E_X[0, \infty, n]}{n\alpha - 2} \left\{ \begin{array}{l} \left(R_m^{2-\alpha n} - R_M^{2-\alpha n}\right) F_Y\left(R_m^{\alpha}\xi_{th}\right) + \zeta_m^{n-\frac{2}{\alpha}} E_Y\left[R_m^{\alpha}\xi_{th}, R_M^{\alpha}\xi_{th}, \frac{2}{\alpha} - n\right] - R_M^{2-\alpha n} \\ F_Y\left(R_M^{\alpha}\xi_{th}\right) - F_Y\left(R_m^{\alpha}\xi_{th}\right) \end{array} \right\} \tag{2.21}$$

where: $\xi_{th} = \dfrac{\rho_{th}}{p_b}$ is the normalized coordination threshold

In the second case, femtocells self-organize through a coordination procedure which is decentralized in nature where both data and signalling channels are fully correlated (due to channel reciprocity). Therefore, the remaining set of interferers is composed of non-detecting femtocells. Likewise, we derive the cumulants for the coordinated TDD-underlay case as follows:

$$\kappa_n(\tilde{\Phi}_2) = \frac{2\nu\pi\lambda p^n}{n\alpha - 2}\left\{\left(R_m^{2-\alpha n} - R_M^{2-\alpha n}\right) E_X\left[-\infty, \tilde{\zeta_m}, n\right] + \zeta_m^{n-\frac{2}{\alpha}} E_X\left[\tilde{\zeta_m}, \tilde{\zeta_M}, \frac{2}{\alpha}\right] - R_M^{2-\alpha n} E_X\left[\tilde{\zeta_m}, \tilde{\zeta_M}, n\right]\right\}$$

Furthermore, after detecting the tagged receiver, intending FUEs rely on the channel reciprocity and use the received beacon strength to estimate their channel attenuation to that victim receiver. Notably, transmitters adapt their link to meet the minimum requirement of their desired receivers while still being able to transmit together with the tagged link. The standard Power Control (PC) algorithm is used by FUs to adjust their power so as to compensate for the desired receiver channel attenuations. We assume that femtocells schedule a random user in every transmission interval, FUs are uniformly distributed within the transmission range of serving cells, and the transmit power is set as a function of the distance between transmitter and receiver pairs, but independently of the interference at that receiver.

Under the assumptions given above, the distribution of the femtocells transmit power is,

$$f_P(p) = \frac{1}{\alpha \beta^{\frac{1}{\alpha}}} p^{-1+\frac{1}{\alpha}} f_R\left[(p/\beta)^{\frac{1}{\alpha}} \right] \tag{2.22}$$

where $d_M = (p/\beta)^{\frac{1}{\alpha}}$ is the radio range of FBSs, such that the received power at the desired user is β, p_m and p_M are the minimum and maximum FUs transmit powers, respectively, and $d_m = 1$ is the minimum distance between an FU and its serving FBS. Finally, the nth cumulants is given as:

$$\kappa_n(\tilde{\Phi}_2) = \frac{2\nu\pi\lambda p^n}{n\alpha - 2}\{\eta_1 + \eta_2 + \eta_3\} \tag{2.23}$$

2.3.4 Simulation results

Let us consider an example where the observation region is determined with Rm = 1m and RM = 100m. The density of interferers is λ = 0.05 FBS/m^2. When operating in the TDD-underlay mode, femtocells choose either slot with equal probability ν = 50%. The radio channel is affected by path loss with exponent α = 3, LN shadowing with σ_{dB} = 6dB, and Nakagami fading with shape factor either m = 2 or 16. In the femtocell tier, transmitters use a fixed power level of $p = 20$ dBm. When using PC with full compensation, femtocells control their transmit power to fully compensate for the average value of the desired receivers' large-scale fading. Figure 2-17 compares the complementary cumulative distribution function (CCDF) of the aggregate CCI from Monte Carlo simulations with those from the LN. As can be seen, the LN approximation matches quite well with the simulation results, though the proposed approximations work slightly better with lower fading variance (m = 16). In the coordinated scenarios, a coordination threshold of ρ_{th} =−40dBm and a MU requesting power of p_b = 0dBm are used. Comparing the aggregate CCI of uncoordinated scenarios with that of coordinated ones, we observe that the two-tier networks under study benefit mostly from avoiding dominant interferers through the self-organizing mechanisms. Indeed, the coordinated cases provide gains due to the formation of dynamic exclusion regions around the tagged receiver. We also evaluate how the coordination mechanisms perform in the two-tier coexistence scenarios by means of the location dependent average channel capacity of the tagged receiver. By using the analytical framework previously established, and assuming all users are allocated on the same bandwidth, W, we initially recover the SIR distribution of the tagged receiver, and then compute the corresponding capacity. Under the assumption of the shadowed fading channel regime, the average channel capacity of the tagged receiver is given as:

$$C \cong W \sum_{k=1}^{K} \frac{w_k}{\sqrt{\pi}} \log 2\left(1 + \exp\left(\frac{\eta_k \sqrt{2\sigma} + \mu}{\theta}\right)\right) \tag{2.24}$$

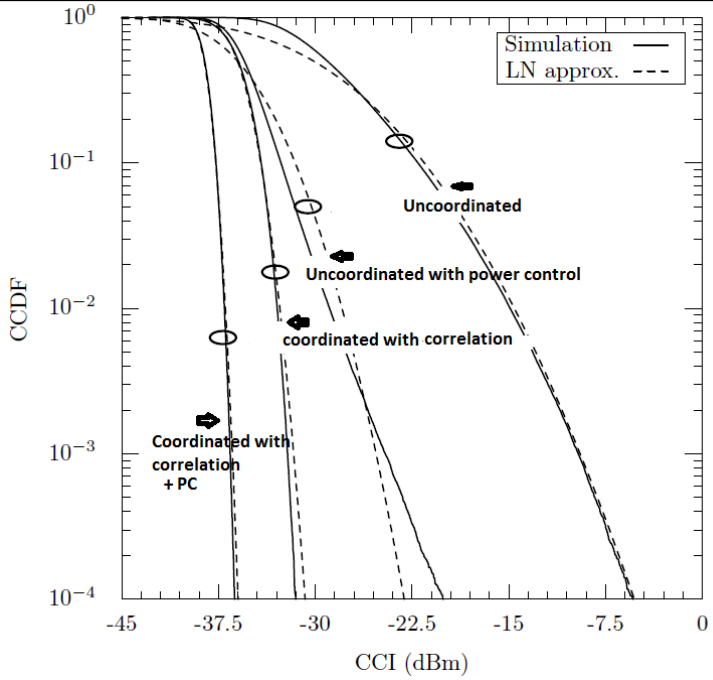

Figure 2-17: CCDF of the aggregate CCI for the uncoordinated coordinated with correlation and power control, respectively.

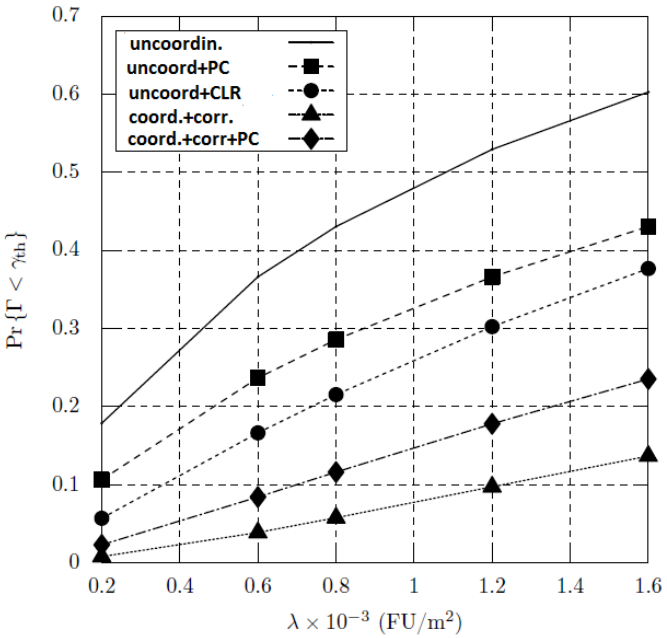

Figure 2-18: Outage Probability at the Tagged Receiver for the uncoordinated and coordinated scenarios, as a function of the femtocell density.

In Figure 2-18, we show the outage probability for increasing density of FUEs. The uncoordinated scenarios present the poorest performance, while in the time-multiplexing scenario the tagged receiver experiences slightly better performance since the CCI is reduced by a factor that is proportional to the number of timeslots available in a UL frame. By avoiding the dominant interferers through the coordination procedure, the tagged receiver performance definitely improves, whereas the extent of the coordination gains depends on the correlation between beacon and data channels. When nodes coordinate, the time-multiplexed scenarios outperform the typical FDD transmission mode. However, by comparing the coordination criteria in the TDD-underlay case, we observe an interesting trade-off between individual link quality and overall spectrum efficiency as in Figure 2-19. In fact when nodes coordinate,

the tagged receiver experiences better link quality since less interferers are active. However, the overall utilization of radio resources is increased since more simultaneous transmissions are allowed at the expense of slightly worse outage figures for the tagged link.

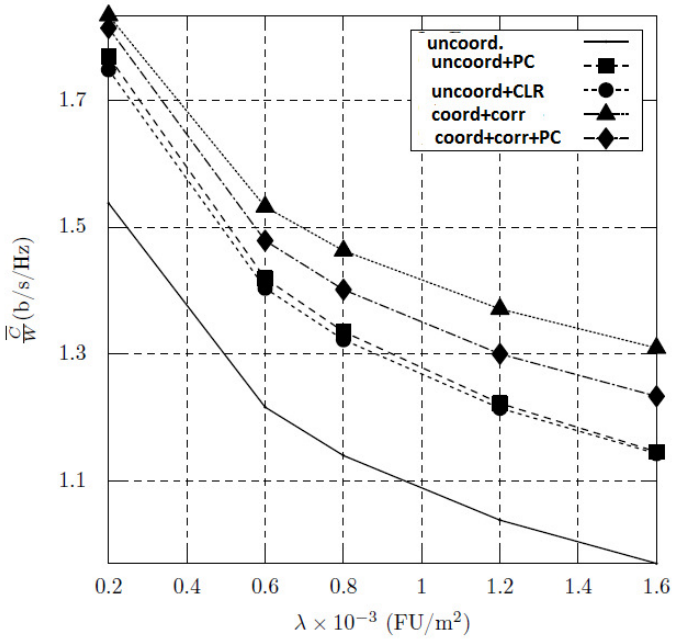

Figure 2-19: Average Spectral Efficiency at the Tagged Receiver for the uncoordinated and coordinated scenarios, as a function of the femtocell density

2.3.5 Conclusions

In this section, we address the CCI problem in two-tier coexistence scenarios. As opposed to the typical spectrum partitioning approaches, the TDD concept is assessed as an alternative to underlay short-range femtocell communications on the Uplink of legacy macrocell deployments. Herein, we consider distributed mechanisms based on the regular busy tones and that rely on minimal signalling exchange to coordinate the underlaid femtocell tier so as to further reduce the co-channel interference. An analytical framework based on stochastic geometry and higher-order statistics through the cumulants concept which captures network dynamics and channel variations is introduced. We use this framework to recover the distribution of the co channel interference and to evaluate the system performance in terms of the outage probability and average spectral efficiency of the tagged link. Our analytical model matches well with numerical results obtained using Monte Carlo simulations. When compared to the uncoordinated deployment, the outage probability of the evaluation scenarios with the coordinated TDD-underlay solution is reduced by nearly 80%, while the average spectral efficiency increases by approximately 90% at high loads.

3. RRM for Indoor standalone femtocells

This section deals with scheduling and RRM algorithms which particularly profit from prior PHY and interference mitigation mechanisms to identify how best to transmit. In the first subsection, the challenges of resource allocation in standalone femtocells are detailed and subsequently some novel decentralized protocols are proposed. The second subsection focuses on RRM and power control scheme combined with successive interference cancellation. Successive interference cancellation is used to allow a macrocell user and a femtocell user to share a common channel on UL to a femtocell access point. Next, the third subsection investigates the issues on layer 2 handover mechanisms in presence of femtocells and some promising algorithms are proposed. Finally, the benefit of Multiple Input Multiple Output (MIMO) transmission and high order modulation for femtocells is presented with detailed simulation studies.

3.1 Decentralised Protocols for Resource Allocation

3.1.1 Problem Statement

Classically, researchers tried to develop bandwidth efficient schedulers to enable heterogeneous systems to coexist within the same bandwidth, thus limiting co-tier and cross-tier interference. However, the femtocell deployment requires a new paradigm because of two main reasons. First, femtocell users FUE can benefit from a high quality DL signal enabled by short range communications, characterizing femtocell deployments. Second, only few users locally compete for a large amount of frequency resource in a given femtocell. Therefore, a femtocell benefits from a huge amount of spectral/power resource. Hence, there is a need for designing a novel approach for reducing interference, improving the spectrum usage and communication robustness in face of undesired interference, and for limiting power consumption. The resource allocation problem in the context of femtocells is interconnected with interference coordination similar to other interference-limited systems. As a result, essentially a resource allocation policy should be integrated with a proper interference-aware policy in a way that would cause minimal interference to the primary users. In the following sub-sections, novel RRM protocols are proposed for radio resource allocation in the context of femtocells to address aforementioned challenges in standalone femtocells.

3.1.2 A RRM Scheduling Algorithm for Self-Organizing Femtocells

In this section, we focus on achieving effective spectral reuse between macrocells and femtocells, while guaranteeing the QoS of users served by both macro and femto BSs We propose a novel resource management scheme that limits the overall interference per RB generated outside the coverage range of a femtocell while reducing the transmission power in each RB. This method does not involve any message exchange neither amongst neighbouring HeNBs nor amongst eNBs and HeNBs.

3.1.2.1 System model

We concentrate on femto-to-femto and femto-to-macro interference in LTE DL scenarios [37]. We consider a mobile wireless cellular network in which mobile terminals and base stations implement an OFDMA air interface based on 3GPP/LTE DL specifications. Each user is allocated one or several RBs in two consecutive slots, i.e., the Time Transmission Interval (TTI) is equal to two slots. We assume that femtocells are deployed according to the 3GPP grid urban deployment model [38]. This model represents a single floor building with 10 m x 10 m apartments placed next to each other in a 5 x 5 grid. The block of apartments belongs to the same region of a macrocell. Each HeNB can simultaneously serve up to 4 users. To consider a realistic case in which some apartments do not have femtocells, we use, a system parameter ρ_d called a deployment ratio that indicates the percentage of apartments with a femtocell. Furthermore, the 3GPP model includes ρ_a, another parameter called an activation ratio defined as the percentage of active femtocells. If a femtocell is active, it will transmit with a certain power over data channels. Otherwise, it will transmit over the control channel.

3.1.2.2 Proposed algorithm

In our vision, femtocells should be "invisible" in terms of interference generated to neighbour cellular users. Nevertheless, femtocells deployment presents a very challenging issue: while HeNBs power consumption and interference range should be small, the coverage range at which UEs can meet their QoS constraints should be large. Based on this observation, we propose a novel RRM algorithm designed to

strongly lower HeNBs DL transmission power. In our proposal, we take advantage of the unusual communication context of femtocells for which locally few UEs compete for a large amount of resources. We come out with a 7 steps RRM algorithm, the Ghost Femtocells (RRM_{ghost}) that reduces transmission energy by using available frequency resources. The detailed description of the proposed algorithm is as follows:

Step 1: [Feedback to HeNB] Each FUE feedbacks to the HeNB its QoS constraints and the, instantaneous Channel State Indicator (CSI) measurements.

Step 2: [Computing Scheduling Matrices] According to the CSI measurements and the selected scheduler algorithm, each HeNB computes scheduling metrics λ_i^j for every attached user *i* on every RB *j*. We assume that RRM_{ghost} implements a Proportional Fair based scheduler, that is

$$\lambda_i^j = \frac{SINR_i^j}{\sum_{k=1}^{K} SINR_i^k} \tag{3.1}$$

where $SINR_i^j$ represents the instantaneous channel condition of the RB *j* observed at user *i* and $\sum_{k}^{K} SINR_i^k$ is the sum of SINRs of *K* RBs that have been already allocated to user *i*. RRM_{ghost} uses the values of this metric as the entries of the scheduling matrices M^{Tx} and M^{Rep} of dimensions $\sum_{k}^{N_f} N_k \times N_{RB}$ where N_f is the number of active HeNBs in the network, N_k is the number of users served by the femtocell k , and N_{RB} is the number of available RBs. In a first phase, based on M^{Tx} , the scheduler allocates to each user the minimum number of RBs that meets QoS and power constraints. Then, in a second phase, the proposed scheduler sorts matrix M^{Rep} to allocate to the served users additional available RBs. These two phases are described below in Steps 3 and 5.

Step 3: [Scheduling] For each user to serve, the HeNB selects the minimum number of RBs that meets QoS and power constraints. It schedules in three iterative steps:

Step 3-a: The HeNB selects the best user-available RB pair *(i,j)* with the best metric in M^{Tx}

Step 3-b: The overall available power at user *i* served by the HeNB *k* is $\hat{P} = P^T / N_k$, where P^T and N_k are the power budget and the number of users of the HeNB *k*, respectively. The HeNB equally splits $\hat{P}$ among the RBs allotted to user *i*, viz. the set $\{RB_i\}$. Then, according to $\{RB_i\}$ and $\hat{P}$ the algorithm selects the highest possible Modulation and Coding Scheme ($M\hat{C}S_i$).

Step 3-c: Then, the HeNB estimates the sum of the Mutual Information *I* given by set $\{RB_i\}$ and $M\hat{C}S_i$.

• When *I* = 0, the selected user-RB pair cannot be served in this scheduling period so the values of the *i-rows* in both M^{Tx} and M^{Rep} are set to zero.

• When $I \geq R_{tg}$, user *i* is served. The values of the *i-th* row in M^{Tx} and M^{Rep} (i, j) are set to zero and the values of the *i-th* row in M^{Rep} are updated according to the scheduler rule (cf. Eq. (3.1)).

• If $I < R_{tg}$, the user *i* is not served yet. The values M^{Tx} (i, j) and M^{Rep} (i, j) are set to zero and the values of the *i-th* rows in M^{Tx} and M^{Rep} are updated according to the scheduler rule (cf. Eq. (3.1)).

Step 4: [MCS Scaling] Given the set of RBs $\{RB_i\}$ allocated to each served user *i*, the algorithm finds the MCS^* of the minimum order that meets the QoS target. If MCS^* is different from $M\hat{C}S_i$, the MCS of user *i*, MCS_i , is set equal to MCS^* . The goal of this process is twofold. First, it improves the transmission robustness. Second, it reduces the padding thus improving the spectral efficiency.

Step 5: [Spreading] The HeNB allocates unused RBs to spread the original message and improve the transmission robustness. Scheduling is done in three iterative steps:

Step 5-a: The scheduler selects the user-available RB pair *(i,j)* that has the best metric in M^{Rep} .

Step 5-b: For each user-available RB pair *(i,j)*, the algorithm checks the Mutual Information *I* given by the entire set of RBs allocated to user *i* and MCS_i :

• If $I < R_{tg}$, additional RB would cause outage, hence the values of the row corresponding to user *I* in M^{Rep} are set to zero.

• When $I \geq R_{tg}$, the original message is spread in the additional RB and M^{Rep} (i, j) is set to zero. Moreover the values of the *i-th* row in M^{Rep} are updated according to the scheduler rule.

Step 5-c: The scheduler process terminates when no more user-RB pairs are available.

Step 6: [Power Scaling] The algorithm estimates the SINR perceived at each served user and reduces the allocated transmission power to meet the SINR threshold given by the target packet error rate (PER) and the selected *MCS* .

Step 7: [Message Reception] Finally, each user collects the information received in each of its allotted RBs and combines these RBs using the Chase combining scheme [39]

3.1.2.3 Simulation results

In this section, we assess the effectiveness of the proposed scheme by comparing its performance with a reference algorithm ($RRM_{classic}$). $RRM_{classic}$ aims at maximizing the spectral efficiency of femtocells while minimizing the probability that users that belong to different cells access to same RBs. Thus, $RRM_{classic}$ attempts to limit the number of RBs allotted to each FUE. Moreover, $RRM_{classic}$ algorithm does not implement MCS and Power scaling (Steps 4 and 6 in RRM_{ghost} algorithm). RRM algorithms are compared in terms of the following energy cost function measured at both the macro and the femto tiers

$$\Gamma_i = \frac{\sum_{j}^{UE_i} N_{i,j} \times P_{i,j}}{\sum_{j}^{UE_i} T_{i,j}} \qquad (3.2)$$

where at TTI i, UE_i, $N_{i,j}$, $P_{i,j}$, and $T_{i,j}$, are the number of active UEs in the (macro/femto) tier, the number of RBs allotted to the user j, the DL power associated to each of these RB, and the perceived throughput at the user j, respectively.

We present simulation results for the system model and its parameters presented in Section 3.1.5.2. The results are averaged over 10^2 runs, each one made of 10^3 TTIs. At the beginning of each run, we independently generate the channel Rayleigh fading coefficients and randomly place HeNBs and FUEs on the deployment grid. In each run, 2 blocks of apartments are randomly dropped in the macrocell area. Moreover, indoor MUEs are randomly distributed in the apartments where HeNBs are not deployed. Note that in the presented simulations, we consider that all deployed HeNBs are active ($\rho_a = 1$) with four FUEs per HeNB.

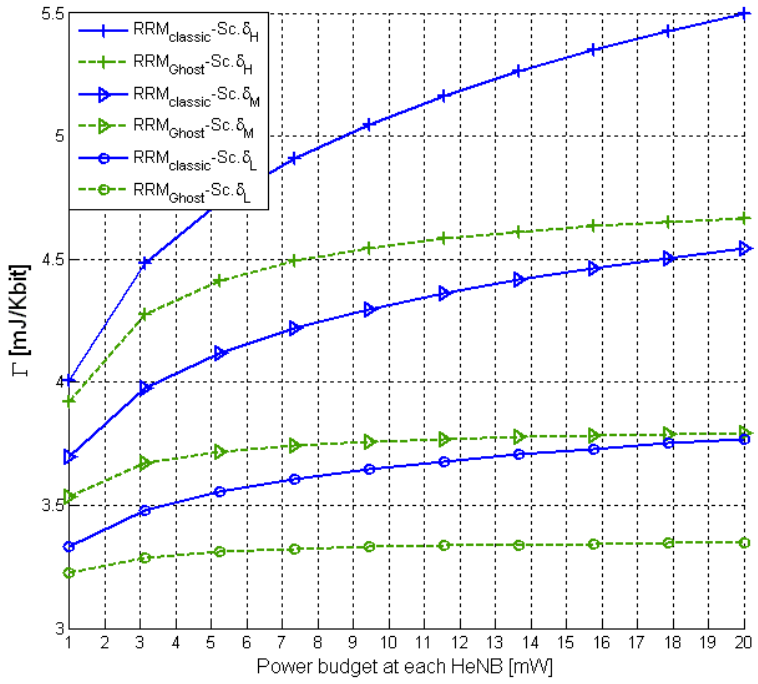

Figure 3-1: Average transmission cost at the macrocell versus power budget at each HeNB in different femtocell deployment scenarios.

Figure 3-1 shows the performance at the macrocell as the energy cost function previously introduced versus the power budget P^T at each HeNB. In the co-channel femtocell deployment, indoor MUE performance is limited by femto-to-macro interference. Some recent research introduced cooperation

within eNBs and HeNBs in order to coordinate the access to the radio medium and avoid the cross-tier interference [7]. However, following the 3GPP Release 10 baseline [40], we do not implement this coordination in our system. Hence, the eNB scheduler is not aware of the RBs exploited by the interfering HeNBs. When the eNB assigns to an indoor user a RB that is used by a neighbour HeNB, this MUE can be exposed to a high level of interference. We aim to evaluate the effect of this interference on MUE when femtocells use the reference $RRM_{classic}$ and the proposed RRM_{ghost} .

To compare these algorithms, we have set the throughput target (T_{tg}) of MUEs and FUEs respectively equal to 300 and 600 kbit/s and considered three different femtocell deployment scenarios:

Scenario δ_L: low density — $\rho_d = 0.3$, circle marked curves.
Scenario δ_A: medium density — $\rho_d = 0.5$, triangle marked curves.
Scenario δ_H: high density — $\rho_d = 0.8$, plus marked curves.

Solid and dashed lines, respectively, correspond to the throughput of $RRM_{classic}$ and RRM_{ghost} schemes. Note that, eNB power is fixed in each allotted RB; therefore, differences of performance between the two approaches are only due to the experienced throughput (which depends on the perceived interference) at MUEs. The results show how RRM_{ghost} strongly limits the impact of the femto-to-macro interference in all scenarios. For instance, under $RRM_{classic}$ and considering a HeNB power budget of 20mW, the proposed RRM_{ghost} gains up to 11%, 16%, and 15% Scenario δ_L, Scenario δ_M, and Scenario δ_H, respectively. This improvement comes from steps 4, 5, and 6 of the proposed scheme (MCS scaling, Spreading, and Power Scaling) that reduce the level of interference experienced in each RB by the MUE. Note that, cross-tier interference increases with the density of femtocells; however, its impact is limited by using the proposed RRM algorithm. Nevertheless, when the deployment ratio is higher than a certain threshold the benefit given by the RRM_{ghost} decreases (cf. Scenario δ_M, and Scenario δ_H); this is due to the higher frequency reuse, which results in higher interference.

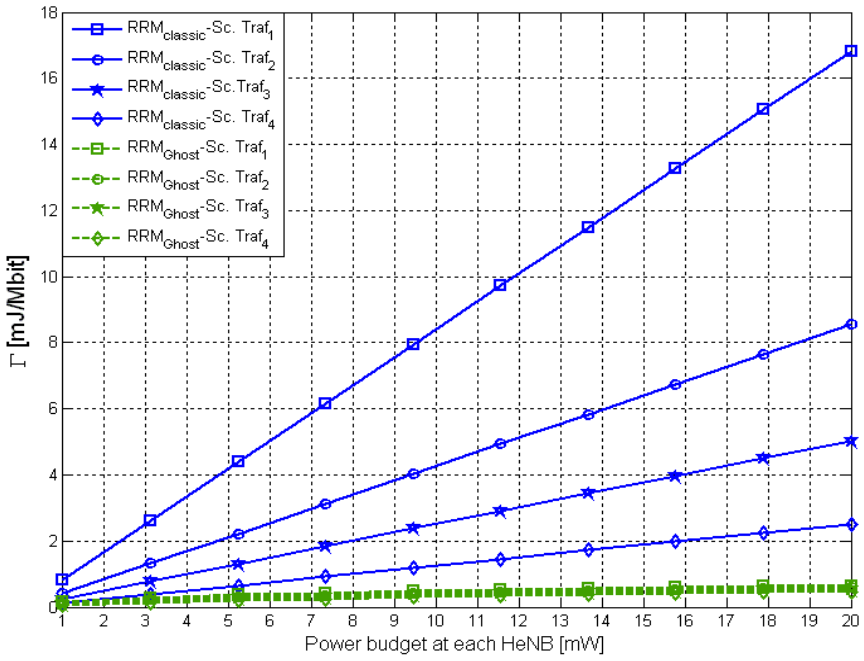

Figure 3-2: Average HeNB transmission cost vs. power budget at each HeNB in different traffic scenarios

Figure 3-2 shows the average transmission cost at the femtocell as a function of the radiated power budget at the HeNB. We consider four different traffic scenarios:

Scenario Traf 1: FUE throughput target T_{tg} = 300 kbit/s, square marked curves.
Scenario Traf 2: FUE throughput target T_{tg} = 600 kbit/s, circle marked curves.
Scenario Traf 3: FUE throughput target T_{tg} = 1 Mbit/s, star marked curves.

As previously mentioned, the eNB does not implement power control scheme and its transmission cost Γ depends only on the interference perceived at the MUE; on the contrary, by using the proposed RRM scheme, HeNBs are able to improve their transmission cost by adapting their output power to the capacity demand. Therefore, performance at HeNBs depends on both the co-tier interference and the used output power. Figure 3-2 shows that transmissions at HeNBs are much less power consuming (in terms of irradiated power) with respect to the eNB transmissions. In fact, there is nearly a factor of 10^3 between Γ measured at the eNB and Γ measured at HeNBs. Moreover, in Figure 3-2 we can observe that our algorithm limits the HeNB transmission cost in each considered scenario. For instance, considering a HeNB power budget equals to 10mW, RRM_{ghost} gains to 94%, 90%, 85%, and 75% in Scenario Traf.1, Scenario Traf.2, Scenario Traf.3, and Scenario Traf.4, respectively. Simulation results show also, that such a gain increases in lightly loaded scenarios, where lower MCSs are required and our algorithm allows to strongly reducing the irradiated power.

3.1.3 Resource Allocation with opportunistic spectrum reuse

Considering a cellular environment, there are several levels of diversity that can be exploited based on the dynamics of channel and environment. Multi-user diversity is quite well-known in radio resource scheduling area to exploit independence across channel quality experienced by a transmitting node to different users in the system. In this manner, users are scheduled at (relatively) good channel conditions to efficiently utilize scarce wireless resources. Route-diversity, on the other hand, provides another degree of freedom to be exploited in wireless environment. Intuitively, users should be served by the transmitting node with the strongest link to them. This factor is usually being considered in routing protocols in general or cell-selection procedures in particular for cellular systems.

Besides the legacy opportunities in the presence of multiuser and multi-route diversity, another level of opportunity arises in a multinode-multiuser environment based on the isolation factor among different pairs of serving node-users to do concurrent transmission, i.e. to reuse the spectrum. This isolation factor is highly dependent to the channel quality gap of a transmitting node to its own users compared to the links to users served by other transmitting nodes. The higher the gap, the better will be the resulting isolation factor. To better explain the concept, an illustrative example is provided in Figure 3-3.

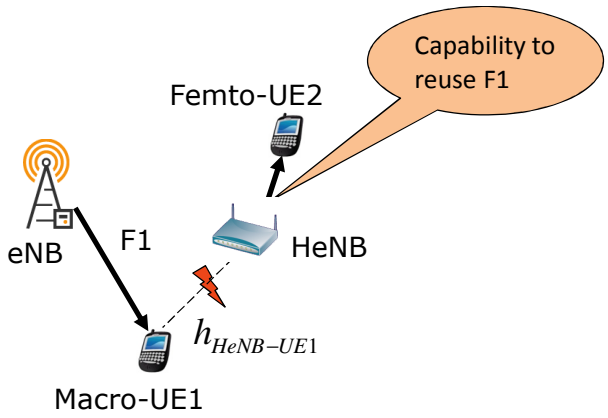

Figure 3-3: Illustrating the concept of opportunistic re-use

As shown, the deep fading condition between a MUE (UE1) and HeNB provides an opportunity to reuse the same resource for concurrent transmission from HeNB to its corresponding user (UE2) as it does not cause any significant interference to the primary transmission. Effectively, this method provides some low cost resources (in terms of interference) in the frequency domain to be utilised by the HeNB to 'serve FUEs.

3.1.3.1 Proposed algorithm

Based on the above concept, here we propose a decentralized algorithm to incorporate opportunistic reuse in radio resource allocation for femtocells:

Listening to primary channel assignments, as illustrated in Figure 3-3, reuse opportunities are quite dependent on the isolation factor among different pairs. So, at the first stage, it is important to categorize channel assignment of primary users based on primary scheduling at the serving node. In this case, the eNB acts as the primary serving node where it supports corresponding MUEs.

Reuse identification, at this stage, the reuse opportunities are identified by estimating the channel between secondary serving node (HeNB) and the primary users (MUE. This estimation is done for each primary user based on the channels that has been assigned to it in previous phase. The reusable resources are the one with faded channel condition on HeNB-primary user links. The fading threshold can be tuned adaptively based on the target level of service for primary macro users.

Secondary scheduling, the identified reusable resources are scheduled according to the adopted scheduling policy in secondary node (HeNB) to the corresponding femto users.

3.1.3.2 Simulation results

To evaluate the efficiency of proposed scheme a set of simulation studies is carried out on the downlink of an OFDMA-based cellular environment comprising seven wraparound cells. The interference is calculated from the first-tier neighbouring cells as well as serving eNB / HeNB for femto / macro users, respectively. The rest of the simulation parameters are as in Table 3-1 that is consistent with LTE assumptions.

Topology	Single block/ 5 x 5 Grid
eNB Power	43 dBm
HeNB Deployment	Standalone
No. Macro UEs	8
No. Femto UEs	4
eNB-to-HeNB distance	0.8 * Cell Radius
Inter-Site Distance	500 m
Speed	3 km/h
Traffic	Full Buffer
Scheduler	PF
Cases	Plain Macro, No Coordination, Opportunistic

Table 3-1: Simulation Parameters

3.1.3.2.1 Indoor-outdoor Scenario

In this scenario, a single femto block (12m x12m) was deployed at the target location (0.8 Cell Radius) while macro users are located outdoors in the surrounding area of the target femto block. Figure 3-4 and Figure 3-5 show the CDF of macro/femto normalized user throughput for two different penetration loss values. As it can be seen, in high levels of penetration loss (20dB), the effect of interference is naturally suppressed and the performance gap of opportunistic algorithm versus no coordination case is marginal. Here, more than 3 times performance improvement is observable in total average throughput compared with plain macro case. The high throughput gain on the femto side is attributed to close distance between HeNB and its corresponding femto users and the exterior wall isolation factor to outdoor macro users. However, in lower levels of penetration loss, there is less natural isolation between macro and femto users and coordination of interference seems crucial.

As shown in Figure 3-5, the proposed opportunistic algorithm can address this issue adequately. As a result, macro users maintain close performance to the benchmark plain case even in low penetration loss regime while the femto users are still able to maintain reasonable throughput (1.8 times improvement in total average throughput over the plain macro) without consumption of any additional frequency resources.

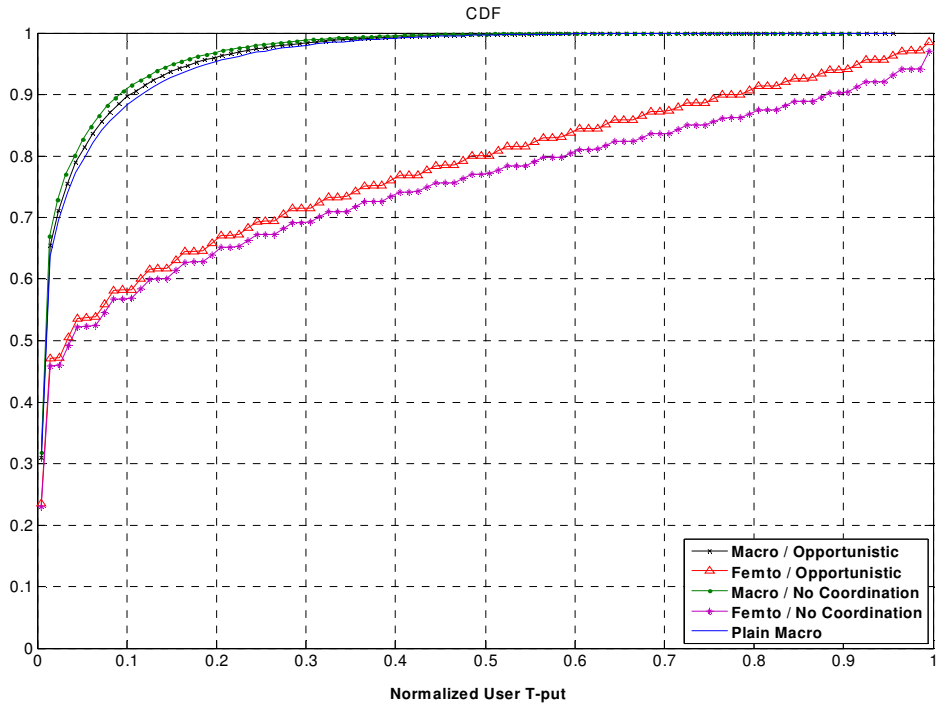

Figure 3-4: Indoor-outdoor results, exterior penetration loss = 20dB

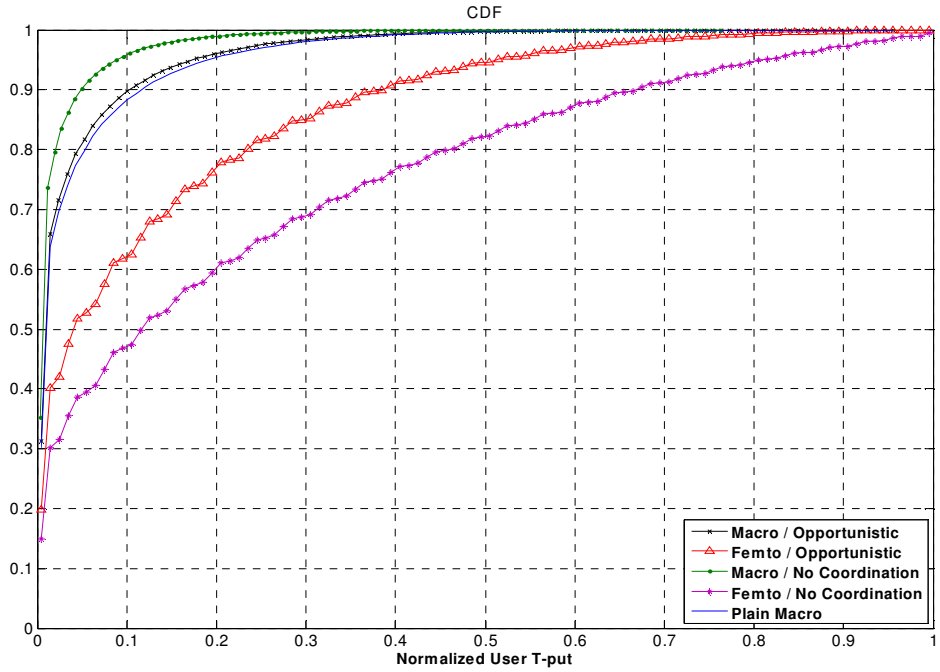

Figure 3-5: Indoor-outdoor results, exterior penetration loss = 10dB

3.1.3.2.2 Fully Indoor Scenario

In this scenario, a single femtocell is located at the central block of a 5x5 grid of blocks (each 10m x 10m) whereas the macro users are located indoor in all the other blocks where no femtocell exists. HeNB power is set to 10 mW. Figure 3-6 and Figure 3-7 show the simulation result for two different penetration loss values similar to previous scenario. As expected, by eliminating the exterior wall loss between macro users and femto access point, the performance of macro users is seriously affected in no coordination case

due to losing the natural isolation factor. Nevertheless, opportunistic reuse can still control efficiently the level of impact on macro users' side. In high penetration loss (20dB), due to sever reduction in reuse opportunities, the average throughput gain is limited over the legacy plain macro case. However, in 10dB penetration loss, still significant gain is observable in total average throughput compared with plain macro case. In this scenario, the plain macro spectral efficiency (1.76 bits/s/Hz- SISO) slightly decreases to 1.62 bits/s/Hz by employing the proposed scheme while the femto cell achieves the spectral efficiency of 1.8 bits/s/Hz.

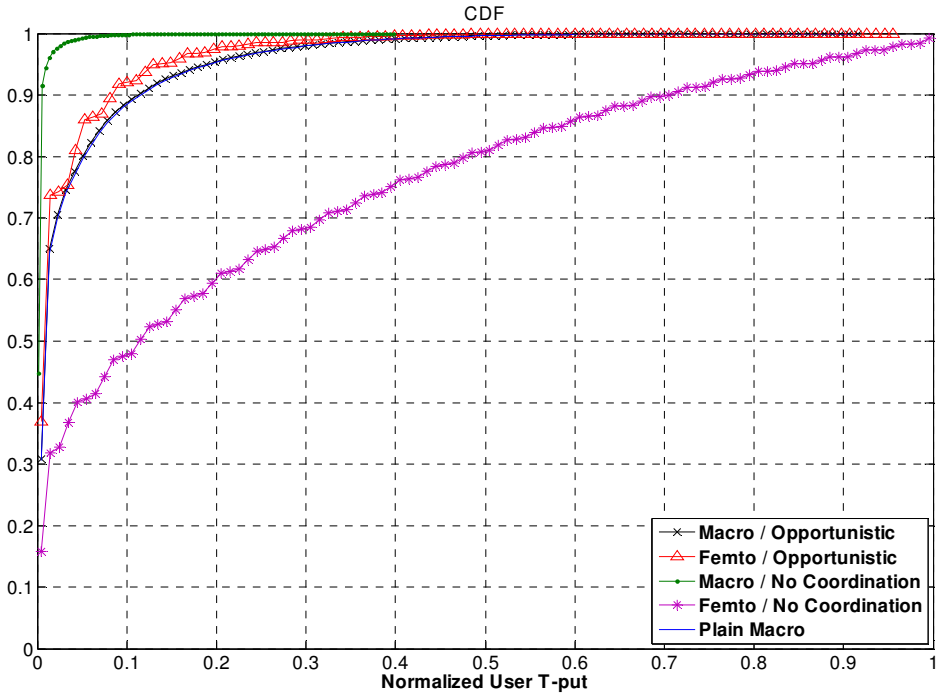

Figure 3-6: Fully Indoor results, exterior penetration loss = 20 dB

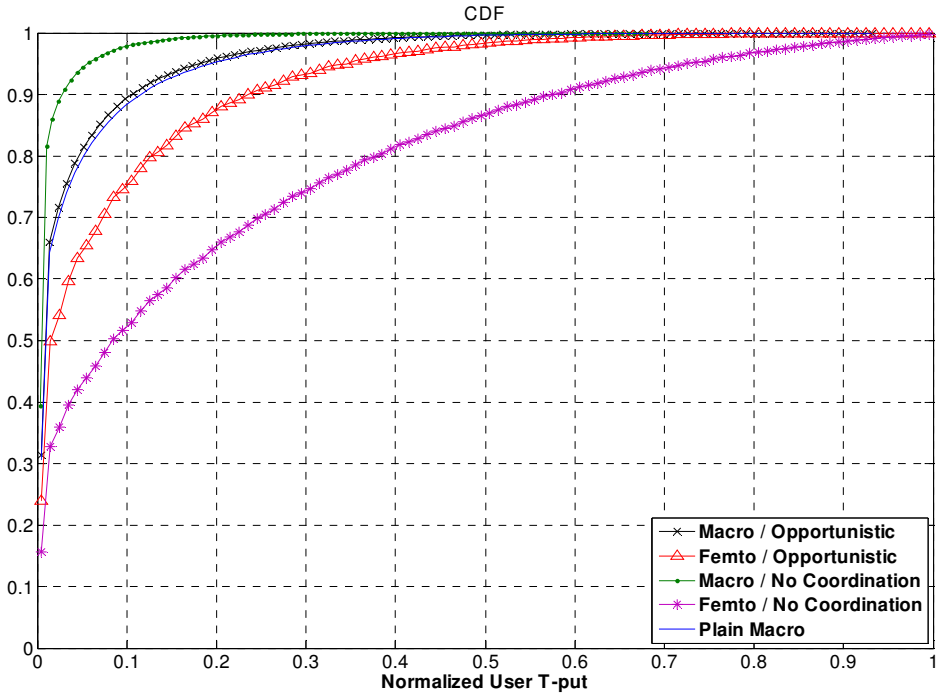

Figure 3-7: Fully Indoor results, exterior penetration loss = 10 dB

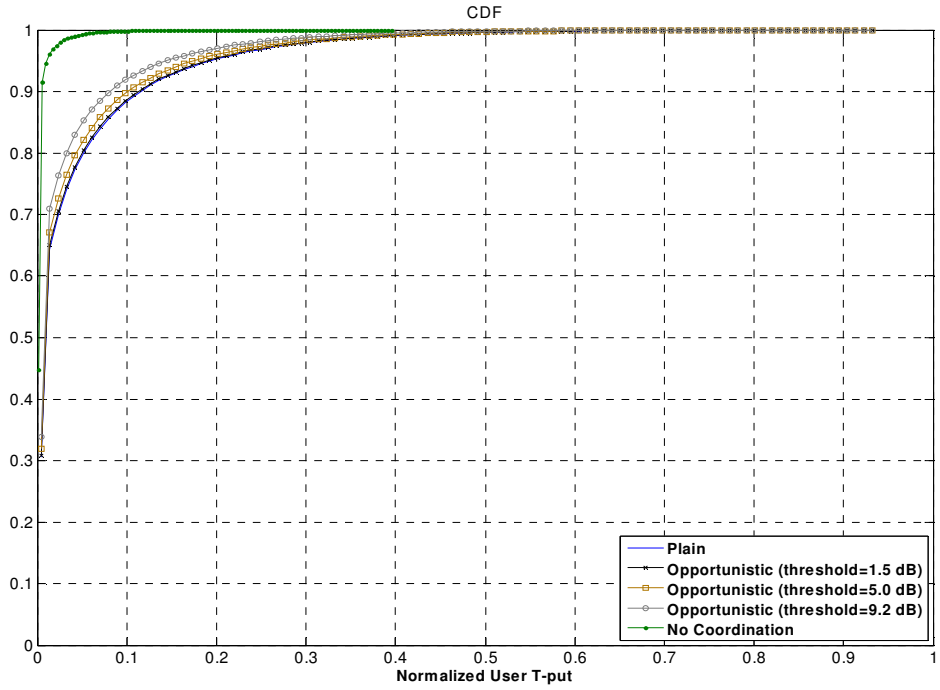

Figure 3-8: Macro fully Indoor results, different interference thresholds

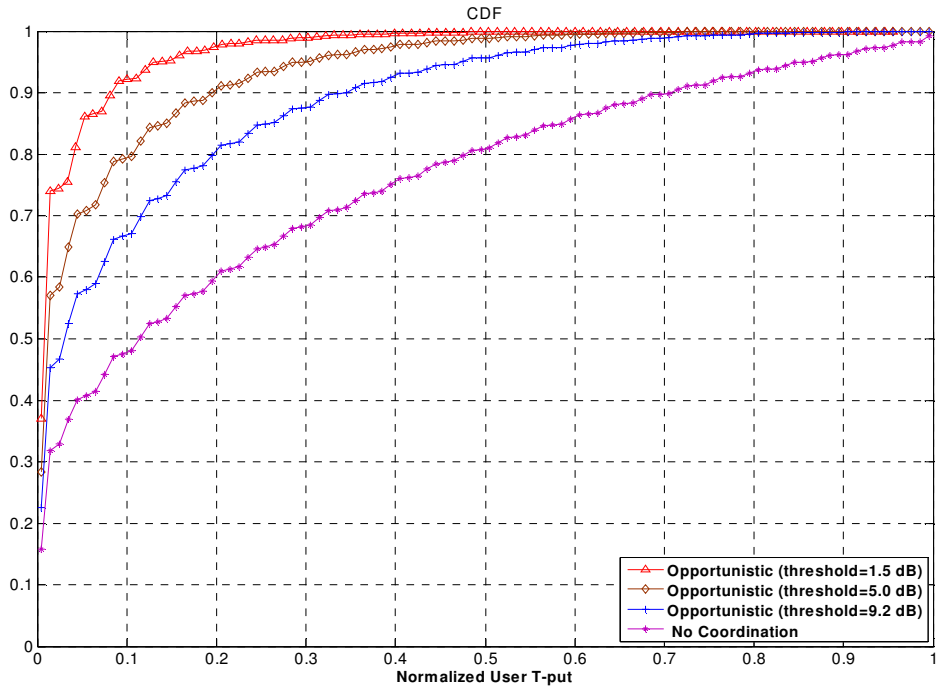

Figure 3-9: Femto fully Indoor results, different interference thresholds

Maintaining the performance of macro users will be at the cost of femto service in opportunistic case. However, the level of this trade-off can be adaptively tuned by controlling the target level of fading threshold in the second step of the algorithm. Figure 3-8 and Figure 3-9 show the CDF of macro and femto normalized user throughput, respectively for different values of fading threshold. As shown, increasing the fading threshold provides more resources to reuse as they appear to be faded from HeNB perspective. However, this would degrade the performance of macro users and the gap to the

benchmarking plain macro scenario increases. Due to better channel condition between the HeNB and its corresponding femto users, the gain on femto side is higher than the level of loss of macro users. This implies that in case macro users have more flexible QoS requirements, it is possible to target higher values for fading threshold.

3.1.4 RRM in Femtocell Downlink Exploiting Location Information

In this sub-section, we focus on the reduction of cross-tier interference via appropriate RRM techniques [41]. Due to fading and unplanned deployment, HeNBs need to change their transmitter parameters dynamically to minimize interference at neighbouring locations. Therefore, femtocell management should be distributed and self-organizing, so that HeNBs can successfully react to changes of the traffic and channel, and minimize interference [42].

In order to overcome the interference issues, several OFDMA-based RRM techniques have been proposed in literature [5] [43] and [47]. In[5], authors allocate the available RBs to avoid interference among HeNBs and MBSs. Power control was used [43] for RRM to minimize the interference. [44] proposed a learning based mechanism for femtocell. In [45], authors proposed an adaptive interference management technique of OFDMA femtocell. There are several proposals to overcome the interference issue using FFR [48]-[52]. However, all these works minimize/avoid the interference among FUEs. In contrast to these, the present work proposes a RRM technique using the interference information at every location within the coverage area.

The main objective of this work is to allocate radio resource among FUEs exploiting radio environment maps (REMs) [53]. We propose an interference-aware local cartography-based RRM (LC-RRM) technique for self-organized standalone HeNBs, where the HeNB system collects interference values measurements at FUEs locations for each RB. The proposed technique consists in a joint power and frequency RB allocation scheme that maximizes the FUE capacity, while keeping interference created at MUES within acceptable limit. In order to achieve this, we introduce the concept of interference cartography (IC) for better resource allocation. The interference cartography (discussed in 3.1.4.2.1) combines radio measurement data with user's location information and provides a complete view of the environment for autonomous decision making [54]. In our work, we use a spatial interpolation algorithm, called Kriging interpolation, to estimate interference values at the unobserved location and make IC diagram for each RB of HeNB coverage area. Thereafter, these RBs are classified based on their interference values using classification technique at desired location. Then, appropriate transmit power is used on these classified RBs for transmission to maximize DL transmission capacity of FUEs, while the interference introduced to the MUE remains within a tolerable limit.

The rest of this section is organized as follows. Section 3.1.4.1 describes the system model of the proposed LC-RRM technique along with analytical formulation. Section 3.1.4.2.1 presents the overview of interference cartography and analyses its formation in the context of present work. The interference classification and dynamic FFR scheme are described in Section 3.1.4.2.2. The power and subcarrier allocation mechanism of proposed LC-RRM technique is described in Section 3.1.4.2.3. Section 3.1.4.3 presents the simulation results.

3.1.4.1 System Model

We consider HeNBs, located within a hexagonal eNBs network, that are using the same frequency band for communication in DL. Since the position of MUEs cannot be known (due to mobility for instance), we only assume that the positions of the MBSs as well as the position of the HeNBs are known.

In this work, the network is based on the 3GPP/LTE DL specifications [37]. Each user is allocated one or several RBs during a time transmission interval (TTI). The overall channel gain is composed of a fixed distance-dependent path loss, a slowly varying component modelled by lognormal shadowing and Rayleigh fast fading with unit power. The received SINR on RB i of k_m-th MUE of m-th eNB can be expressed as

$$\beta_{i,k_m}^{m} = \frac{G_{i,k_m}^{mm} P_i^m}{\sigma^2 + \sum_{a=1\neq m}^{M-1} G_{i,k_m}^{aa} P_i^a + \sum_{h=1}^{H} G_{i,k_m}^{hm} P_i^h} \tag{3.3}$$

where $G_{i,k_m}^{mm(resp.aa)}$ is the channel gain between MUE k_m and serving eNB m (resp. eNB a) on RB i, G_{i,k_m}^{hm} the channel gain between MUE k_m and neighbouring HeNB h on RB i. $P_i^{m(resp.a)}$ is the transmit power on RB i by m-th (resp. a-th) MeNB. Similarly, P_i^h is the transmit power of neighbouring HeNB

h on RB i. M and H are the total number of eNBs and HeNBs respectively. σ^2 is the white noise power spectral density.

In case of a FUE, it is interfered by all eNBs and adjacent HeNBs. The received SINR of a FUE k_h of h-th HeNB on RB i can be similarly given by

$$\beta_{i,k_h}^{h} = \frac{G_{i,k_h}^{hh} P_i^h}{\sigma^2 + \sum_{m=1}^{M} G_{i,k_h}^{mh} P_i^m + \sum_{b=1\neq h}^{H-1} G_{i,k_h}^{bb} P_i^b} \tag{3.4}$$

where $G_{i,k_h}^{hh(resp.bb)}$ is the channel gain between FUE k_h and serving HeNB h (resp. b), and G_{i,k_h}^{mh} the channel gain between FUE k_h and eNB m on RB i. In our channel model, the channel gain between FUE k_h and serving HeNB h is given by

$$G_{i,k_h}^{hh} = PL_{k_h}^{h}(d_{k_h}^{h}) \times \eta_{k_h}^{h} \times \zeta_{ik_h}^{h} \tag{3.5}$$

where $PL_{k_h}^{h}$, $\eta_{k_h}^{h}$ and ζ_{i,k_h}^{h} are the distance-dependant channel gain, the shadowing, and the fast fading component that depends on the RB i for k-th user of h-th HeNB. In this work, we consider different pathloss models for eNB and HeNB.

From now on, we will concentrate on a particular HeNB h, and its associated FUEs. An FUE whose serving femto is h, will be denoted by k to alleviate notations.
The transmission rate of FUE k is given by

$$C_k = \sum_{i=1}^{N} a_{i,k} R_{i,k}^{h}(G_{i,k}^{hh}, P_i^h) \tag{3.6}$$

where N is the total number of RBs, $a_{i,k}$ is the binary assignment variable and $R_{i,k}^{h}$ is the Shannon capacity of FUE k at i-th RB, expressed as

$$R_{i,k}^{h} = B_i \log_2\left(1+\beta_{i,k}^{h}\right) \tag{3.7}$$

where B_i is the bandwidth of the RB i. As mentioned earlier, our objective is to allocate the appropriate RBs to meet FUE's QoS with power and interference constraints. Thus, the optimization problem can be formulated as follows:

$$\textit{Optimize} \quad \sum_{k=1}^{K} C_k = \sum_{k=1}^{K}\sum_{i=1}^{N} a_{i,k} R_{i,k}^{h}(G_{i,k}^{hh}, P_i^h) \tag{3.8}$$

Subject to

$$I_{i,k_m} = \sum_{a=1\neq m}^{M-1} G_{i,k_m}^{aa} P_i^a + \sum_{h=1}^{H} G_{i,k_m}^{hm} P_i^h \leq I_{th}^{m}$$

and

$$I_{i,k_l} = \sum_{m=1}^{M} G_{i,k_h}^{mh} P_i^m + \sum_{b=1\neq h_l}^{H-1} G_{i,k_l}^{bb} P_i^b \leq I_{th}^{h}$$

$$0 \leq \sum_{k=1}^{K}\sum_{i=1}^{N} a_{i,k} P_i^h \leq P_{Tot}, a_{i,k} \in \{0,1\}$$

for any MUE k_m belonging to eNB m and for any FUE k_l belonging to HeNB l, with l different from h. K is the number of FUEs per HeNB. I_{i,k_m} (resp. I_{i,k_h}) are interference terms (see denominators of Eq (3.3) (resp. Eq. (3.4)). I_{th}^{m} and I_{th}^{h} are the interference thresholds for these interferences terms.

3.1.4.2 Proposed algorithm

Figure 3-10 shows the system model of the proposed LC-RRM technique. As shown in the figure, it consists of two main functional modules: IC manager and femtocell spectrum manager (FSM) with spectrum allocation module. The IC manager consists of measurement collection module (MCM) and IC database. MCM collects the available interference values for each RB at every current users. These interference values for each RB are then stored in the IC database. IC database adds interference values for any new location and updates the value for already existing locations. With this process, IC database is up-to-date at any point of given time. By gathering these interference values, IC manager makes the cartography diagram for each RB of its coverage area.

This IC diagram helps FSM module for resource allocation among FUEs. The FSM module, which can control several HeNBs or a standalone HeNB, assigns RBs with appropriate transmit power to users to satisfy QoS. Here, we consider resource allocation technique for a standalone HeNB. The RBs and transmit power are selected based on the interference at desired user location and the interference threshold limit at neighbouring locations. The interference threshold at a given receiver is the maximum

interference level acceptable by the receiver (i.e. maximum level of interference that does not cause any quality of service degradation). Moreover, knowledge of the locations of MUEs may help to determine the corresponding interference threshold. It depends on the particular user with specific QoS and might differ for different users. The threshold value is very sensitive for different worst case MUE, discussed more in [55].

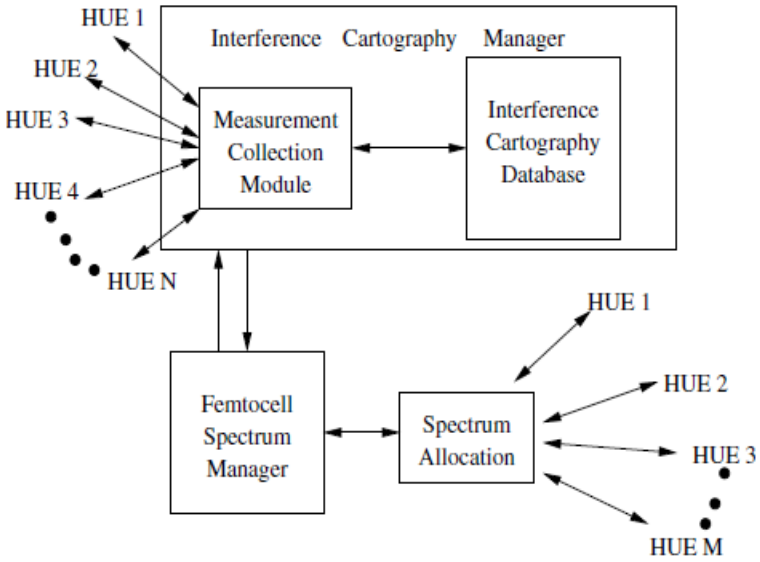

Figure 3-10: System model framework of LC-RRM technique

3.1.4.2.1 Interference Cartography and its Construction

The interference cartography [54] is based on the aggregation of the interference information, measured by entities of several HetNet users at a central unit. The central unit combines these aggregated values with geo-localization information, and performs advanced signal processing techniques to render complete and reliable information. It provides a viable picture of the environment for efficient detection, analysis and decision by updating this information on a database, known as REM [56]. To achieve certain level of accuracy and reliability in measured data, large amounts of measurement data may be needed in constructing a cartography that relies only on reported measurements. Furthermore, with the rapidly increasing level of technological advances in digital signal processing, it is possible to implement efficient signal processing techniques that achieve high levels of accuracy and reliability with a small proportion of measurement data [53].

In our wireless network simulator, we use interference values of each RB at the current user's location as REM information. These interference values are used to form the IC database, whose size is limited to those RBs with characteristics provided by current users. Using IC database, IC manager estimates interference values at the desired location using spatial interpolation. The spatial interpolation is a statistical procedure that estimates missing values at unobserved locations within a given area, based on a set of available observations of a random field. This interpolation is mainly based on spatial autocorrelation. One such interpolation technique is Kriging interpolation technique [57], used in this work. In order to implement the interpolation, we consider the data set $y(1),...,y(n)$ are the realization of a stochastic model with mean, $\mu(.)$, and (symmetric) variance-covariance matrix, Σ. Given a sample of size n, the best linear unbiased predictor of any unsampled point on the surface can be obtained by simple Kriging.

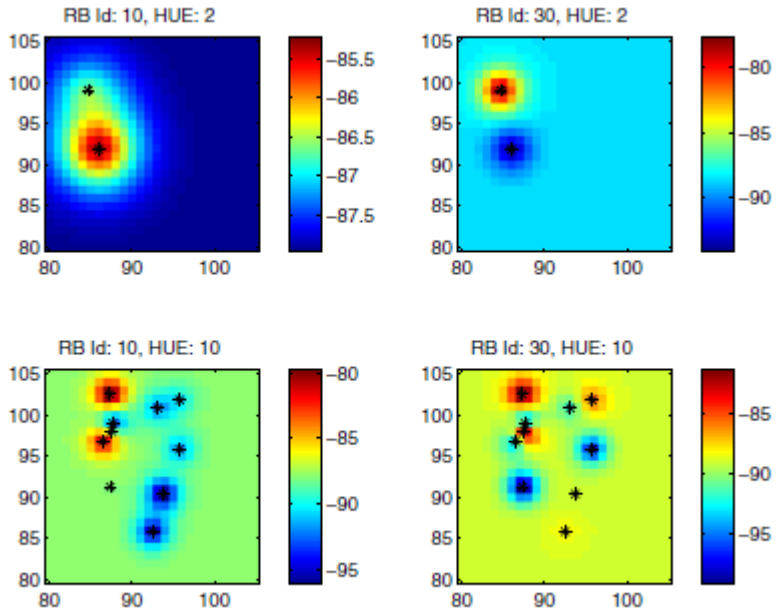

Figure 3-11: A typical interference cartography diagram for RB Id 10 and RB Id 30 with different FUEs in HeNB coverage area (10 × 10 meter). HeNB access point located at (90, 95). Star marks represent the FUE locations. The unit of interference is dBm.

To predict the attribute value at site x, (x), which is not included in the sample, compute:

$$\tilde{y}(x) = \mu(x) + C^T \Sigma^{-1}(\mathbf{y} - \Omega) \tag{3.9}$$

where $C^T = (cov(y(x), y(1)),...,cov(y(x), y(n))$. Σ, as noted, is an $n \times n$ symmetric matrix with (i, j)-th element equal to $cov(y(i), y(j))$, $\mathbf{y} = (y(1),..., y(n))^T$, $\Omega = (\mu(1),...,\mu(n))^T$ and $\mu(x)$ is the mean evaluated at site x. The second term in (7) identifies the simple Kriging weights, $C^T \Sigma^{-1}$, assigned to each data point, that yields the best linear unbiased predictor of the unknown attribute value.

As shown in Figure 3-10, by accessing the interference values from IC database, IC manager makes the cartography diagram for each RB using Kriging interpolation of HeNB coverage area. Figure 3-11 shows the IC diagram for two different RBs of a particular HeNB with two different numbers of FUEs. As shown in the figure, the interpolation algorithm estimates more accurately at the unobserved locations with larger database. The interference values are different for different RBs at a particular location. Using this constructed IC diagram, the RBs are split into different categories by interference classification scheme. These classified RBs are then being used to allocate to FUEs based on proposed dynamic FFR scheme, discussed in next section.

3.1.4.2.2 Interference Classification and Dynamic Fractional Frequency Reuse

In the literature, some theoretical investigations propose to classify perceived interference at user into five regimes, namely *noisy*, *weak*, *moderately weak*, *strong* and *very strong* interference regimes [58]. In [59], the authors simplify interference classification which reduces the processing complexity in comparison to the other classification. This paper classifies the interference into three regimes.

Noisy interference regime: The noisy regime corresponds to the most conventional way for processing interference, *i.e.*, as thermal noise. If the perceived neighbour signal is too weak, then the interference can be processed as additional noise.

Strong interference regime: Here, interference is so strong that it causes no degradation in comparison to a scenario without interference. Such a regime is known in the literature as the *very strong* interference regime. One main advantage of this regime is that the optimal scheme can be used to decode the interfering data while treating information data as noise, then subtracting interference to the received signal and eventually decoding the information signal cleaned from interference. Interference is then cancelled out.

Jointly decoding regime: With this regime, perceived inter-cell interference is not strong enough to be decoded alone and not weak enough to be treated as noise; destination jointly decodes information and interference for recovering the information signal. This regime lies between *noisy* and *strong interference* regimes. The bounds of applicability of the three different regimes with satisfaction the rate and power constraints with macrocell as a known interferer are given by (described by (14) in [59]):

$$\begin{aligned}
&1.\ \textit{Noisy} && \begin{cases} \gamma_i = A_i\left(1+f_j\cdot\gamma_j\right) \\ \gamma_j \le \dfrac{A_j}{f_j} \end{cases} \\
&2.\ \textit{Jointly decoding} && \begin{cases} \gamma_i = A - f_j\cdot\gamma_j \\ \dfrac{A_j}{f_j} \le \gamma_j \le \dfrac{A_j}{f_j}\left(1+\gamma_i\right) \end{cases} \\
&3.\ \textit{Strong Interference} && \begin{cases} \gamma_i = A_i \\ \gamma_j \ge \dfrac{A_j}{f_j}\left(1+\gamma_i\right) \end{cases}
\end{aligned} \tag{3.10}$$

where $A_i, A_j, f_i, f_j, \gamma_i$ and γ_j are defined in [59].

The above classification is valid in the case of one single interferer We thus assume in the sequel, that the FUE is interfered by one MeNB, which is the dominant interferer. Interference created by other MeNBs if any, will be considered as noise.

Having knowledge of the interference values, for a given location, RBs are classified according to the above classification and allocated to user based on our proposed dynamic FFR scheme. The general FFR scheme is very suitable for OFDMA-based systems, and has been used for interference mitigation, where the whole spectrum is divided into several subbands in frequency and time scale [18][20][59]. Each sub-band is differently assigned to centre zone and edge region of the cell. While reuse factor of the centre zone is one, the edge region adopts a larger reuse factor. As a result, interference in the centre zone is removed, and interference in the edge region is substantially reduced. At the same time, system throughput is also enhanced. Most of the previous works are based on fixed FFR. In this work, we propose a dynamic FFR among femtocell users with reuse factor one, for both central and edge zone.

In our proposed dynamic FFR scheme, we use the RBs of two categories, noisy and interference cancellation regime for allocation among users. The allocation of RBs is motivated by users' location within HeNB coverage area. In our allocation scheme, we divided FUEs into two categories based on their location, *i.e.* pathloss, central users and edge users. The proposed dynamic FFR uses the RBs in interference cancellation regime for edge user and the RBs in noisy interference regime for central users for allocation. The RBs in interference cancellation regime are used for edge user to mitigate higher pathloss and shadowing effect. The shadowing effect cannot be anticipated by interpolation algorithm during the formation of cartography diagram. Therefore, there may be a possibility of incorrect estimation of interference values if a user is in the shadowing region, which will have a higher impact for high pathloss. In addition to this, the effect of other obstruction can also be mitigated by this kind of RB allocation. Indeed, the wrong estimation of interference can affect the power allocation, which may produce strong interference at the nearby MUEs. To mitigate this, we consider the RBs in interference cancellation regime for edge users. Since the interference will cancel out with an optimal decoding scheme, these RBs can be used for communicating to edge users. Using this dynamic FFR scheme, we will discuss the joint RBs and power allocation procedure in the next section.

3.1.4.2.3 RRM Technique among Femtocell Users for Standalone Femtocell

Based on the above-mentioned assumptions, we will use the following procedure for allocating the RBs with proper transmit power to FUEs. The flowchart of the LC-RRM is described in Figure 3-12. The allocation module in Figure 3-10 uses location-based interference values from IC database and allocates the RBs to FUE with the help of FSM. At first, IC manager collects the interference values at the current scheduled users locations on each RB and stores them in the IC database. This operation happens periodically and IC manager refreshes the values in IC database. The refreshment happens whenever there is an update on power allocation, user activation, additional resource allocation etc. Using these values, IC manager forms the cartography diagram for each RB. When a new user wants to join the HeNB, IC manager uses IC diagram to determine the interference values of each RBs at user location. The

standalone HeNB then classifies the RBs based on their interference values. Having knowledge of user location, the proposed dynamic FFR scheme chooses the RBs for possible allocation. On each chosen classified RB, HeNB selects transmit power in an iterative way. For each iteration, HeNB estimates interference values by producing IC diagram on each available RB at the neighbouring areas. During each iteration, HeNB checks the interference values produced at the nearby area, which should be under the threshold limit. The threshold limit is different for MUEs and FUEs. In both cases, it depends on current QoS condition. However, it also depends on the deployment scenario of eNBs and HeNBs and the receiver sensitivity of MUEs and FUEs. Thus, for each value of transmit power, IC manager forms IC diagram for extended coverage area, so that the possible interference values after transmission can be checked at the neighbouring HeNBs users and worst case MUEs [55] for interference limit. By this process, the RRM algorithm selects the transmit power for each available RB. The number of RBs is selected with best modulation and coding value to meet rate and power constraints. In this way, FSM with allocation module selects the transmission parameters for FUEs as well as keeps the interference at neighbouring area within the threshold limit.

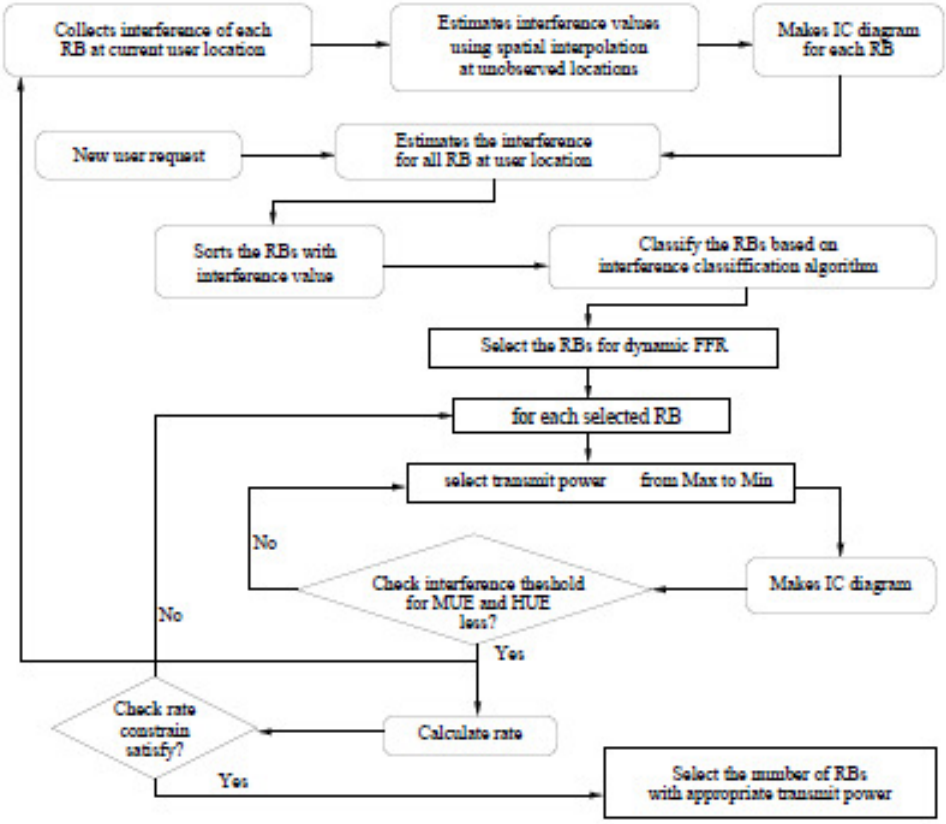

Figure 3-12: Flow chart of the proposed LC-RRM technique

3.1.4.3 Simulation Results

We benchmark the proposed algorithm by considering the network where MBSs and HeNBs share the same spectrum. The maximum power of eNBs and HeNBs are 46 and 10 dBm respectively. The HeNBs are deployed according to the 3GPP grid urban deployment model within a hexagonal structure of 19 eNBs with intersite distance of 500 m. Each eNB transmits continuously and with maximum power. As a consequence, only a particular HeNB is simulated, while others are used for down-link interference generation only. In this model, a single floor building is considered, where 10 m x 10 m apartments are placed next to each other in a 5 x 5 grid. Each HeNB can simultaneously serve a maximum number of 4 users. The combined deployment/activation ratio of HeNBs is 20%.

Figure 3-13 shows the IC diagram of before and after transmission for two different RBs with two FUEs. As shown in the figure, interference values change after transmission due to power allocation on the RB. These values are different for different RBs at a particular location. These estimated interference values are being used for checking the interference threshold limit at neighbouring location. Based on these IC diagram, appropriate transmit power has been chosen for each RB, while the interference introduced to the MUE remains within a tolerable limit. Thus, with the help of IC diagram, LC-RRM technique selects

appropriate transmit power on each RB.

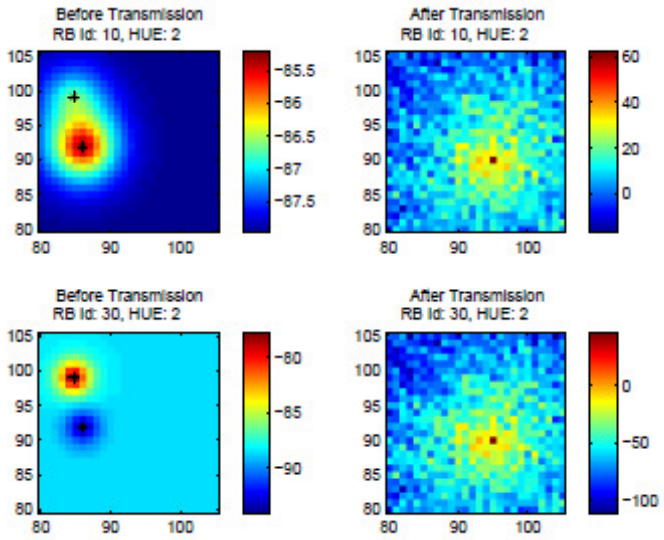

Figure 3-13: Interference cartography diagram (25 × 25 meter) at before and after transmission for two different RBs. HeNB access point located at (90, 95). Star marks represent the FUE locations. The unit of interference is dBm.

The average throughput of the proposed LC-RRM technique is shown on Figure 3-14 for central and edge users. As expected, the throughput for edge user is slightly lower than the central user at a particular HeNB transmit power due to the distance from HeNB access point. The figure also shows the comparison between with and without the proposed LC-RRM technique. The throughput gain is higher for edge user than for the central user due to our dynamic FFR scheme. In Figure 3-15, we plotted the average achievable transmission rate of FUE versus interference introduced to the worst-case MUE. Since HeNB does not have the knowledge of MUE location, we consider a worst-case MUE, co-located with FUE

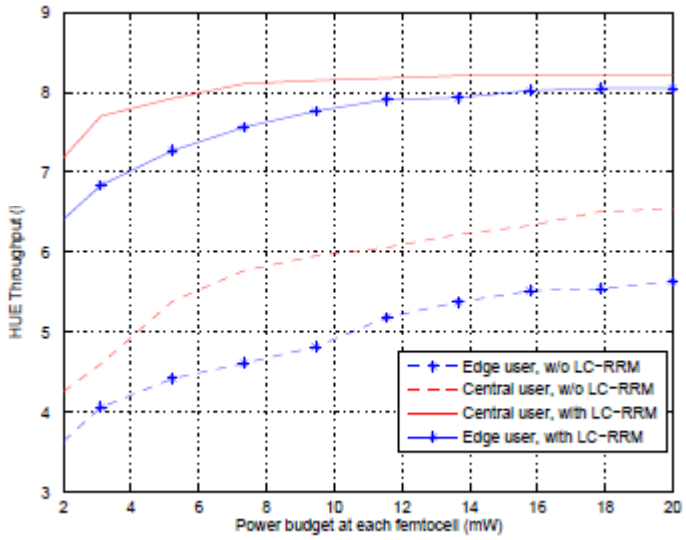

Figure 3-14: Average FUE throughput in Mbps for central user and edge user in a particular HeNB.

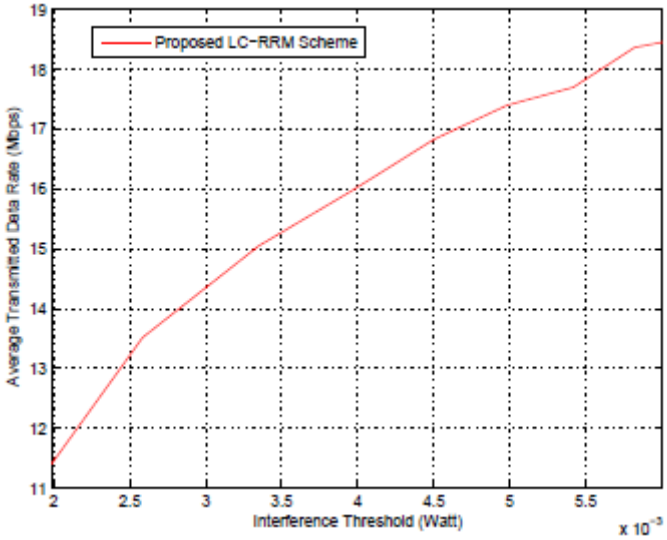

Figure 3-15: Maximum average transmitted data rate of FUE versus interference introduced to the worst-case MUE.

3.1.5 Conclusions

Future 3GPP/LTE femtocells deployment is expected to be dense: a large population of potential interferers will need to share scarce frequency resources while few users will locally have access to a large amount of resources. Classical resource allocation and interference mitigation techniques cannot address the challenge of limiting interference between neighbour femtocells and maintaining a high level of reliability for macro UE communications. We have obtained some important results facilitating coexistence of femto and macro users. Initially, we have designed RRM_{ghost}, a novel radio resource management scheme that makes femtocells "invisible" from the macro users. This RRM scheme limits the undesired effects of interference by exploiting the scarcity of users vs. available spectrum in a femtocell. Each femto user can then use more spectrum, while reducing the radiated power (in each RB) required to meet target QoS constraints. Subsequently, another decentralized approach was proposed for radio resource allocation in femtocell networks based on opportunistic reuse. As shown, this method can efficiently control the level of resulting interference on macro performance. As discussed, in indoor-outdoor scenario, high levels of natural isolation can naturally suppress the impact on macro cells whereas in low penetration loss case, the opportunistic reuse algorithm hugely outperform the no coordination case by maintaining the quality of macro users. Similar promising performance is observable in fully indoor case. On the other hand, we proposed an interference-aware LC-RRM technique for standalone femtocell where power and RBs are allocated to FUEs efficiently by combining location information. It has been observed that the proposed technique is notably effective to improve the throughput of FUEs. The proposed LC-RRM technique provides the upper bound of the interference at the MUEs.

3.2 Successive Interference Cancellation on the UL of Femtocell Transmission

3.2.1 Problem Statement

We develop a comprehensive methodology and evaluate the performance of the two-tier cellular network overlaid with femtocells during the UL. We propose a femtocell power control scheme that relies on minimal coordination with the cellular base station users. We use a simple interference sensing procedure in the femtocells to assign channels to femtocell users. We show that these two techniques alone yield beneficial gains for users in terms of power savings and for the network in terms of additional throughput. We then develop a decision rule in which macrocell users should join a nearby femtocell. Successive interference cancellation is used to allow a macrocell user and a femtocell user to share a common channel and UL to a femtocell access point. We show that these two additional techniques significantly improve the gains already realized from the power control and channel assignment scheme developed.

We consider the network's UL bandwidth to be divided into N_c orthogonal channels that are fully shared between the two networks. In the context of this work, we consider a given channel to be a frequency slot as in a Frequency Division Multiple Access (FDMA) or OFDM system, however nothing prevents the system from allocating resources as time slots in a TDMA system. We further assume that $M = N_c$ so that there is one MUE per channel and then a random number of FUEs sharing the UL channel as well. For a MUE link to exist on a given channel, we require a minimum SINR threshold of β_M to be satisfied. A similar minimum threshold β_F must be satisfied for a FUE link to exist.

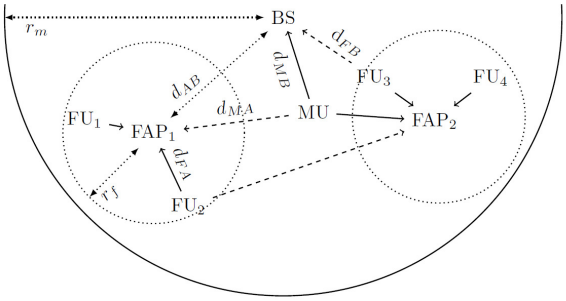

Figure 3-16: Topology illustrating the numerous distances and connections between nodes.

Finally, we assume that a given HeNB can only support a maximum of F links where each link must be on different channels. Due to the nature of the fully shared spectrum, the two networks will interfere with each other. To account for the interference from the FUEs to the MeNB, we assume that there exists a margin κ_M in the SINR at the MeNB which determines how much interference is allowed at the MeNB. We consider a similar margin κ_F to exist in the SINR at the HeNB. We assume the MeNB can tolerate more interference than a given HeNB and thus make the assumption that $\kappa_M >> \kappa_F$. Using our distance based pathloss model, modelling the interference on the various links is equivalent to varying the pathloss exponent. For FUEs communicating with HeNBs, we use α for the pathloss exponent. We use an exponent of γ for MUEs when they interfere with the HeNBs or when they connect to a nearby HeNB. Finally, we use ϕ as the exponent for MUE links with the MeNB as well as the FUE interference to the MeNB and other HeNBs.

3.2.2 Joint Power Control, Channel Assignment and Handover Mechanism

Femto user power control is managed by the HeNB, however the process is aided by the MeNB. The value κ_M controls how much interference is allowed at the MeNB and is incorporated into the power control that the MeNB performs for each MUE on their respective channel. We can see the effects of the power control in the MUE link by looking at the SNR of a given channel C_k at the MeNB, where after rearranging terms, gives a bound on the transmit power of MUEs as:

$$\frac{P_{T_M} d_{MB}^{-\phi}}{\sigma_n^2} \geq \kappa_M \beta_M$$
$$P_{T_M} \geq \kappa_M \beta_M \sigma_n^2 d_{MB}^{\phi} \quad (3.11)$$

where d_{MB} is the distance between a MUE and the MeNB and P_{T_M} is the transmit power of the MUE. If we assume that MUEs transmit at the required minimum just found, then by looking at the SINR of a given channel C_k at the eNB and after rearranging terms

$$\frac{P_{T_M} d_{MB}^{-\phi}}{I_k + \sigma_n^2} \geq \beta_M$$
$$\sigma_n^2 (\kappa_M - 1) \geq I_k \quad (3.12)$$

we can upper bound the total amount of interference allowed on that channel in terms of κ_M. We know however that I_k is the sum interference from all femtocells on channel C_k. If we divide I_k by the average number of femtocells N_f, we can calculate the amount of interference allowed per femtocell.

Furthermore, each channel in a given femtocell can only be used by a single FUE. Thus, the interference at the MeNB from a given FUE on channel C_k is simply $P_{T_F} d_{FB}^{-\phi}$. The amount of overhead for the MeNB to learn d_{FB} for every FUE in the network could be quite high. We can make a close approximation however by assuming a worst case location for a FUE as being on the edge of the femtocell, closest to the MeNB. We illustrate this in Figure 3-16 where we show a femto user FU3 on the edge of HeNB2. Due to the relative small size of the femtocell, we can approximate each FUE distance by $d_{AB} - r_f$, the difference of the distance from the HeNB to the MeNB and the femtocell radius. Because the HeNBs are stationary, the overhead to know the distance to the HeNBs is low. Thus for any FUE in a given femtocell, its own distance to the MeNB will always satisfy $d_{FB} \geq d_{AB} - r_f$. We can combine all of these concepts with the interference bound and write:

$$\frac{\sigma_n^2(\kappa_M - 1)(d_{AB} - r_f)\phi}{N_f} \geq P_{T_f} \tag{3.13}$$

which is an upper bound on the transmit power of each FUE in the network for all C_k channels. We assume that the MeNB knows d_{AB} for each femtocell and it knows N_f, and thus can set a maximum transmit power for each femtocell. Due to the fact that the total interference at the MeNB from all the FUEs is constrained by κ_M, each MUE will always be able to satisfy its required SINR threshold when connecting to the MeNB. Thus in terms of outage performance, a MUE has no reason to connect to a HeNB instead of the MeNB. However, depending on the operating point of the network, a MUE can achieve gains in terms of power savings if it were to connect to a nearby HeNB. We can define a decision rule in which each MUE can decide whether to access the MeNB or a nearby HeNB. With power savings as the end goal, we can say that a given MUE on channel C_k should connect to a nearby HeNB if the transmit power needed to connect to the HeNB, denoted by P_{T_A}, is less than the power needed to connect to the MeNB, P_{T_M}. If we write the SINR at a femtocell access point on a given channel C_k and rearrange terms, we get:

$$\begin{aligned} &\frac{P_{TA} d_{MA}^{-\gamma}}{I_k + \sigma_n^2} \geq \kappa_F \beta_M \\ &P_{TA} \geq \kappa_F \beta_M (I_k + \sigma_n^2) d_{MA}^{\gamma} \end{aligned} \tag{3.14}$$

which is a lower bound on the power needed to connect to the HeNB. Note that the bound is proportional to the distance from the MUE to the HeNB, d_{MA}, as well as the interference observed by the HeNB on channel C_k. Furthermore, the bound is scaled by κ_F for further robustness against any additional interference the MUE-HeNB link may encounter. Thus if we define the decision rule for which a MUE should connect to a HeNB as $P_{T_M} > P_{T_A}$ and use the minimum powers derived above, after rearranging terms we get:

$$d_{MB}^{\phi} > \frac{\kappa_F (I_k + \sigma_n^2) d_{MA}^{\gamma}}{\kappa_M \sigma_n^2} \tag{3.15}$$

which gives the decision rule in terms of the network parameters, the interference at the HeNB on channel C_k, and the path-loss of the two different links. We assume that there is a mechanism in place in which MUEs can either learn the distances of the two links or the path-loss of those links. Using the decision rule, MUEs can coordinate with a nearby HeNB to be admitted to the femtocell and be power controlled as if it were just another FUE. Recall however that a HeNB can only support F links and those links could be in use by the FUEs in the femtocell. As a solution, we propose that the MUE share one of the channels actively in use by a FUE. We intend for the sharing to be made possible through successive interference cancellation at the HeNB. We will give more details on this in the following sections.

Each HeNB manages the channel assignment for the F femto users within its own femtocell. It is in the best interest of the FUEs in terms of power consumption and link outage to use the channels with the least amount of interference. To achieve this, we assume that if there is a MUE who wishes to join the femtocell on a given channel C_k, and if the SINR requirements for a FUE can be met on that channel, the MUE should be assigned to C_k. In doing so, the high power signal the MUE uses to get to the MeNB, which causes high interference to the HeNB, can be lowered to a level that is manageable by the HeNB. It is important that HeNBs exploit the sharable channels whenever possible as the number of non-shared

channels available for use in the femtocell may be less than the number of FUEs who desire a link. If there are FUEs who cannot be serviced by a shared channel with a MUE, we assume that HeNBs measure the interference I_k on a given channel C_k. We assume each HeNB measures the interference on all of the N_c channels and orders them with respect to their interference powers. Thus without loss of generality, we consider each HeNB to maintain a set of channels $C_1 > C_2 > ... > C_{N_c}$ such that $I_1 < I_2 < ... < I_{N_c}$. Each HeNB can then assign the best non-shared channels to any of the users still requiring a link. If there are no channels in which a FUE can establish a link with its HeNB, then the user does not receive a channel and is considered to be in outage.

3.2.3 Successive Interference Cancellation

We utilize SIC as the means in which a MUE and a FUE can communicate with a femtocell access point in a multiple access manner. SIC has been shown as a feasible technique in OFDM networks for both uncoded and coded systems. The performance of SIC depends largely on the channel estimation of the interfering signal so that it can be successfully subtracted from the received signal. For our system, we intend the macrocell user to be the primary user and the femto user to be the interfering user. The FUE is located very close the HeNB and is often slow moving or stationary. Thus channel estimation for a femto user link should be highly accurate. Following the methodology in [60], both the FUE and MUE transmit simultaneously and the femtocell access point regenerates the interfering signal and subtracts it from the received signal. After decoding the FUE's signal, the femtocell access point can then decode the macro user's signal. Using this strategy, we are able to achieve the joint decoding and both the MUE and FUE can achieve their desired SINR threshold while sharing a single channel.

3.2.4 Numerical Results

We now present the simulation results for the architecture described above with the network parameters in Table 3-2. As a comparison, we show results for two schemes. The first scheme we consider is one that uses the femtocell user power control and channel assignment described above but does not allow a MUE to handover to the femtocell. We denote this scheme as PC. The second scheme we consider is one that incorporates the macrocell to femtocell handover enabled by the successive interference cancellation in addition to the power control and channel assignment as in the PC scheme. We label the second scheme as SIC for convenience. In Figure 3-17 we show the percentage of macro users that handover to a nearby femtocell versus the average number of femtocells per macrocell. We can immediately see that as femtocells are added to the network, a percentage of the MUEs does handover to the femtocells. When the average number of femtocells reaches ten, we can see that the percentage of handovers levels off at about 30% and remains constant for the range of N_f shown. Recall that the decision rule that determines whether a MUE should handover to a FUE is a function of the interference at the HeNB as well as the pathloss between the MUE and the HeNB. As N_f increases, the number of femtocell users causing interference in the network also increases which in turn should decrease the threshold of the decision rule. However, due to the constant value the handover percentage maintains suggests that the dominating factor of the threshold is not the interference but rather the pathloss of the channel. Due to the distance based pathloss model and the uniform distributions of the users, there will be an average pathloss realized per link in the network which will upperbound the probability of a handover occurring. If we were to change the value of γ, the pathloss exponent for the MUE-HeNB link, we would be able to realize different values in the handover probability.

System Parameters	Value
Average number of femtocells (N_f)	[0, 50]
Number of channels (N_C)	25
Number of macro users (M)	25
Number of femto users per femtocell (F)	2
Minimum macro user SINR (β_M)	20 dB
Minimum femto user SINR (β_F)	25 dB
SINR margin at the BS (κ_M)	3 dB
SINR margin at the FAP (κ_F)	0.5 dB
Noise power (σ_n^2)	-103 dBm
Macrocell/femtocell radius (r_m, r_f)	400m, 30m
Pathloss exponents (α, γ, ϕ)	2, 3, 3.5

Table 3-2: Simulation Parameters

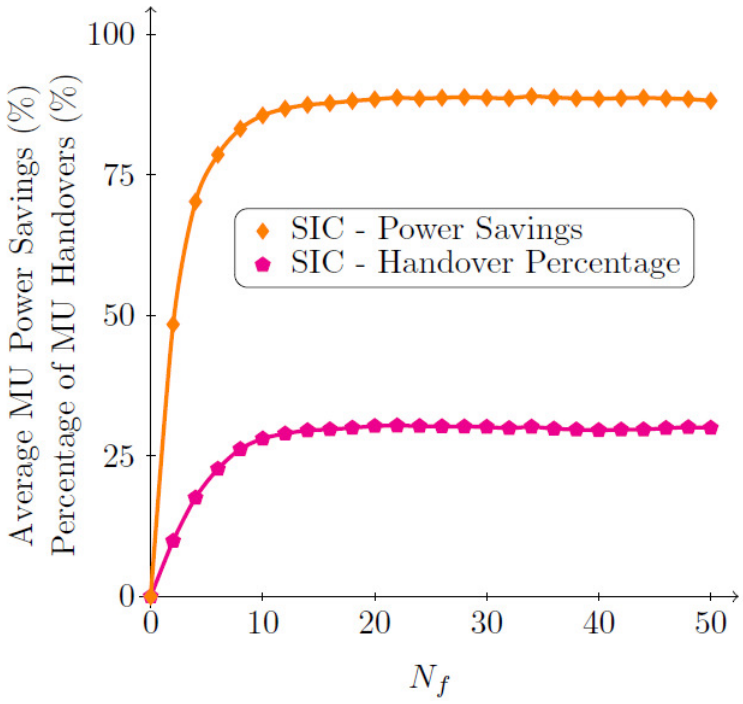

Figure 3-17: Average number of macro user handovers and their corresponding average power savings vs. the average number of femtocells per macrocell. SIC is used to allow for a macrocell user and femtocell user to share a common channel.

We mentioned above that as macro users access a nearby HeNB rather than the MeNB, they will be able to lower their transmit power. Also in Figure 3-17, we plot the average transmit power savings for a macrocell user in the network versus the average number of femtocells. We can immediately notice that the shape of the power savings curve is identical to the curve for the percentage of macrocell user handovers that occur. Intuitively, this makes sense that the percentage savings will be proportional to the number of handovers. What is interesting to note however is the amount of savings that are realized. For the 30% handover probability, a corresponding 90% of power savings is realized. Thus, even though only a small percentage of the MUEs actually handover, the reduction in their transmit power is significant enough to realize large savings as a whole for the network.

We have just shown that allowing MUEs to access a nearby HeNB rather than the MeNB can result in significant gains from the perspective of a given macrocell user. Gains are also realized from the FUEs perspective as well. As MUEs lower their transmit power to connect to a nearby HeNB, the amount of interference they cause to other femtocells also decreases. This will in turn increase the likelihood of FUEs in those other femtocells being able to establish a link. In Figure 3-18 we plot the average number of femtocell users who are able to maintain a link at the required SINR with their corresponding HeNB. We show curves for both the PC scheme without the handover process and the SIC scheme that allows the handover to occur. We can clearly see that the SIC scheme outperforms the PC scheme and at high values of N_f, large gains in the number of users served are realized. We also note that at smaller values of N_f, the PC scheme's performance decays at a faster rate than SIC. Then around $N_f = 25$, the two schemes begin to decay at the same rate. As more femtocell users are served in the network, we will see additional gains in terms of network throughput. Recall that the M macro users are always guaranteed a channel of at least an SINR level of β_M from either the MeNB or a nearby HeNB. Thus, the macro user component of the sum rate will always be equal to $M \log(1+\beta_M)$ whether or not the femtocell network is present. Any gains in the sum rate will come from the additional FUE links that are being added to the network. Due to the interference management in the femtocells, femto user links are power controlled to SINR levels of $\kappa_F \beta_F$. When calculating the rates of the links however, we consider that the additional power used in the power control does not contribute any extra rate over the link. Thus, we can formally write the rate for a given femtocell user i as:

$$R_{FU_i} = \begin{cases} \log(1+\beta_F), & if \quad \beta_F \le SINR_{FU_i} \le \kappa_F \beta_F \\ 0, & otherwise \end{cases} \tag{3.16}$$

where FUEs are considered to be in outage if they cannot meet their required SINR. Having defined the rate per femtocell user, and knowing that there are on average N_f femtocells per macrocell and F femto users per femtocell, we can write the sum rate gain as:

$$R_{gain} = \frac{1}{M \log(1+\beta_M)} \sum_{i=1}^{FN_f} R_{FU\,i} \tag{3.17}$$

where the gains from the femtocell component of the sum rate are calculated as a percentage of the sum rate of the macrocell user only network. We can derive an upper bound on the sum rate gain from the scenario that all FUEs in each femtocell are able to satisfy their required SINR threshold with their corresponding femtocell access point. We know that there are on average FN_f femtocell users per macrocell, thus it is easy to show that the maximum sum rate gain satisfies the condition:

$$R_{gain} < FN_f \log(1+\beta_F) = R_{\max} \tag{3.18}$$

where the upper bound is linear in the average number of femtocells per macrocell. In Figure 3-19 we plot the average sum rate gain of the network for the two schemes considered above. In addition, we plot the upper bound on the sum rate gain. We can immediately see that the SIC scheme outperforms the PC scheme in terms of the sum rate gain achieved. As N_f increases, we see that the amount of gain of the SIC scheme over PC scheme also increases. We further note that the SIC scheme is significantly closer to the maximum sum rate gain than the PC scheme for all values of $N_f > 10$.

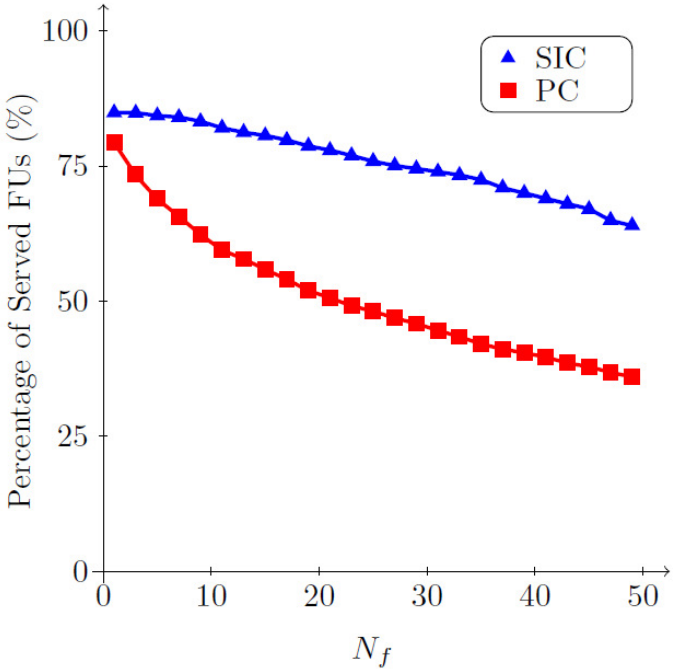

Figure 3-18: Average number of femtocell users who are served by their corresponding femtocell access points versus the average number of femtocells per macrocell.

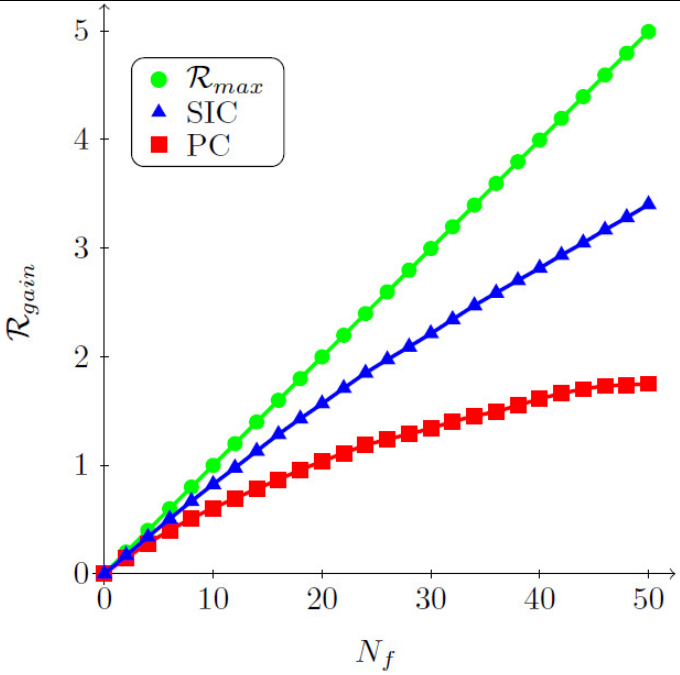

Figure 3-19: Average sum rate gain of a power control (PC) scheme that does not allow macro user handover versus the same scheme that does allow macrocell user handover using SIC

3.2.5 Conclusions

We have analyzed practical femtocell architecture and quantified both user level and network level gains that can be achieved. We developed a femtocell user power control scheme that relies on minimal coordination from the macrocell to operate. A channel sensing scheme was used to assign femtocell users with channels that exhibit low interference levels. Simulations show that this scheme achieves good performance in terms of sum rate gain and in the number of femto users served in the network. We then developed a decision rule in which macro users could connect to a nearby femtocell access point rather than the MeNB. We utilize successive interference cancellation to allow femto and macro users to share a common channel and connect simultaneously to the femtocell access point. Using this second scheme, we show that even more gains from both the user and network perspectives can be realized over the first scheme. Taking $N_f = 35$ as an example, 30% of macro users joined a nearby femtocell which in turn yielded an average power savings of 90% per macro user, 30% more femtocell users being served by femto access points, and almost a 100% increase in the sum rate gain. Thus, with a relatively small change to the structure of the macrocell network, significant gains for both macrocell and femtocell users as well as the network as a whole can be realized.

3.3 Layer 2 Hand over

3.3.1 Problem Statement

While the coexistence between femtocell and macrocell in the same spectrum is expected to substantially increase the spectral efficiency, a number of challenges lie ahead which can undermine this coexistence. Among these challenges, the interference between macro and femtocells is a major concern, especially when those systems are non-cooperative [61]. Thus, femtocells need to self-organise to control the interference generated towards the macrocell layer, and also neighbouring femtocells. In this direction, the Handover (HO) behaviour is critical to the support of seamless QoS when a mobile user traverses cell boundaries. Hard HO procedure is used in 3GPP LTE for both intra-eNB handover and inbound/outbound handover between eNBs and HeNBs. Each handover process comprises a set of parameters to control the HO procedure, such as measurement period, hysteresis and time-to-trigger. To support seamless mobility across the cell boundaries, “too early” and “too late” handover triggers should be avoided. If a handover is initiated before it approaches the actually required crossing point, the UE may hand over back to the source cell within a short period, causing the so called “ping-pong” effect. If a handover is initiated after the UE has moved out of the coverage of the current serving cell, the radio link with the current serving

cell may be disconnected before a handover can be completed. In this case, radio link failure recovery procedure has to be engaged which may lead to a significantly increased service interruption time. While recent work [69][70][71] has evaluated the impact of different handover parameters on the performance in terms of HO failure rate and HO number for LTE macrocells via computer simulation, little work has been done for femtocell scenarios. Furthermore, an analytical framework to model HO behaviour without resorting to time-consuming computer simulation is necessary.

3.3.2 Open, Closed and Hybrid Access Femtocells

In the concept of TDD-underlaid femtocells is introduced and two mechanisms (centralized and distributed) for interference management, which are based on the graph colouring theory, are proposed. Results revealed the efficacy of the TDD-underlay approach to cope with interference among adjacent femtocells while using local information only. We intend to extend the TDD-underlay concept by incorporating a mechanism for jointly coordinating macrocell users when the macrocell UL band is shared. Such solution would have to address technical issues related to the open, closed and hybrid access policies in femtocell deployments [62]-[65].

3.3.2.1 System Model

Macrocell operates in FDD mode, where UL and DL transmissions occur in two separate bands. Femtocells operate in TDD mode over the UL band of macrocells. The rationale behind the deployment of the UL band is that, when the eNB and HeNBs are far enough from each other, femto transmissions produce a limited interference at the eNB. The macrocell is underlaid with randomly distributed femtocell networks. MUEs are uniformly distributed over the macrocell deployment area. Transmitters use omni-directional antennas. In each femtocell site, four FUEs are randomly uniformly distributed. Finally, we assume perfect synchronization among all femtocells.

Let us consider UL femtocell transmissions within the macrocell uplink band. Let $|h_{j,i}^{(n)}|^2$ denote the channel gain between Femto UE j and HeNB i over carrier n. Moreover, let σ^2 be the variance of additive white Gaussian noise at HeNB i. The transmit power of Femto UE j over carrier n is denoted by $p_{j,i}^{(n)}$. Hence, the average Signal-to-Noise and Interference Ratio (SINR) experienced by HeNB i in carrier n is given as:

$$SINR_{i,j}^{(n)} = \frac{p_{i,j}^{(n)} \times |h_{i,j}^{(n)}|^2}{\sigma^2 + \underbrace{\sum_{k \neq j} p_{i,k}^{(n)} \times |h_{i,k}^{(n)}|^2}_{femto} + \underbrace{\sum_{m \neq i} p_{i,m}^{(n)} \times |h_{i,m}^{(n)}|^2}_{macro}} \quad (3.19)$$

where $p_{i,k}^{(n)}$ is the transmit power of neighbouring interfering femtocell k and $p_{i,m}^{(n)}$ is the transmit power of macrocell user m over carrier n.

Herein, we address the aforementioned TDD underlay concept to manage interference in macrocell-femtocell networks. Each femtocell carries out independent measurements over the whole spectrum and selects the least interfered subcarriers. In order to allow for a maximum number of simultaneous transmissions among femtocells, each HeNB constructs a map of interfering links based on which, it runs a list colouring scheduling algorithm and jointly schedules Femto UEs with a given duplexing method (i.e., UL or DL) over each used subcarrier and timeslot. We propose a hybrid access control policy in which highly interfering Macro UEs are absorbed inside a femtocell.

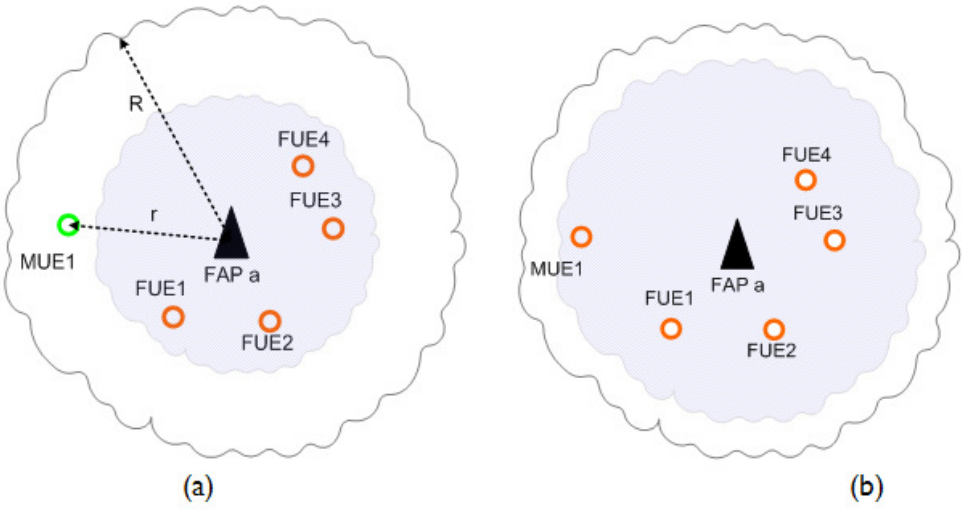

Figure 3-20: (a) The Macro UE$_1$ is within transmission range R, (b) The Macro UE$_1$ absorbed by femtocell a.

To tackle the problem of macro-to-femtocell interference, we propose the following procedure:

When in a given femtocell, a transmission link experiences an SINR lower than a predefined threshold γ for longer than a timeout τ , the algorithm is triggered.

1) The femtocell access point increases the transmit power on the interfered subcarrier.

2) The femtocell access point monitors if the adjustment was sufficient to restore its SINR above the threshold. If not, it estimates the distance r from the interfering Macro UE i (Figure 3-20 (a)).

3) If Macro UE i falls inside the maximum transmission range R of the femtocell access point, it is *absorbed* in a handover procedure (Figure 3-20(b)). Once absorbed, Macro UE i is scheduled in a TDD mode on its own original used subcarrier. In other words, when it is associated to the femtocell, the Macro UE benefits from a better SINR (since transmissions are coordinated by the same HeNB), at the expense of sharing resources with other Femto UEs.

4) Conversely, when Macro UE i is out of the transmission range ($r > R$), HeNB has to switch to another subcarrier (through an intra-handover procedure) and vacate the current one, in favour of Macro UE i .

3.3.2.2 Flow-chart of the proposed algorithm

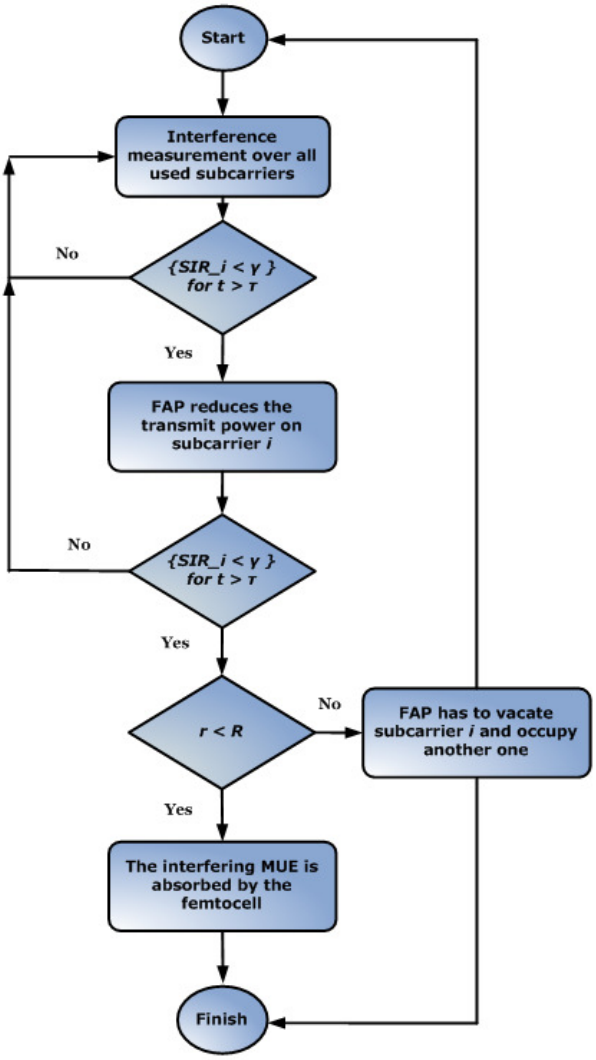

Figure 3-21: Algorithm chart for the proposed femtocell access policy.

3.3.2.3 Simulation Results

We evaluate the proposed algorithm through computer simulations. In the open access mode, a Macro UE associates with the femtocell that provides the best SINR, while in the closed access mode, CSG femtocells only serve their own subscribers. Finally, the hybrid approach allows a limited number of Macro UEs to connect to the underlay femtocell tier depending on the criteria defined above. The table below summarizes the assumed configuration parameters used throughout the simulations.

Parameter	Value
Number of macro users	100
Number of femto users per femtocell	4
Number of femto cells	64
Femto SINR threshold (γ)	10dB
Timeout τ	5 s
Femto UE transmit power (p)	20 dBm
Noise power (σ^2)	-104 dBm
Macro cell radius	2 km
Femtocell Max Tx range (R)	30m

Table 3-3: Considered simulation parameters

Figure 3-22 shows that the hybrid access provides a trade-off between open and closed access policies as the absorption of macrocell users only happens under particular conditions. In terms of outage probability (i.e., rate < 300kbps for the Macro UE over one physical resource block of 180 KHz), a femtocell with closed access policy mainly suffers from excessive interference brought by close Macro UEs on the UL. Conversely, an open access policy may require a large number of inter-femtocell handover which triggers higher outage probabilities, because of excessive number of handover failures. The proposed hybrid solution offers two main benefits: (a) it provides a better QoS for Macro UEs at the cost of sharing its subcarriers and backhaul (b) it mitigates the interference from the Macro UEs and reduces the number of handovers resulting in lower outage probabilities as shown in Figure 3-23. For more information on the proposed approach, please see [66].

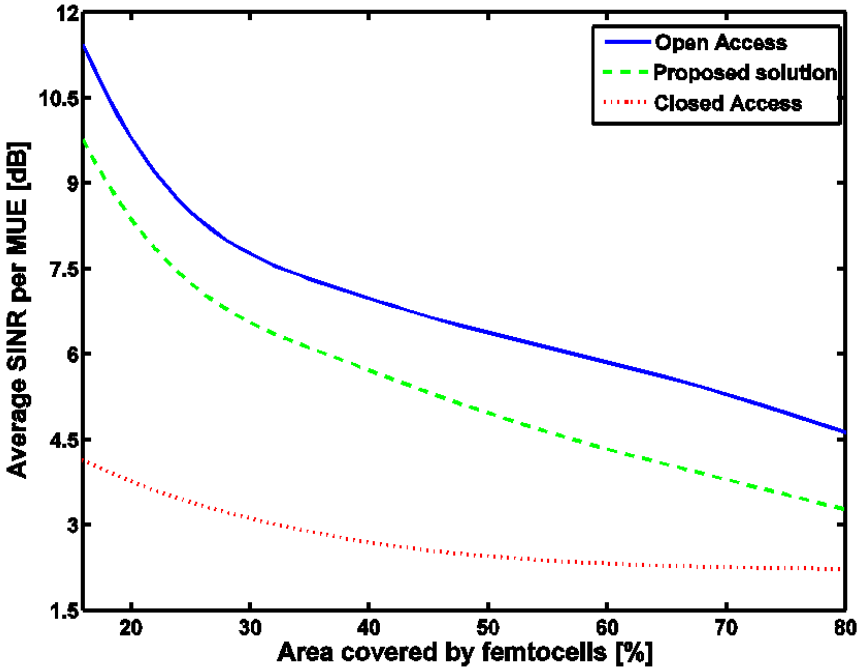

Figure 3-22: Average signal to interference plus noise ratio per Macro UE as a function of the density of indoor femtocells, in closed, open and hybrid femtocell access policies.

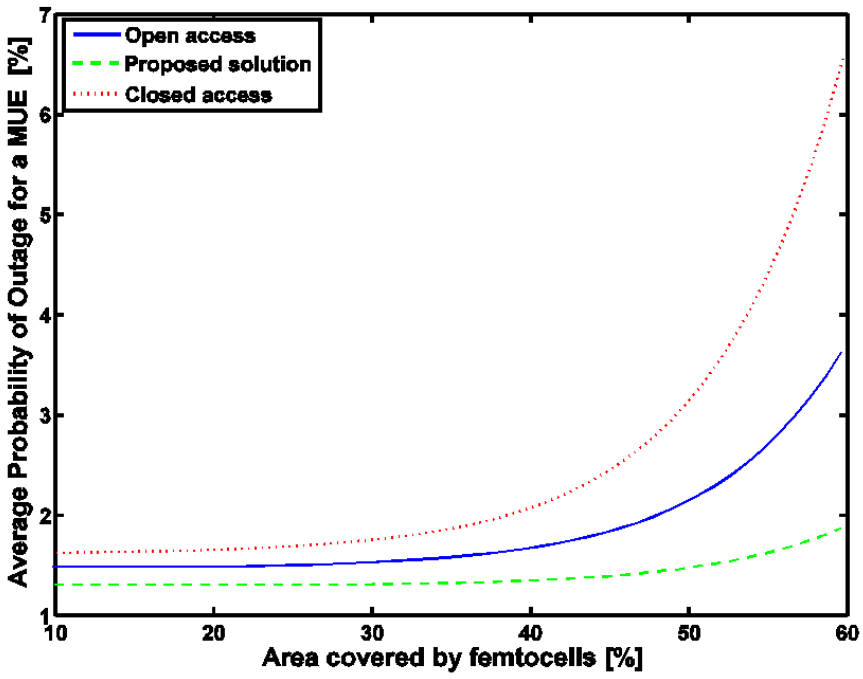

Figure 3-23: Average outage probability per Macro UE as function of the femtocell density in closed, open and hybrid femtocell access policies.

3.3.3 Handover Decision Optimization

In this section, we present an analytical study for inbound/outbound HO taking specific LTE/ LTE-A parameters and femtocell scenarios into account, highlighting important HO parameters via this analytical study.

3.3.3.1 System Model

We consider a hierarchical cell structure in which a HeNB is deployed within the coverage of a macro base station (m-BS). For inbound mobility scenario, a mobile station is moving from the m-BS to the HeNB in a straight line at constant velocity v. For outbound mobility scenario, the moving direction is reversed. The two base stations are separated by a distance D. The Received Signal Strength (RSS) measured by the mobile station is affected by path loss, shadowing and fast fading effect. A Layer 3 filter is used in LTE to filter out the effect of the signal fluctuation and measurement errors [67][68]. The filtered measurement is updated every measurement period T_s at the UE as the output of a first-order Infinite Impulse Response (IIR) filter:

$$y_i[k] = (1-a)\,y_i[k-1] + a x_i[k] \tag{3.20}$$

where $x_i[k]$ is the latest received measurement result from the physical layer for base station i, $y_i[k-1]$ is the last filtered measurement result, and $y_i[k]$ is the updated filtered measurement result used for evaluation of reporting criteria. $a = \frac{1}{2^{K/4}}$ is the forgetting factor, where K is the filter coefficient. Similar to previous work [72][73], fast fading effect is assumed to be averaged out by filtering since it has a much shorter correlation distance compared to shadow fading.

As the filtered measurement is updated every measurement period T_s, a discrete-time approach is applied following the procedure in [72]. The moving distance between the two consecutive measurement periods d_s is determined by $d_s = v \cdot T_s$. Let k denote the kth measurement period from the starting base station, the RSS at a base station i (i denotes either eNB or HeNB), when a mobile is at a distance kd_s from the starting base station, is formulated as:

$$x_i[k] = m_i[k] + w_i[k] \tag{3.21}$$

where $m_i[k] = P_{i,t} - PL_i[k]$ models the impact of path loss on the RSS, in which $P_{i,t}$ denotes the transmission power of the base station i and $PL_i[k]$ denotes the path loss from the base station i at the distance kd_s, and $w_i[k]$ represents the log-normal shadow fading with mean zero and variance $\sigma_{w_i}^2$ at the distance kd_s. The autocorrelation function of the process $\{w_i[k]\}$ is modelled by [74]:

$$R_{w_i}(l) = \sigma_{w_i}^2 e^{(-|l|d_s / d_{0,i})} \tag{3.22}$$

where $d_{0,i}$ is the correlation distance for base station i, which determines how fast the shadowing correlation decays with the distance. According to the model in [72], the shadow fading process can be represented as a first-order autoregressive process by:

$$w_i[k] = b_i w_i[k-1] + v_i[k] \tag{3.23}$$

where $b_i = \exp(-d_s / d_{0,i})$ and $v_i[k]$ is a zero-mean stationary white Gaussian noise process with variance $\sigma_{v_i}^2 = (1-b^2)\sigma_{w_i}^2$. By converting 0 into Z-domain as an input signal $X_i(z)$ and converting L3 filtering function 0 into Z-domain as a transfer function $H_i(z)$, the output response in Z-domain is given by $Y_i(z) = H_i(z)X_i(z)$. By taking the inverse Z-transform, the filtered signal is obtained as:

$$\begin{aligned} y_i[k] = {} & (1-a+b_i)\,y_i[k-1] - (1-a)b_i\,y_i[k-2] \\ & + a m_i[k] - a b_i m_i[k-1] + a v_i[k] \end{aligned} \tag{3.24}$$

Following a similar approach as in [72], the statistical properties of the process $\{y_i[k]\}$ can be derived. The details are omitted here due to the limitation of the space.

The difference in the filtered measurements is represented as:

$$y_\Delta[k] = y_i[k] - y_j[k] \tag{3.25}$$

where $y_i[k]$ and $y_j[k]$ denote the filtered RSS from source base station and destination base station

along the moving trajectory, respectively. The handover from i to j will be triggered at interval k if the following criterion is satisfied:

$$y_j[k-n]-y_i[k-n]>H \ \ (y_\Delta[k-n]<-H), \qquad \forall n\in\{0,1,...,\mathrm{TTT}\} \tag{3.26}$$

where H is the hysteresis and TTT is the Time-To-Trigger (TTT) window. This implies that the handover will be triggered only if the RRS from j is better than the one from the serving base station by a value of H and this condition is satisfied for the next consecutive TTT measurement periods. Both the hysteresis and the TTT have been used in 3GPP to reduce the effect of the signal fluctuation. And both can be set to zero to enable fast HO triggering, which means that the handover will be triggered immediately as long as the RSS from another base station is better than the current serving base station. As the HO trigger is determined by a series of consecutive filtered measurement results, we model it as a multivariate Gaussian random variable $\mathbf{y}_\Delta=\{y_\Delta[k-L], y_\Delta[k-L+1],...y_\Delta[k]\}$ with the Probability Density Function (PDF) given by:

$$f_{\mathbf{y}_\Delta}(\mathbf{y}_\Delta)=\frac{1}{(2\pi)^{(L+1)/2}|\boldsymbol{\Sigma}|^{1/2}}\exp\left(-\frac{1}{2}(\mathbf{y}_\Delta-\mathbf{m})'\Sigma^{-1}(\mathbf{y}_\Delta-\mathbf{m})\right) \tag{3.27}$$

where $\mathbf{m}$ is the mean vector and $\boldsymbol{\Sigma}$ is the covariance matrix. Both can be derived based on 0.

3.3.3.2 Handover Analysis

Following the procedure used in [73], let $P_{i|j}[k]$ denote the probability of handover from base station j to i at interval k and $P_{j|i}[k]$ vice versa. Let $P_{ho}[k]$ denote the probability that a handover occurs at interval k, $P_i[k]$ and $P_j[k]$ denote the probability of the mobile being assigned to base station i and j at interval k, respectively. Assuming a handover can be completed within one measurement period, $P_i[k]$, $P_j[k]$ and $P_{ho}[k]$ can be recursively calculated as:

$$\begin{aligned}
P_i[k] &= P_i[k-1](1-P_{j|i}[k])+P_j[k-1]P_{i|j}[k]\\
P_j[k] &= P_i[k-1]P_{j|i}[k]+P_j[k-1](1-P_{i|j}[k])\\
P_{ho}[k] &= P_i[k-1]P_{j|i}[k])+P_j[k-1]P_{i|j}[k]
\end{aligned} \tag{3.28}$$

Let $I[k]$ and $J[k]$ denote the event that the mobile is assigned to base station i and j at interval k, respectively. The conditional probability $P_{i|j}[k]$ and $P_{j|i}[k]$ can be calculated in the following:

$$\begin{aligned}
P_{i|j}[k] &= \frac{P\{J[k-1],I[k])}{P\{J[k-1]\}}\\
&= \frac{P\{y_\Delta[k-N-1]>-H, y_\Delta[k-N]<-H,..., y_\Delta[k]<-H\}}{1-P\{y_\Delta[k-N-1]<-H, y_\Delta[k-N]<-H,..., y_\Delta[k-1]<-H\}}
\end{aligned} \tag{3.29}$$

$$\begin{aligned}
P_{j|i}[k] &= \frac{P\{I[k-1],J[k])}{P\{I[k-1]\}}\\
&= \frac{P\{y_\Delta[k-N-1]<H, y_\Delta[k-N]>H,..., y_\Delta[k]>H\}}{1-P\{y_\Delta[k-N-1]>H, y_\Delta[k-N]>H,..., y_\Delta[k-1]>H\}}
\end{aligned} \tag{3.30}$$

3.3.3.3 Analytical results

In this section, we present the numerical results derived from the analytical model. A femto BS is deployed in an outdoor environment. The values of the model parameters are given in Table 3-4. The results are presented for inbound mobility scenario, where a mobile station is moving from a macro BS towards a femto BS. The outbound mobility scenario can be analyzed following the similar method.

Parameter	Value
Pass loss model	$PL = 15.3 + 37.6\log_{10}(d)$
Shadowing standard deviation for macrocell	8 dB
Shadowing standard deviation for femtocell	6 dB
Shadowing correlation distance for macrocell	50 m
Shadowing correlation distance for femtocell	30 m
Measurement period	500 ms
UE moving speed	1 m/s
Distance between macro BS and femto BS	500 m

Table 3-4: Parameters for numerical evaluation

We first set the hysteresis $H = 1$ and the TTT window $TTT = 0$ and evaluate the impact of the filter coefficient K. As shown in Figure 3-24, the assignment of the MS to the femto BS is delayed by a high value of K since a high value of K implies a high weight for the previous measurement result when using the averaging filter. The HO delay may cause the HO failure. However, by using a high value of K, the impact of the measurement fluctuation can be mitigated and the HO probability can be greatly reduced as shown in Figure 3-25. This implies that the number of total HOs and unnecessary HOs is reduced. There is always a trade-off between the HO delay and the number of HOs. We then fix the filter coefficient $K = 4$ and the TTT window $TTT = 0$ to evaluate the impact of the hysteresis H. Similar results are found in Figure 3-26 and Figure 3-27. A high value of H may reduce the HO probability at the cost of the delayed HOs. Finally, we fix the filter coefficient $K = 4$ and the hysteresis $H = 1$ to evaluate the impact of the TTT window. Again, the results shown in Figure 3-28 and Figure 3-29 indicate that a high value of TTT can reduce the chance that a HO is unnecessarily triggered by the measurement fluctuation. An interesting point is that compared to the hysteresis parameter, the TTT window cause less HO delay.

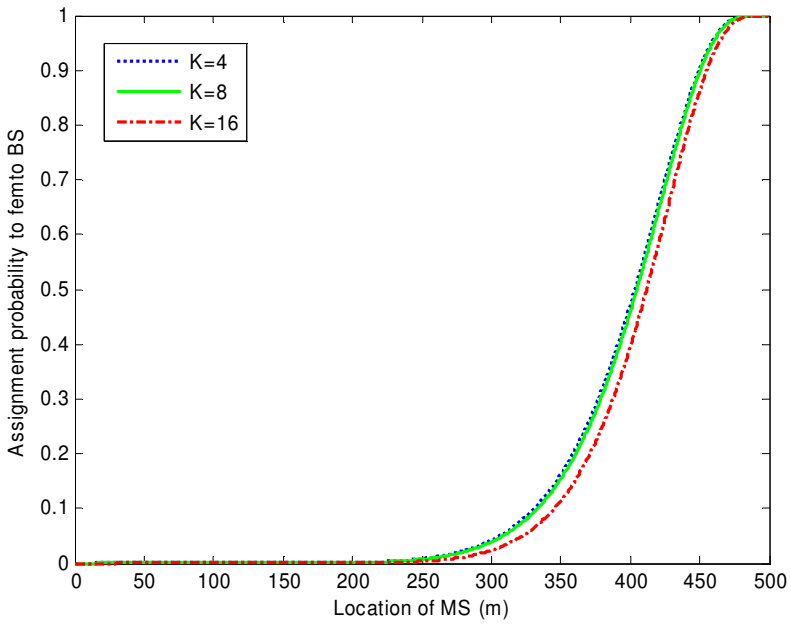

Figure 3-24: Impact of filter coefficient on assignment probability to femto BS

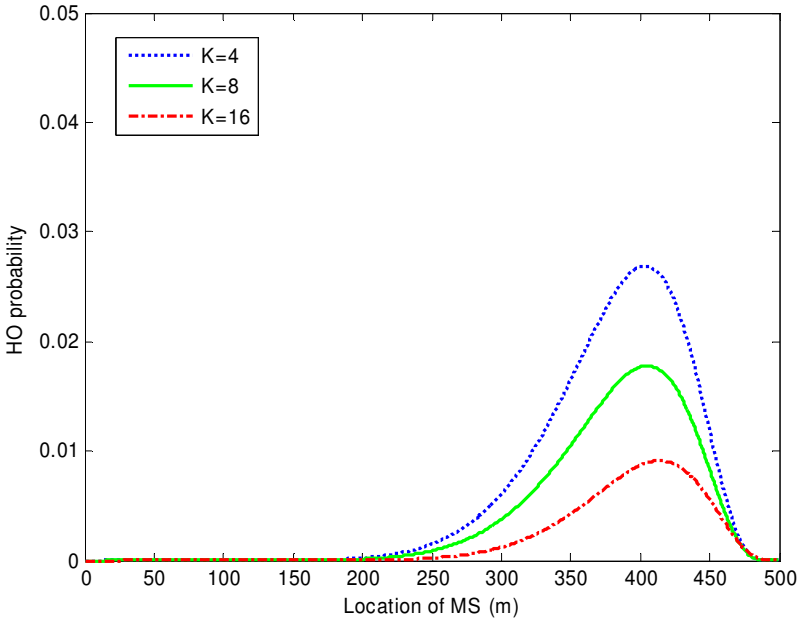

Figure 3-25: Impact of filter coefficient on HO probability

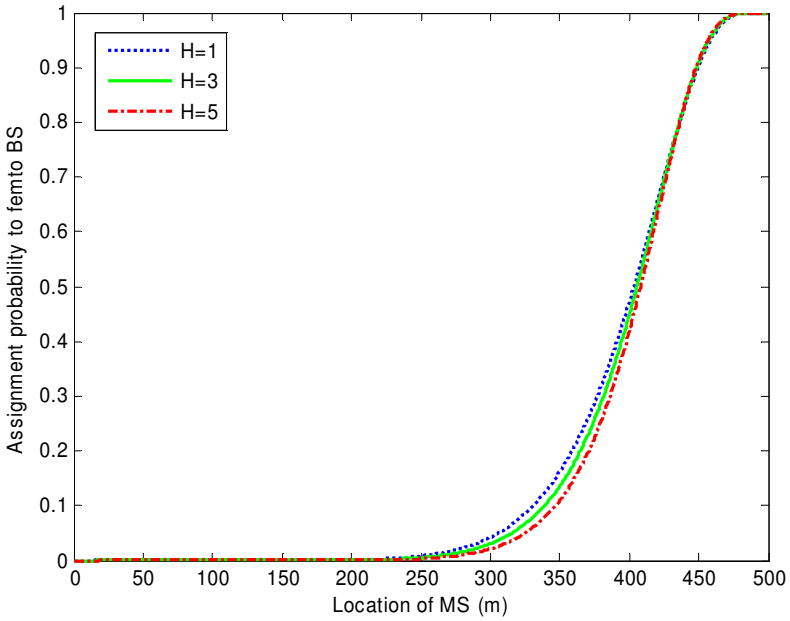

Figure 3-26: Impact of hysteresis on assignment probability to femto BS

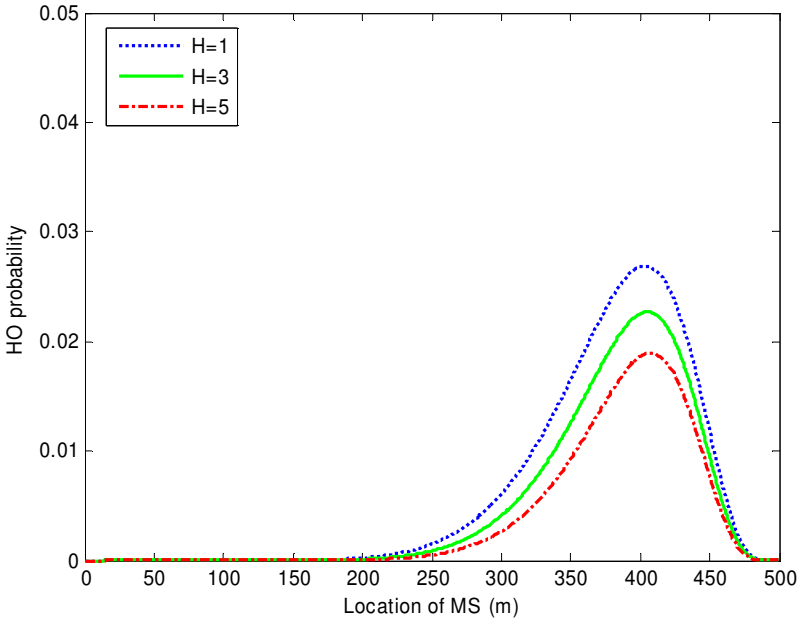

Figure 3-27: Impact of hysteresis on HO probability

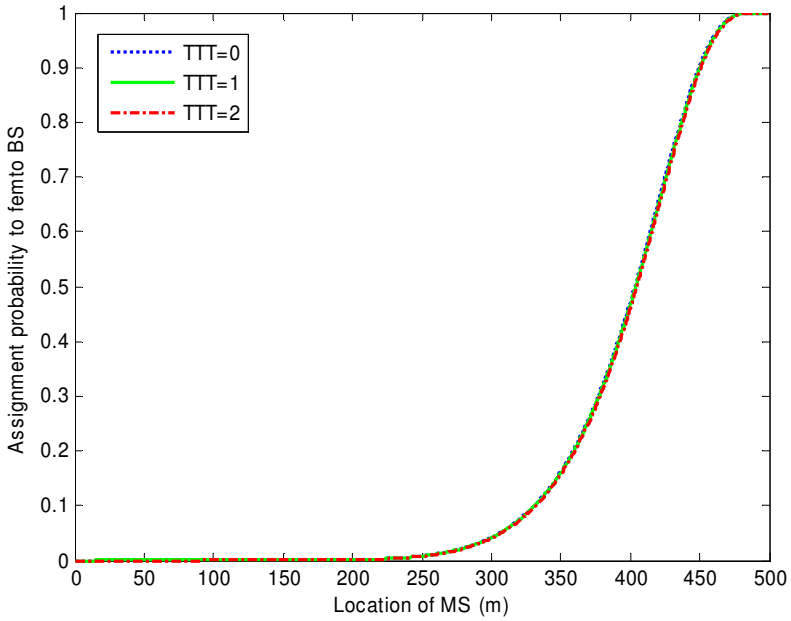

Figure 3-28: Impact of TTT window on assignment probability to femto BS

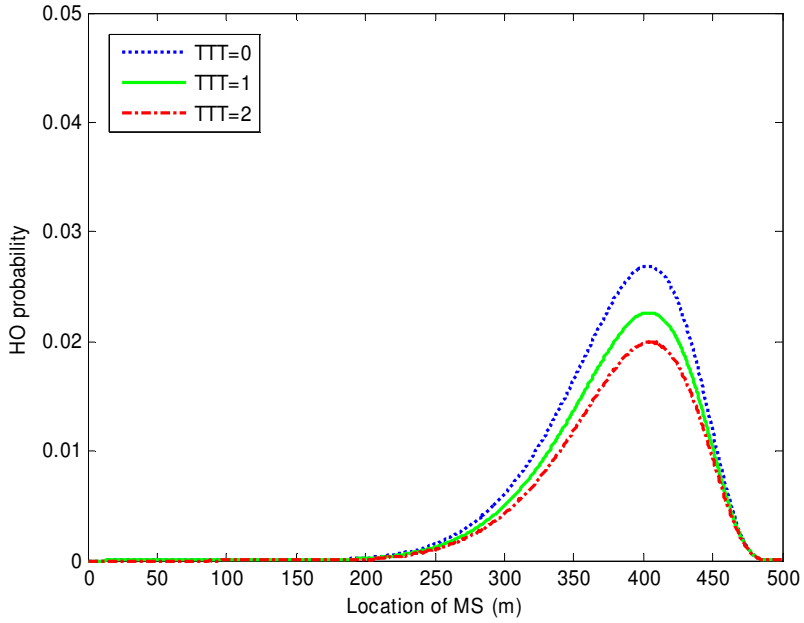

Figure 3-29: Impact of TTT window on HO probability

3.3.4 Conclusions

In this section, we have investigated different strategies of femtocell access policies, namely the closed, open and hybrid policies. It turns out that interesting trade-offs exist in which open access is not always the best and optimal strategy. In fact, the hybrid approach is shown to be preferable in terms of outage probability at the expense of lower average SINRs. Furthermore, the impact of various HO parameters has been evaluated via an analytical model. Due to the plug-and-play nature and large deployment of femtocells, the legacy subjective configuration of HO parameters based on long-term field statistics is not feasible. It is crucial to self-optimize HO parameters in order to minimize the number of unnecessary handovers and reduce HO delays. The developed analytical model provides an offline tool to pave the way in this direction in line with 3GPP assumptions as demonstrated for some critical parameters.

3.4 MIMO and High Order Modulation for Femtocell in HetNet Deployment

3.4.1 Problem Statement

An average spectral efficiency of 8bits/s/Hz over the whole bandwidth is quite difficult to achieve in downlink considering a femtocell transmission power of 10dBm. In a suburban scenario where no femto-femto interference occurs, a 4x4 antenna configuration is needed to reach this target (8.18bits/s/Hz) when considering classical MMSE receiver at the user equipment side [77].

Going from suburban to urban environment emphasises the femto-femto interference which can be moderated to highly aggressive according to the femtocell model employed [78] (and the femtocell deployment probability). By allocating the whole spectrum to the femtocell users, even the 4x4 configuration standalone femtocell does not provides the targeted spectral efficiency (4.95bits/s/Hz for the Dual-Stripes model with 10% femtocell deployment ratio) due to interference [77]. This target may be achieved using advanced receiver at the user equipment side, e.g., receiver based on spatial interference cancellation such as iterative successive interference cancellation also known as turbo equalisation (9.46bits/s/Hz for Dual-Stripes model with 10% femtocell deployment ratio in case of perfect spatial interference cancelling which may be reached after convergence of the turbo process). However, the exploitation of the whole spectrum by the femtocell at any time may also lead to severe macro-femto interference in Heterogeneous Network (HetNet) with femtocells deployed under a CSG access policy. This macro-femto impact was not reflected in the simulations performed in [77] where no macrocell users were forced to be in the vicinity of a femtocell.

To reduce the interference (both for femto and macro users), the frequency domain nature of the LTE radio access has been intensively exploited in BeFEMTO through partitioning schemes such as SFR or FFR at the macrocell or at the femtocell level as described in this final deliverable. However, reducing the bandwidth allocated to one user also reduces its throughput even though its spectral efficiency is improved by virtue of higher Signal to Interference-plus-Noise Ratio (SINR). If the use of multiple antennas which increases the maximum number of spatial multiplexing streams to be sent can compensate the bandwidth reduction (if the radio conditions are good enough after partitioning), it has to be kept in mind the cost and the form factor of a femtocell which cannot integrate 8 antennas as actually proposed in LTE. However, due to the low level of power envisaged (10dBm) the linearity of the power amplifier should permit the use of modulation order higher than the 64-QAM.

In this subsection, we present a downlink LTE-compliant resource allocation algorithm at the femtocell level which only serves one user at a time over a (dynamic) part of the total available bandwidth. The blank created in the frequency domain can then be exploited either by the surrounding macrocells or femtocells for their own scheduling. This direct loss in the throughput is compensated by the use of multiple antennas enabling more spatial streams if the channel conditions permit it. A fully LTE-compliant version of the RRM algorithm boosts the power of the subcarriers carrying the data transmission based on the maximum specified value (factor 2), while a beyond LTE Release-11 version allocates the totality of the 10dBm transmit power to these subcarriers and introduces higher modulation order (namely the 256-QAM).

3.4.2 System model

In LTE, the downlink radio access relies on OFDMA. Due to the OFDM nature of the access, the resources to allocate are subcarriers spaced out by 15kHz, where:

12 consecutive subcarriers form a Resource Block (RB),

N_{RB} consecutive RBs form a Resource Block Group (RBG),

N_{RBG} consecutive RBGs form a subband,

N_{SB} consecutive subbands form a bandwidth part.

The LTE system bandwidth defines N_{RB} (called P in [81]), N_{RBG} (the product N_{RB}* N_{RBG} is called k in [81]) and N_{SB} (called Nj in [81]). Figure 3-30 details the bandwidth repartition in a 10 MHZ LTE system. The bandwidth effectively available for allocation is made of 50 RBs (9MHz).

Assuming a Type 0 allocation, one User Equipment (UE) can receive information on the data PDSCH channel on any set of RBGs signalled by a bitmap on the control PDCCH channel [81]. This resource allocation is made at the base station.

To perform the scheduling operation, one LTE base station requests that each attached UE reports specific feedback related to the configured transmission mode. Assuming the classical MIMO closed-loop spatial multiplexing, namely transmission mode 4 in LTE standards, this feedback is made of three components [81]:

- **Rank Indicator** (RI): RI defines the number of independent streams a UE can support (decode). It cannot be greater than the minimum number of transmit (base station side) and receive (UE side) antennas.
- **Precoding Matrix Indicator** (PMI): PMI is the index of the precoding matrix to apply which splits the supported streams defined by RI over the base station transmit antennas.
- **Channel Quality Indicator** (CQI): According to the PMI and RI, the streams are gathered into codewords. One CQI reflects the modulation and coding schemes to apply to a codeword ensuring a transmission of it with a block error rate lower than 10%. To lower the signalling, a maximum of two codewords (thus, CQIs) can be transmitted to one UE no matter the antenna configuration.

The minimum granularity of the reporting is usually the subband [81], except the aperiodic M-best subband reporting (mode 2-0 and 2-2) which works with RBGs.

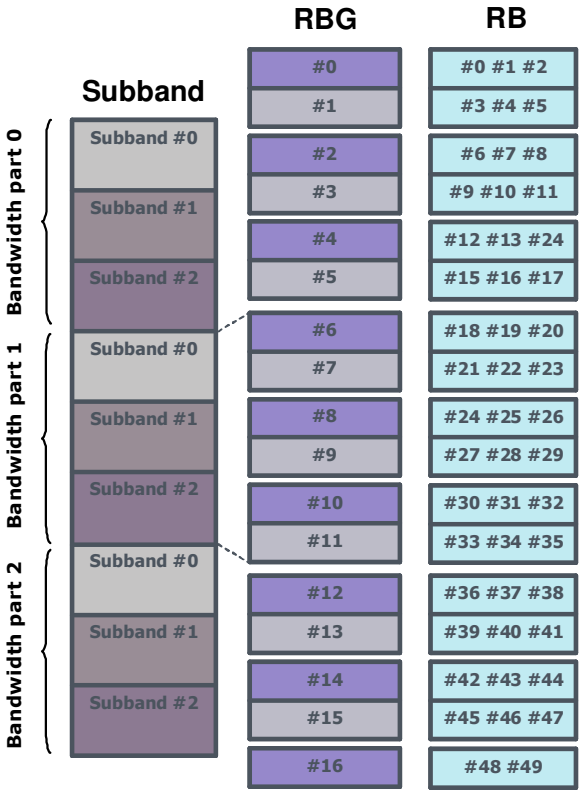

Figure 3-30: Bandwidth repartition for an LTE 10Mhz system

The highest modulation currently specified in LTE is the 64-QAM [81]. We propose to introduce the 256-QAM since FUEs usually experienced higher SINR values. In system level simulations, the truncated Shannon bound can be used as a link to system interface to derive the spectral efficiency from the effective SINR, which comes from the compression of the SINRs computed on the allocated subcarriers [82]. This bound is given by:

$$\eta_t = \begin{Bmatrix} \min(\eta_{\max}, \alpha \log_2(1+SINR) & SINR_t > SINR_{\min} \\ 0 & SINR_t \le SINR_{\min} \end{Bmatrix}, \quad (3\text{-}31)$$

where usually $\alpha = 0.6$, $\eta_{\max} = 4.4$ and $SINR_{\min}(dB) = -10$ for the downlink [83]. We extend this bound by using $\eta_{\max} = 6.4$, which corresponds to a 256-QAM associated with a 4/5 coding rate. Figure 3-31 gives the classical truncated Shannon bound as well as our extended version:

We consider an LTE downlink macrocell/femtocell co-channel deployment. Within this HetNet, the femtocells apply an independent CSG access policy. This means that the Macrocell User Equipment (MUE) can only be connected to a macrocell base station (eNB in LTE) while a Femtocell User Equipment (FUE) can be attached to either a macrocell or its CSG femtocell (called Home eNB in LTE) depending on it radio channel conditions. We assume that the 256-QAM is supported by all equipments within the HetNet. According to LTE, the scheduling is performed every millisecond or Time Transmit Interval (TTI).

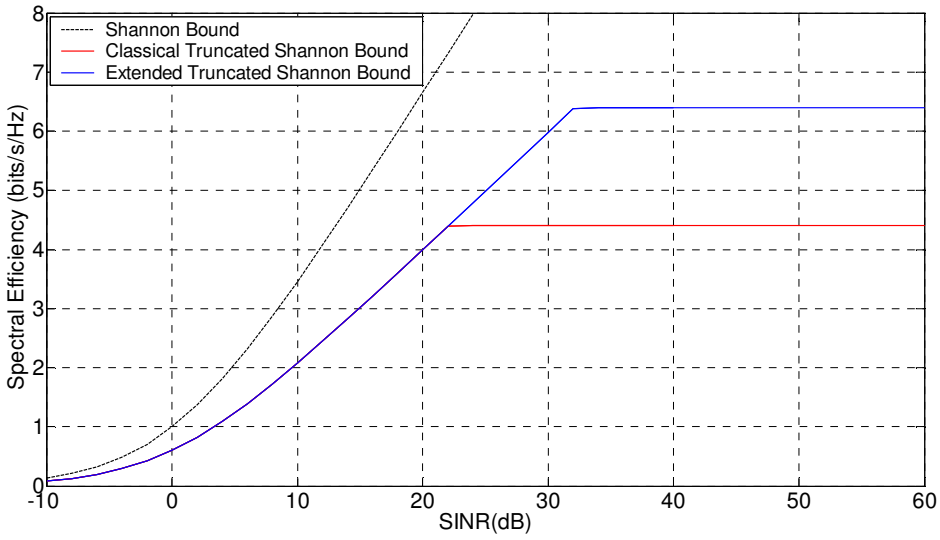

Figure 3-31: Truncated Shannon bound

3.4.3 Proposed algorithm

The femtocell resource allocation algorithm only schedules one user at a time on its data channel (known as PDSCH). By doing so and adopting three symbols for the control channel (known as PDCCH), we can rely on a sparse allocation of the PDCCH (as evocated section 2.1.2) to assume a perfect decoding of the downlink control information at both the macro and femtocell level.

Based on an exhaustive reporting on all subbands (made possible using the aperiodic reporting higher-layer-configured mode 3-1 [81]), the femtocell associates to each attached mobile the set of its N best subbands. The set size is initialised at (roughly) half the bandwidth size keeping the subband split specified in LTE standards (e.g., since a LTE 10MHz bandwidth is divided into 9 subbands, $N = 4$ in this case).

Since only one user is scheduled at a time (to leave blank space for other cell users) on half the bandwidth, the femtocell will not transmit at its full power when doing so. However, the specifications allow a user-specific power weighting of all the subcarriers carrying data for a given user. This power offset is signalled to the user through the parameter P_A [81], which can take 8 values, the maximum being $P_A = 3\text{dB}$ [84]. This means that we can only boost the power by a factor of 2 (which explains why we target a usage of half the bandwidth for the femtocell in order to stay close to the maximum transmission power).

Once the subbands determined and the power offset set to 3dB, the mobile is requested to perform its reporting on these subbands exclusively as the femtocell will schedule it on these resources and with this power boost (using the same aperiodic reporting mode 3-1 but restricted to those subbands only instead of the whole bandwidth).

If the report falls below a given threshold, the mobile is requested to perform a new report over the whole bandwidth while its $N-1$ best subbands will be selected for transmission. This process can go on until only one subband is left. Figure 3-32 depicts the proposed scheduling algorithm per user.

The strict compliancy with the LTE standard implies that the power boost on all the subcarriers carrying data could not exceed 2 even if the number of subbands in the set decreases (standard approach). We propose to go beyond by allowing more flexible P_A values such that the average transmit power stays the same using a part or the whole bandwidth (i.e. 10dBm, the BeFEMTO target). With this power flexibility, we also introduce the higher 256-QAM modulation in the downlink (extended approach). Since the transmit power is low (and equally distributed per antenna in a MIMO configuration), the linearity of the power amplifier required to support a 256-QAM at the femtocell transmitter should be acceptable.

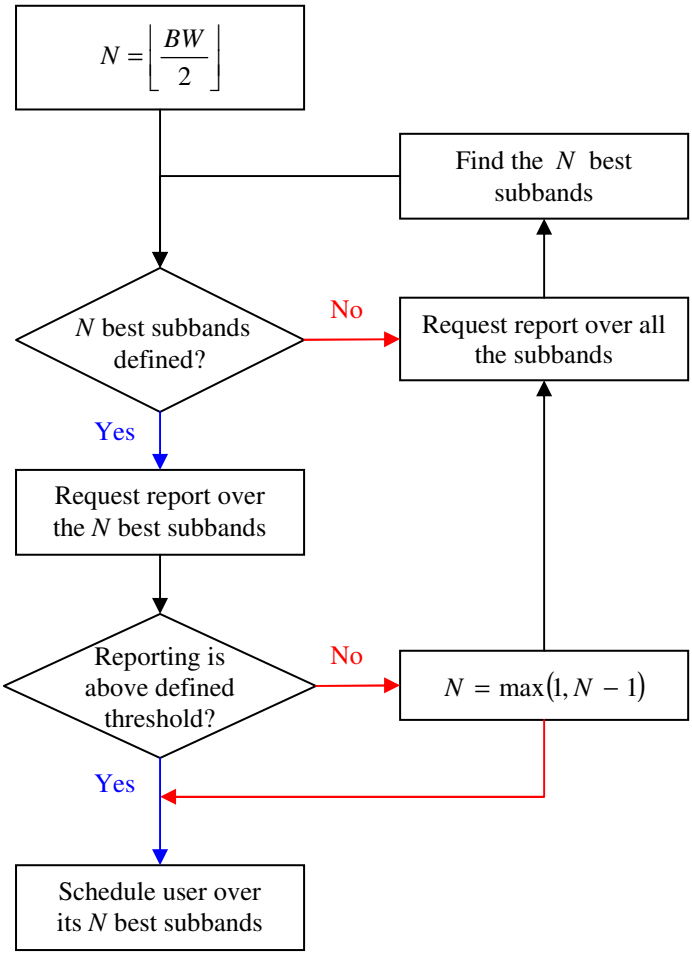

Figure 3-32: Per user scheduling approach

3.4.4 Simulation results

3.4.4.1 Simulation assumptions

In order to assess in a large scale environment the standard resource allocation mechanism and its extended version (with the use of high order modulation (up to 256QAM) and constant transmitted power), we rely on Monte-Carlo system-level simulations. We consider an urban HetNet deployment with femtocells deployed in a classical Dual-Stripes femtocell model (with only one floor) and applying a CSG access policy. Table 3-5 summarizes the macrocell layout, Table 3-6 describes the femtocell model and Table 3-7 gives the user equipment parameters.

Each macrocell handles 15 User Equipments (UEs) and we force an average of 35% of them to be dropped within a Dual-Stripes model to add macro-femto interference in top of the existing femto-femto one. The macrocell relies on a proportional fairness scheduling algorithm and allocates to one UE one subband (leading to 9 UEs scheduled per TTI for our 10MHz system).

For the femtocell scheduling, we compare the whole bandwidth attribution to one user per TTI with our proposed subband allocation mechanism following either the standard approach or the extended one (with high order modulation and fixed transmission power). The subband set size reduction is triggered when the user reporting indicates that only a rank one transmission with a spectral efficiency lower than 2 bits/s/Hz is supported.

We gather the spectral efficiency of the FUEs and the indoor MUEs (the most impacted by the femtocell deployment). We also collect the indoor MUEs outage ratio (proportion of times where one user equipment reports a CQI equals to zero) for both populations.

System Parameters		Value
Carrier Frequency		2GHz
Bandwidth		10MHz
Time Transmit Interval (TTI)		1ms
Macrocell Layout		**Value**
Inter-Site Distance		500m
Number of Sites		7
Number of Sectors per Site		3
Transmission Power (Sector)		46dBm
Antenna	Boresight Gain	14dBi
	Front to Back Ratio	25dB
	Angle Spread at -3dB	70°
	Gain	See [77], (6.1)
	Spacing (wavelength)	10λ
Pathloss		See [77], Table 6-8
Shadowing	Standard Deviation	8dB
	Correlation Inter-Site	0.5
	Intra-Site	1
Channel Profile		SCME UMa (See [85], line of sight not applied)
Number of UEs per Sector		15
Indoor Probability		0.35 (drop in a Dual-Stripes)
Scheduler		Proportional Fair
Resource Allocation per TTI		One subband per user
RI/CQI/PMI Reporting Period in TTI		5TTI
RI/CQI/PMI Processing Delay in TTI		1 (report issued at TTI by the mobile is available at TTI+1 at the cell)

Table 3-5: Urban Macrocell Assumptions

Femtocell Layout		Value
Cluster Model		Dual-Stripes
Number of Clusters		21 (uniform drop)
Number of Floors per Cluster		1
Number of Blocks per Floor		40 (2 stripes of 2 x 10 blocks)
Block size		10m x 10m
Femtocell Deployment Ratio per Block		10% (uniform drop)
External Wall Attenuation		20dB
Internal Wall Attenuation		5dB
Femtocell Transmission Power		10dBm
Antenna Gain (omni)		0dBi
Pathloss		See [77], Table 6-10
Shadowing	Standard Deviation	4dB
	Correlation	0
Channel Profile		SCME UMa (See [85], line of sight not applied)
Number of UEs per Femtocell		1 (uniform drop within one femtocell)

Table 3-6: Urban Dual-Stripes Femtocell Assumptions

User Equipment		Value
Antenna	Gain (omni)	0dBi
	Spacing (wavelength)	0.5λ
Noise Figure		9dB
Thermal Noise Density		-174dBm/Hz
Speed		3km/h

Table 3-7: User Equipment Assumptions

3.4.4.2 Classical MMSE receiver

Table 3-8 and Table 3-9 show the average spectral efficiency and the outage for various antenna configurations when the UEs are equipped with classical MMSE receiver with the standard subband allocation algorithm engaged at the femtocell side, respectively. For comparison purpose, the same statistics are displayed with a full bandwidth allocation.

Antenna configuration		2x2	4x2	4x4
FUE	Standard Subband Allocation	4.1743	4.9924	6.0648
	Full Bandwidth Allocation	3.4603	4.1763	5.2976
Indoor MUE	Standard Subband Allocation	2.1153	2.3926	3.5666
	Full Bandwidth Allocation	1.5308	1.7403	2.5777

Table 3-8: Spectral efficiency (bits/s/Hz) with standard resource allocation algorithm

Antenna configuration		2x2	4x2	4x4
Indoor MUE	Standard Subband Allocation	2.95%	2.07%	1.65%
	Full Bandwidth Allocation	19.77%	18.32%	14.42%

Table 3-9: Outage ratio (%) with standard resource allocation algorithm

Obviously, the higher is the antenna configuration, the better are the statistics. We note that the subband allocation algorithm increases the spectral efficiency for both the FUEs and the indoor MUEs. In addition, the indoor MUEs outage is drastically reduced: below 3% and 1.7% for the 2x2 and 4x4 configurations, respectively. The subband allocation leaves more room for MUEs (and FUEs) to be scheduled. However, the FUE average spectral efficiency does not reached 8 bits/s/Hz (6.0684bits/s/Hz in 4x4).

Table 3-10 and Table 3-11 show the same statistics as previously but with the extended algorithm (which enable the 256-QAM). In average, the indoor MUEs present the same performance gain in terms of spectral efficiency with the standard or extended subband allocation algorithm. Indeed, the blank left for them stay the same between the two versions of the algorithm. Regarding the outage, they experience higher ratios since the extended algorithm keeps the transmission power equals to 10dBm no matter the number of subbands used. However, those values are still drastically lower than the full band allocation: below 3.5% and 1.9% for 2x2 and 4x4 configurations, respectively. At the femtocell side, the use of a higher modulation brings higher spectral efficiency for the FUEs compared to the standard approach. The 4x4 configuration brings an average of around 7bits/s/Hz, which is a bit lower than the BeFEMTO target of 8bits/s/Hz.

Antenna configuration		2x2	4x2	4x4
FUE	Extended Subband Allocation	4.8501	5.7581	7.0136
	Full Bandwidth Allocation	3.7696	4.5298	5.794
Indoor MUE	Extended Subband Allocation	2.0929	2.3809	3.5388
	Full Bandwidth Allocation	1.5307	1.7411	2.5784

Table 3-10: Spectral efficiency (bits/s/Hz) with extended resource allocation algorithm

Antenna configuration		2x2	4x2	4x4
Indoor MUE	Extended Subband Allocation	3.43%	2.35%	1.86%
	Full Bandwidth Allocation	19.77%	18.58%	14.42%

Table 3-11: Outage ratio (%) with extended resource allocation algorithm

The CDF of the spectral efficiency for the 4x4 configuration and the extended subband allocation algorithm, given in Figure 3-33, shows that 30% of the FUEs experiences a spectral efficiency higher than 8bits/s/Hz with femtocells transmitting at 10dBm.

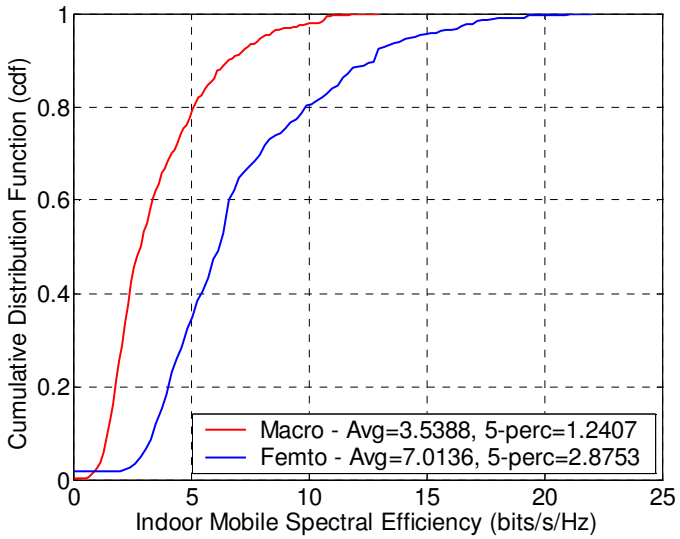

Figure 3-33: Indoor UE spectral efficiency for 4x4 configuration with extended subband allocation

3.4.4.3 Advance receivers

For comparison, the extended subband allocation simulations are redone with an advanced receiver at the UE side which perfectly cancels the spatial interference leading to independent stream detection at the UE side. Such receiver may be implemented using the turbo equalisation principle or iterative successive interference cancellation process.

Antenna configuration		2x2	4x2	4x4
FUE	Extended Subband Allocation	6.334	7.8829	14.1343
	Full Bandwidth Allocation	4.8092	6.1542	10.8813
Indoor MUE	Extended Subband Allocation	2.551	2.8799	4.8799
	Full Bandwidth Allocation	1.8473	2.0652	3.5875

Table 3-12: Spectral efficiency (bits/s/Hz) with extended resource allocation algorithm and perfect spatial interference cancellation

Antenna configuration		2x2	4x2	4x4
Indoor MUE	Extended Subband Allocation	4.72%	3.40%	3.44%
	Full Bandwidth Allocation	20.66%	19.18%	15.36%

Table 3-13: Outage ratio (%) with extended resource allocation algorithm and perfect spatial interference cancellation

The use of an advanced receiver improves the spectral efficiencies of both type of UEs, but the gap is wider when considering the FUEs. Indeed, the FUEs experienced better radio conditions, thus they report higher rank (RI > 1). The multiple streams sent to the FUEs benefit from the perfect spatial interference cancellation. As shown in Table 3-12, the 4x4 configuration with the proposed subband allocation algorithm in conjunction with higher order modulation (up to 256-QAM) allows FUEs to experience an average spectral efficiency of around 14bits/s/Hz. According to Table 3-13, the indoor MUE outage stays really low (3.44% compared to 15.36% for the full bandwidth allocation at the femtocell side).

The CDF of the spectral efficiency for the 4x4 configuration given in Figure 3-34 shows that more than

77% of the FUEs experienced a spectral efficiency higher than 8/bits/s/Hz within the 10dBm power budget.

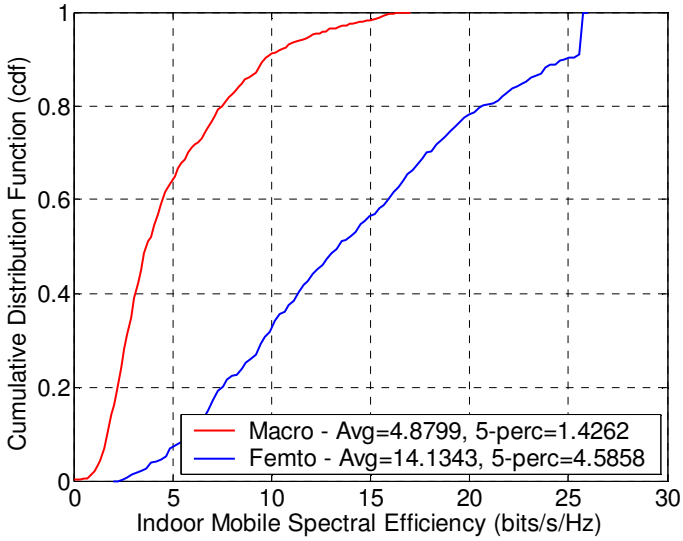

Figure 3-34: Indoor UE spectral efficiency for 4x4 configuration with extended subband allocation and perfect spatial interference cancellation

Finally, even the 4x2 configuration is close to the BeFEMTO target of 8bits/s/Hz at 10dBm, with an average FUE spectral efficiency of 7.88bits/s/Hz and an indoor MUE outage kept around 3.4%. Having only two receive antennas reduces the complexity of the advanced receiver which will have only up to two streams to detect.

3.4.5 Conclusions

If the full bandwidth is allocated by a CSG femtocell in a co-channel HetNet deployment, then non-authorised users in the vicinity of the femtocell may report many outages (CQI equals to zero) reducing their scheduling occasions. In our proposed allocation algorithm, the femtocell only schedules one user at a time on maximum half the system bandwidth leaving blanks for non-authorised users. Power offset is applied on the subcarriers carrying the data in order keep the transmission power as close as possible to the maximum transmission power of 10dBm. With classical receiver, the use of high order modulation (up to 256-QAM) and more flexible power offset (allowing the maximum transmission power to be transmitted on any set of subbands) definitely improves the spectral efficiency of the femtocell users. The 4x4 configuration exhibits on average 7bits/s/Hz which is close to the BeFEMTO target of 8bits/s/Hz while reducing significantly the indoor macrocell user outage (from 14.4% to 1.9%) Without the 256-QAM, this average femtocell user spectral efficiency goes down to 5.8bits/s/Hz.

The introduction of advanced receiver which cancels the spatial interference in MIMO configuration (such as iterative successive interference cancellation) enables the 4x4 configuration with the 256-QAM to beat the BeFEMTO target with an average of 14bits/s/Hz, while preserving a low outage of the indoor macrocell users. With two receive antennas at the user side (meaning a simpler implementation and less signal processing for the advance receiver), the average spectral efficiency is really close to 8bits/s/Hz under the 10dBm power constraint.

By default the femtocell only uses up to half of its bandwidth, leaving sufficient room for other macro/femto users. However, if non-unauthorized user is in the vicinity of the femtocell, then this may appear as a waste of resources. Therefore, mechanism could be envisaged to trigger the presented resource allocation algorithm only when an unauthorised user comes close, by monitoring the uplink for instance to detect the presence of other users.

Simulation results were presented with only one user attached to the femtocell. In case of femtocell multi-user scheduling, the proposed algorithm still applies without any change since only one user is scheduled at a time. However, attention should be paid such that a femtocell user should be scheduled over sufficient consecutive TTIs, such that when the neighbouring cells schedules their users, they do it based on a coherent reporting by the time they receive it.

4. Conclusions and Achievements

This report presented the innovative concepts along with the promising results of the research activities carried out during the 2.5 years of the BeFEMTO project within Work Package 3.

Initially, interference management approaches between unplanned indoor standalone femtocells and overlay macrocells were explored. As shown, in case of femto-to-macrocell interference on the control channel, interference-reducing techniques such as sparseness yield promising gains for UEs trapped within the coverage of active femtocells. On data channel part, a novel low-complexity distributed ICIC scheme was proposed. It has been observed through a simulation study that the proposed scheme can substantially increase both the critical performance and the system performance of the network. Furthermore, a complementary dynamic algorithm was introduced to mitigate interference for victim macro user equipments which are impacted by an aggressor femto cell in the vicinity. The algorithm exploits the channel condition of the victim MUE so that the soft frequency reuse in femto cell only implicates the least number of required subbands. It was shown that the proposed algorithm not only improves the throughput of the victim MUE but also maintains femto cells throughput.

Moreover, multi-operator indoor band sharing was examined where full sharing versus partial sharing of macrocell and femtocells spectrum bands was discussed. As shown, an adaptive sharing was crucial where the level of sharing with femtocells can be controlled based on the density of femto deployment and the activation ratio per sector.

The concept of TDD underlay at UL was also investigated where a distributed self-organizing mechanism based on the concept of busy tones was proposed. When compared to the uncoordinated deployment, the outage probability of the evaluation scenarios with the coordinated TDD-underlay solution was reduced by nearly 80%, while the average spectral efficiency increased by approximately 90% at high loads.

The impact of decentralized approaches for radio resource allocation was examined. Here, a novel scheduler exploiting the wireless spectrum in a two tier-network was proposed. The proposed resource management scheme limits the overall interference per RB generated outside the coverage range of a femtocell while reducing the transmission power in each RB. Subsequently, another decentralized approach was proposed for radio resource allocation in femtocell networks based on opportunistic reuse. As shown, this method could efficiently control the level of resulting interference on macro performance. Moreover, in case macro users have more flexible QoS requirements, it is possible to target higher values for fading threshold resulting better performance on FUE side. Thereafter, an interference-aware LC-RRM technique was presented where power and RBs are allocated to FUEs efficiently by combining location information.

One contribution also focused on a novel RRM and power control scheme combined with Successive Interference Cancellation. Here, SIC was used to allow a macrocell user and a femtocell user to share a common channel and UL to a femtocell access point. Simulations showed that the scheme (excluding SIC) achieves good performance in terms of sum rate gain and in the number of femto users served in the network. Utilizing SIC, even more gains from both the user and network perspectives could be realized. Finally, different access control policies for standalone femtocells were studied highlighting interesting tradeoffs between closed, open and hybrid access. In fact, the hybrid approach was shown to be preferable in terms of outage probability at the expense of lower average SINRs. Furthermore, the impact of handover parameters were evaluated via analytical methods and it was highlighted that handover decision process should be a function of important factors, such as interference, traffic load, and backhaul capability.

Finally, the benefit of MIMO transmission and high order modulation on femtocells was evaluated based on detailed simulation studies. In brief, the introduction of advanced receiver which cancels the spatial interference in MIMO configuration (such as iterative successive interference cancellation) could enable the 4x4 configuration with the 256-QAM to beat the BeFEMTO target with an average of 14bits/s/Hz, while preserving a low outage of the indoor macrocell users. With two receive antennas at the user side (meaning a simpler implementation and less signal processing for the advance receiver), the average spectral efficiency seemed really close to 8bits/s/Hz under the 10dBm power constraint.

5. References

[1] M. Alouini and A. Goldsmith, "Area Spectral Efficiency of Cellular Mobile Radio Systems", *IEEE Transactions on Vehicular Technology*, vol. 48, no. 4, pp. 1047–1066, 1999.

[2] V. Chandrasekhar, J. Andrews, and A. Gatherer, "Femtocell Networks: A Survey", *IEEE Communications Magazine*, vol. 46, no. 9, pp. 59–67, 2008.

[3] J. D. Hobby and H. Claussen, "Deployment Options for Femtocells and their Impact on Existing Macrocellular Networks", *Bell Labs Technical Journal*, vol. 13, no. 4, pp. 145–160, Feb. 2009.

[4] R.-T. Juang, P. Ting, H.-P. Lin, and D.-B. Lin, "Interference Management of Femtocell in Macro-Cellular Networks", in Proc. of the *IEEE Wireless Telecommunications Symposium (WTS)*, Tampa, U.S.A., Apr. 2010, pp. 1–4.

[5] D. Lopez-Perez, A. Valcarce, G. de la Roche, and J. Zhang, "OFDMA Femtocells: A Roadmap on Interference Avoidance", *IEEE Communications Magazine*, vol. 47, no. 9, pp. 41–48, June 2009.

[6] J. Espino and J. Markendahl, "Analysis of Macro-Femtocell Interference and Implications for Spectrum Allocation", in Proc. of *the IEEE Personal, Indoor and Mobile Radio Communications (PIMRC)*, Tokyo, Japan, September 13–16 2009, pp. 2208–2212.

[7] Z. Bharucha, A. Saul, G. Auer, and H. Haas, "Dynamic Resource Partitioning for Downlink Femto-to-Macro-Cell Interference Avoidance", *EURASIP Journal on Wireless Communications and Networking (special issue on Femtocell Networks)*, vol. 2010, no. Article ID 143413, p. 12 pages, May 2010.

[8] Z. Bharucha, H. Haas, A. Saul, and G. Auer, "Throughput Enhancement through Femto-Cell Deployment", *European Transactions on Telecommunications*, vol. 21, no. 4, pp. 469–477, Mar. 2010, (invited).

[9] H. Mahmoud, I. Guandvenc, and F. Watanabe, "Performance of Open Access Femtocell Networks with Different Cell-Selection Methods", in Proc. of *the 71st IEEE Vehicular Technology Conference (VTC)*, May 16–19 2010, pp. 1–5.

[10] J. Weitzen and T. Grosch, "Comparing Coverage Quality for Femtocell and Macrocell Broadband Data Services", *IEEE Communications Magazine*, vol. 48, no. 1, pp. 40–44, Jan. 2010.

[11] 3GPP, "New Work Item Proposal: Enhanced ICIC for non-CA based Deployments of Heterogeneous Networks for LTE", March 16–19, 2010.

[12] D. Lopez-Perez, I. Guvenc, G. de la Roche, M. Kountouris, T. Q.S. Quek and J. Zhang, "Enhanced Inter-Cell Interference Coordination Challenges in Heterogeneous Networks", *IEEE Wireless Communications*, June 2011.

[13] Y-J. Hong, N. Lee, and B. Clerckx, "System Level Performance Evaluation of Inter-cell Interference Coordination Schemes for Heterogeneous Networks in LTE-A System", in Proc. of *IEEE Globecom workshop on Femtocell Networks*, Dec. 2010.

[14] R. Madan, J. Borran, A. Sampath, N. Bhushan, A. Khandekar, and T. Ji, "Cell Association and Interference Coordination in Heterogeneous LTE-A Cellular Networks" *IEEE Journal on Selected Areas in Communications*, Dec. 2010.

[15] Z. Bharucha, H. Haas, G. Auer and I. Cosovic, "Femto-Cell Resource Partitioning", *in Proc. of IEEE Globecom workshops*, Nov. 2009.

[16] Y. Wu, D. Zhang, H. Jiang, Y. Wu, "A Novel Spectrum Arrangement Scheme for Femto Cell Deployment in LTE Macro Cells", in Proc. of *the IEEE Personal, Indoor and Mobile Radio Communications (PIMRC)*, Sept. 2009.

[17] S. Sesia, I. Toufik, and M. Baker, LTE - *The UMTS Long Term Evolution: From Theory to Practice*, 1st ed., S. Sesia, I. Toufik, and M. Baker, Eds. Wiley, 2009.

[18] 3GPP TS 36.211, "Physical Channels and Modulation (Release 9)", v 9.1.0, Mar. 2010.

[19] 3GPP TS 36.212, "Multiplexing and Channel Coding (Release 9)", v 9.2.0, Jun. 2010.

[20] 3GPP TS 36.213, "Evolved Universal Terrestrial Radio Access (E-UTRA) Physical layer procedures (Release 9)", Dec. 2010.

[21] 3GPP TR 36.921, "Evolved Universal Terrestrial Radio Access (E-UTRA); FDD Home eNodeB (HeNB) Radio Frequency (RF) Requirements Analysis (Release 9)," v 9.0.0, Mar. 2010.

[22] 3GPP TSG RAN WG4 R4-092042, "Simulation Assumptions and Parameters for FDD HeNB RF Requirements", May 2009 from www.3gpp.org/ftp/Specs/.

[23] ITU-R Working Party 5D (WP5D) - IMT Systems, "Report 124, Report of correspondence group for IMT.EVAL," May 2008, United Arab Emirates.

[24] T. S. Rappaport, Wireless Communications: Principles and Practice, 2nd ed. Prentice Hall, ISBN: 0130422320, Dec. 2001.

[25] K. Brueninghaus, D. Astely, T. Salzer, S. Visuri, A. Alexiou, S. Karger, and G.-A. Seraji, "Link Performance Models for System Level Simulations of Broadband Radio Access Systems," in Proc. of *the 16th IEEE International Symposium on Personal, Indoor and Mobile Radio Communications (PIMRC)*, vol. 4, Berlin, Germany, Sept. 11–14 2005, pp. 2306–2311.

[26] M. Rahman, H. Yanikomeroglu, "Inter-Cell Interference Coordination in OFDMA Networks: A Novel Approach Based on Integer Programming", in Proc. of *the IEEE Vehicular Technology Conference (VTC)*, May 2010, pp.1-5

[27] GLPK (GNU Linear Programming Kit). Version 4.47. [Online]. Available: http://www.gnu.org/software/glpk/.

[28] M. Sternad, T. Ottosson, A. Ahlen, A. Svensson, "Attaining both coverage and high spectral efficiency with adaptive OFDM downlinks", in Proc. of *the IEEE Vehicular Technology Conference (VTC)*, Oct. 2003. pp.2486-2490

[29] 3GPP R1-050507, Huawei, "Soft frequency reuse scheme for UTRAN LTE", TSG RAN WG1 Meeting #41, Athens, Greece, May 2005.

[30] 3GPP R1-050594, Alcatel, "Multi-cell Simulation Results for Interference Co-ordination in new OFDM DL", TSG RAN WG1 LTE Ad Hoc on LTE, Sophia Antipolis, France, Jun. 2005.

[31] 3GPP TSG RAN, "3GPP TR.36.814, Evolved Universal Terrestrial Radio Access (E-UTRA); Further advancements for E-UTRA physical layer aspects," v9.0.0, Mar. 2010.

[32] D. S. Baum, J. Hansen, G. D. Galdo, M. Milojevic, J. Salo, and P. Kysti, "An Interim Channel Model for Beyond-3G Systems Extending the 3GPP Spatial Channel Model (SCM)," in Proc. of *the IEEE Vehicular Technology Conference (VTC),* Spring, May 2005.

[33] 3GPP TS 36.214 "Evolved Universal Terrestrial Radio Access (E-UTRA); Physical layer; Measurements", V10.0.0, Dec. 2010.

[34] K. Ramadas and R. Jain, "WiMAX System Evaluation Methodology," WiMAX Forum, Tech. Rep., Jan. 2007.

[35] C.H. Lima, M. Bennis, M. Latva-aho, "Coordination Mechanisms for Self-Organizing Femtocells in Two-Tier Coexistence Scenarios" *IEEE Transaction in Wireless Communications*, June 2012.

[36] S. Resnick, A Probability Path. Birkhäuser Boston, 1999.

[37] 3GPP TR.25.814, "Physical Layer Aspects for Evolved UTRA (Release 7)," v7.1.0, Sept. 2006.

[38] 3GPP TSG-RAN4#51, Alcatel-Lucent, picoChip Designs, and Vodafone, "R4-092042, Simulation assumptions and parameters for FDD HeNB RF requirements," May 2009.

[39] D. Chase, "Code Combining–A Maximum-Likelihood Decoding Approach for Combining an Arbitrary Number of Noisy Packets," *IEEE Transactions on Communications*, vol. 33, no. 5, pp. 385–393, May 1985.

[40] 3GPP TSG-RAN1#62, "R1-105082, Way Forward on eICIC for non- CA based HetNets," Aug. 2010.

[41] S. Geirhofer, L. Tong, and B. M. Sadler, "Interference-aware ofdma resource allocation: a predictive approach," *IEEE Military Communications Conference (MILCOM)*, pp. 1–7, Nov. 2008.

[42] P. Thulasiraman and X. Shen, "Interference aware resource allocation in hybrid hierarchical wireless networks," *Computer Networks (Elsevier),* vol. 54, no. 13, pp. 2271-2280, Sept. 2010.

[43] Kulkarni, "Radio Resource Management Considerations for LTE Femto Cells," ACM-SIGCOMM,

2010.

[44] M. Nazir *et al*, "Learning based mechanisms for interference mitigation in self-organized femtocell networks", *Signals, Systems and Computers (ASILOMAR),* Nov. 2010.

[45] Ji-Hoon Yun and K.G. Shin, "Adaptive interference management of OFDMA femtocells for co-channel deployment," *IEEE Journal on Selected Areas in Communications,* pp 1225-1241, Jun. 2011.

[46] T. Weiss and F. K. Jondral, "Spectrum pooling: an innovative strategy for the enhancement of spectrum efficiency," *IEEE Commun. Mag.,* vol. 43, no. 3, pp. S8-S14, Mar. 2004.

[47] V. Kuppusamy and R. Mahapatra, "Primary user detection in OFDM based MIMO cognitive radio," *3rd International Conf. Cognitive Radio Oriented Wireless Netw. Commun. (CrownCom 2008),* pp. 1-5, 2008, Singapore.

[48] H. Lei, L. Zhang, X. Zhang, and D. Yang, "A novel multi-cell OFDMA system structure using fractional frequency reuse," in Proc. of *the IEEE International Symposium on Personal, Indoor and Mobile Radio Communications (PIMRC),* Sept. 2007.

[49] H.-C. Lee, D. C. Oh and Y. H. Lee, "Mitigation of inter-femtocell interference with adaptive fractional frequency feuse," in Proc. of *the IEEE International Conference on Communications (ICC),*pp.1-5, 23-27, May 2010.

[50] Ju Yong Lee *et al*, "Interference analysis for femtocell deployment in OFDMA Systems Based on Fractional Frequency Reuse," *IEEE Communications Letters,* April 2011.

[51] Taeyoung Lee *et al*, "Resource allocation analysis in OFDMA femtocells using fractional frequency reuse in Proc. of *the IEEE International Symposium on Personal, Indoor and Mobile Radio Communications (PIMRC), 2010.*

[52] Poongup Lee *et al*, "Interference management in LTE femtocell systems using fractional frequency reuse,"*Advanced Communication Technology* (ICACT), 7-10 Feb. 2010.

[53] Bruce Fette, *Cognitive Radio Technology,* Second Edition, 2009, Academic Press.

[54] Alaya-Feki *et al* "Informed spectrum usage in cognitive radio networks Interference cartography," IEEE PIMRC 2008.

[55] J. Nasreddine, J. Riihijärvi, P. Mähönen, "Location-based adaptive detection threshold for dynamic spectrum access," in Proc. of *the IEEE Dynamic Spectrum Access Networks* (DySPAN 2010), Singapore, April 2010.

[56] D2.1 State of the Art Review document, "Flexible and spectrum-aware radio access through measurements and modeling in cognitive radio systems," FP7 ICT-248351 FARAMIR project

[57] D.G. Krige, "A statistical approach to some basic mine valuation problems on the Witwatersrand," Journal of the Chemistry, Metal and Mining Society of South Africa, vol. 52, pp. 119-139, 1951.

[58] R.H. Etkin, D.N.C. Tse and H. Wang, "Gaussian interference channel capacity to within one bit," *IEEE Transactions on Information Theory*, vol. IT-54, no. 12, pp. 5534--5562, Dec. 2008.

[59] C. Abgrall, E. Calvanese Strinati and J.C. Belfiore, "Distributed power allocation for interference limited networks", in *Proc. of the IEEE Personal, Indoor and Mobile Radio Communications (PIMRC),*2010

[60] B. Kaufman, E. Erkip, J. Lilleberg, B. Aazhang, "Femtocell Interference Mitigation Through Succes- sive Interference Cancellation and Cellular Handover," *IEEE International Conference on Communications: Workshop on Heterogeneous Networks (ICC)*, Jun. 2011.

[61] D. López-Pérez, A. Valcarce, A. Ladanyi, G. de la Roche, and J. Zhang, "Intracell handover for interference and handover mitigation in OFDMA two-tier macrocell-femtocell networks", to appear in *EURASIP Journal of Wireless Communications and Networking,* 2010

[62] G. de la Roche, A. Valcarce, D. López-Pérez, and J. Zhang, "Access control mechanisms for femtocells", *IEEE Communication Magazine*, vol. 48, no. 1, pp. 33-39, Jan. 2010

[63] Femtoforum working group, "Wireless in the Home & Office: the need for both 3G femtocells and WiFi access points," http://www.femtoforum.org/femto/publications.php, Jan. 2010.

[64] Mobile Broadband Access at Home, "Informa Telecoms & Media," Aug. 2008.

[65] Presentation by Picochip, “2nd International Conference on Home Access Points and Femtocells,” www.avernevents.com/dallasfemto2007/purchase presentations.htm.

[66] F. Pantisano, K. Ghaboosi, M. Bennis and M. Latva-aho, “Interference Avoidance via Resource cheduling in TDD Underlay Femtocells,” in Proc. of *the IEEE Personal, Indoor and Mobile Radio Communications (PIMRC),* 26-29 Sept. 2010, Istanbul, Turkey

[67] 3GPP TS 36.300, “Evolved Universal Terrestrial Radio Access (E-UTRA) and Evolved Universal Terrestrial Radio Access Network (E-UTRAN); Overall description; Stage 2”

[68] 3GPP TS 32.521, “Telecommunication management; Self-Organizing Networks (SON) Policy Network Resource Model (NRM) Integration Reference Point (IRP); Requirements”

[69] M. Anas, F. D. Calabrese, P.-E Ostling, K. I. Pedersen, P. E. Mogensen, "Performance Analysis of Handover Measurements and Layer 3 Filtering for Utran LTE," in Proc. of *the IEEE Personal, Indoor and Mobile Radio Communications (PIMRC)*, Sept. 2007

[70] K. Dimou, M. Wang, Y. Yang, M. Kazmi, A. Larmo, J. Pettersson, W. Muller, Y. Timner, "Handover within 3GPP LTE: Design Principles and Performance," in Proc. of *the IEEE Vehicular Technology Conference,* 2009-Fall, Sept. 2009

[71] P. Legg, H. Gao, J. Johansson, "A Simulation Study of LTE Intra-Frequency Handover Performance," in Proc. of *the IEEE Vehicular Technology Conference,* 2010-Fall, Sept. 2010

[72] A. E. Leu, B. L. Mark, "A discrete-time approach to analyze hard handoff performance in cellular networks," *IEEE Transactions on Wireless Communications*,, vol.3, no.5, pp. 1721- 1733, Sept. 2004

[73] N. Zhang, J. M. Holtzman, "Analysis of handoff algorithms using both absolute and relative measurements," *IEEE Transactions On Vehicular Technology*, vol.45, no.1, pp.174-179, Feb. 1996

[74] D. Giancristofaro , "Correlation model for shadow fading in mobile radio channels," Electronics Letters , vol.32, no.11, pp.958-959, 23 May 1996

[75] 3GPP TS25.104 v9.3.0 (2010-03), “Base Station (BS) radio transmission and reception (FDD) (Release 9)”

[76] 3GPP TS25.105 v10.0.0 (2010-06), “Base Station (BS) radio transmission and reception (TDD) (Release 10)”

[77] BeFEMTO D2.3, “The BeFEMTO System Concept and its Performance”, ICT 248523 FP7 BeFEMTO project, June 2012.

[78] M. Maqbool, M. Lalam, and T. Lestable, “Comparison of femto cell deployment models for an interference avoidance technique,” in Proc. of *Future Network & Mobile Summit* (FUNEMS’11), Jun. 2011.

[79] BeFEMTO IR3.2, “Radio Access Specs and Promising Techniques for Indoor Standalone Femtocells, “Promising Interference and Radio Management Techniques for Indoor Standalone Femtocells”, ICT 248523 FP7 BeFEMTO project, Dec. 2009.

[80] BeFEMTO IR3.3, “Promising Interference and Radio Management Techniques for Indoor Standalone Femtocells”, ICT 248523 FP7 BeFEMTO project, Dec. 2010.

[81] 3GPP TS 36.213, “Evolved Universal Terrestrial Radio Access (E-UTRA) Physical layer procedures (Release 9)”, v9.0.0, Dec. 2010.

[82] K. Brueninghaus, D. Astely, T. Sälzer, S. Visuri, A. Alexiou, S. Karger, and G.-A. Seraji, “Link performance models for system level simulations of broadband radio access systems,” in Proc. of *the IEEE Personal, Indoor and Mobile Radio Communications (PIMRC)*, vol. 4, Sept. 2005.

[83] Femto Forum, “Interference management in OFDMA femtocells,” White Paper, Feb. 2010, Available online: www.femtoforum.org

[84] 3GPP TS 36.331, “Evolved Universal Terrestrial Radio Access (E-UTRA); Radio Resource Control (RRC); Protocol specification (Release 9)”, v9.4.0, Sept. 2010.

[85] D. S. Baum, J. Hansen, G. D. Galdo, M. Milojevic, J. Salo, and P. Kysti, “An Interim Channel Model for Beyond-3G Systems Extending the 3GPP Spatial Channel Model (SCM),” in Proc. of *the IEEE Vehicular Technology Conference (VTC)*, Spring, May 2005.